

LDA + DMFT Investigation of NiO

Von der Mathematisch-Naturwissenschaftlichen Fakultät
der Universität Augsburg
zur Erlangung eines Doktorgrades der Naturwissenschaften
genehmigte Dissertation

von
Xinguo Ren
aus
China

November 2005

Vorsitzender: Priz-Doz Dr. Alexander Krimmel
Erstgutachter: Prof. Dr. Dieter Vollhardt
Zweitgutachter: Priz-Doz Dr. Volker Eyert
Prüfer: Prof. Dr. Ulrich Eckern, Prof. Dr. Siegfried Horn

Tag der mündlichen Prüfung: 16.02.2006

CONTENTS

Introduction	1
1. Electronic-Structure Calculations with Density Functional Theory	5
1.1 Density Functional Theory	5
1.2 Single-Particle Description and Local Density Approximation	8
1.2.1 Kohn-Sham Approach	8
1.2.2 Local Density Approximation	9
1.3 The Linear Muffin-Tin Orbital Method	11
1.3.1 Energy Band Methods	11
1.3.2 Linear Muffin-Tin Orbitals	13
1.3.3 The LMTO Band Calculation	16
1.4 Wannier Functions	19
2. The LDA+DMFT Approach	23
2.1 The Hubbard Model	23
2.2 Dynamical Mean-Field Theory	27
2.2.1 The Infinite Dimension Limit	27
2.2.2 DMFT Equations — Exact Solution of the $D = \infty$ Hubbard Model	29
2.2.3 Quantum Monte-Carlo Method	31
2.2.4 Case Studies with DMFT	35
2.3 The LDA+DMFT Formulation	38

3. LDA+DMFT Investigation of NiO	43
3.1 Introduction	43
3.1.1 Crystal Structure	43
3.1.2 Electronic and Magnetic Properties	44
3.1.3 Previous Studies	46
3.2 Method and Results	48
3.2.1 Wannier Function Construction	51
3.2.2 LDA Results	54
3.2.3 LDA+DMFT Results and Comparison with Experiment	56
3.3 Conclusions	60
4. Towards A Self-Consistent LDA+DMFT Scheme	63
4.1 General Motivation	63
4.2 Flow Diagram and Formulation	64
4.3 Difficulties and Challenges	68
5. Summary and Outlook	71
Appendix	73
A. Proof That The External Potential Is A Unique Functional of The Ground-State Density	75
B. Estimation of The Local Magnetic Moment and The Coulomb Interaction Parameter	77
C. Energy Moment Calculation from Matsubara Green function	79
Bibliography	82
Curriculum Vitae	89
Acknowledgements	91

INTRODUCTION

From a microscopic *ab-initio* point of view, a solid material is an interacting many-particle system involving both ions and electrons. However, according to the Born-Oppenheimer approximation (Born and Oppenheimer, 1927), the ions and electrons can be treated separately. Indeed, many properties of solids can be well described by the electronic degree of freedom, while the ions only contribute through a static potential. The resultant electronic Hamiltonian is still far too complicated to be fully solved and immediately requires further approximations, among which the one-electron approximation plays an important role. Within this approximation, the electron-electron interaction is taken into account at a mean-field level, behaving like an effective potential, and therefore the many-electron problem reduces to a single-electron one described by a single-electron Schrödinger equation. Solving this Schrödinger equation leads to the energy band theory of solids. The effective potential can be determined in different ways, governed by different approximations, among which the Hartree-Fock (HF) approximation (Hartree, 1928; Fock, 1930) is the most famous example. At present the most satisfactory picture for single-electron theory is based on the density functional theory (DFT) (Hohenberg and Kohn, 1964) through Kohn-Sham's approach (Kohn and Sham, 1965). The single-particle approximation is very successful for explaining the properties of weakly correlated systems, e.g., simple metals, ordinary insulators and some semiconductors, but generally fails for systems with strongly correlated electrons such as Mott insulators, cuprates, manganites and rare earth systems. A satisfactory description of these systems requires an explicit treatment of the interactions between electrons.

The problem of understanding the properties of strongly correlated materials is one of the main challenges for modern condensed matter physics. In this case one has to go beyond the one-electron approximation and employ more sophisticated treatment of electron-electron interaction. For that purpose, practically one has to restrict oneself to the most important orbitals so that the many-electron interactions can be explicitly treated. For instance, the valence d electrons are the most relevant ones responsible for the properties of transition metal compounds, and a model Hamiltonian can be formulated involving only these electrons. The simplest model appropriate for the strongly correlated electrons is one-band Hubbard model (Gutzwiller, 1963; Hubbard, 1963), in which only the on-site Coulomb

interaction is considered, whereas the long-range ones are neglected. However, it turned out even for such a highly simplified model it is still very difficult to solve, and the exact solution only exists for one dimension. Therefore various approximations were developed to gain insights into the model and to arrive at some understandings of the experimental behaviors for real materials in the end. Dynamical mean-field theory (DMFT) is such an approximation which maps the the lattice model onto a quantum impurity model subject to a self-consistent condition (Metzner and Vollhardt, 1989b; Georges and Kotliar, 1992; Jarrell, 1992). The particular advantages of DMFT lie in two aspects: first, it is a “controlled” approximation meaning that it has a well-defined limit— the infinite coordination number (or the infinite dimensions) where the theory becomes exact (Metzner and Vollhardt, 1989b); second, the practical solution of DMFT consists in solving an effective Anderson impurity model (Anderson, 1961) iteratively and several analytical and numerical techniques have existed to deal with it. The application of DMFT to Hubbard model has produced fruitful results and substantial progress has been made in understanding the nature of Mott metal-insulator transition (Georges *et al.*, 1996; Rozenberg *et al.*, 1999; Blümer, 2002).

The model Hamiltonian approach is helpful in understanding some qualitative features or identifying the underlying physical mechanism of the strongly correlated systems, but it can’t explain the detailed features of real materials. This is not surprising since the material-specific information can’t be contained in a highly-simplified, Hubbard-like model. On the other hand, the efforts of describing the real materials at a quantitative level persist, and for that purpose the model Hamiltonian approach has to be used with the help of the “*ab-initio*” approach for incorporating the material-specific information. This is actually the basic idea of the LDA+DMFT approach formulated by Anisimov *et al.* (1997b) (see also Lichtenstein and Katsnelson (1998)) in which the band-structure calculation based on DFT within its local density approximation (LDA) and the DMFT treatment of the localized orbitals are combined. The strategy here is based on the observation that although LDA often leads to qualitatively wrong results for the strongly correlated materials, it can usually provides quite reliable parameters for these systems. These parameters can be in turn used to construct a many-body Hamiltonian which is specific for the particular material under study. In most of the practical applications of LDA+DMFT, one first performs a LDA band calculation to drive a material-specific generalized model Hamiltonian, and solve this Hamiltonian by DMFT.

In the past few years LDA+DMFT approach has been successfully applied to transition metals, e.g. nickel (Lichtenstein *et al.*, 2001), transition metal compounds, e.g. $\text{La}_{1-x}\text{Sr}_x\text{TiO}_3$ (Anisimov *et al.*, 1997b; Nekrasov *et al.*, 2000), LiV_2O_4 (Nekrasov *et al.*, 2003), $\text{Ca}(\text{Sr})\text{VO}_3$ (Nekrasov *et al.*, 2005), V_2O_3 (Held *et al.*, 2001a; Keller, 2005), and *f*-electron systems such as plutonium (Savrasov *et al.*, 2001) and cerium (Held *et al.*, 2001b). In this thesis, we will use the

LDA+DMFT approach to investigate the electronic structure of NiO. NiO is a classical Mott insulator which has been under intensive studies for many years. The recent theoretical investigations mainly fall into two categories, i.e., the calculations from first principles and that based on the localized cluster model. However, a satisfactory description of its electronic spectrum is still not available, and this is due to the reason that the first principles studies usually can not treat the strong local Coulomb interaction adequately whereas the local cluster approach completely ignores the band effect which also plays an important role in this system. In this connection it is very interesting to see if the LDA+DMFT approach works better for NiO, considering its previous successes for strongly correlated materials. It turns out that within the LDA+DMFT approach the calculated energy gap and local magnetic moment are in good agreement with experiment, and the obtained electronic energy spectrum shows impressive quantitatively improvement over previous results.

The plan of this thesis is as follows. In chapter 1 we give an account of the density-functional based band structure calculations which is the starting point for performing a LDA+DMFT calculation. In particular, Emphasis will be given to LDA which is the most commonly used approximation for carrying out the self-consistent band structure calculations. Then we will introduce one of the most favorable methods for calculating the band structures of transition metal compounds, namely linear muffin-tin orbital (LMTO) method (Andersen, 1975), within which the LMTO basis is used for solving the one-electron Schrödinger equation. Finally we discuss the concept of Wannier functions (WFs) and its historical development, and point out its usefulness in realistic modelling of materials with localized orbitals.

An introduction of the LDA+DMFT approach in general is then presented in Chapter 2. In this chapter we first give an elementary review of the stereotyped strongly-correlated fermionic lattice model, namely the Hubbard model. This is followed by a presentation of the DMFT equations, illustrating how a lattice model, in the limit of infinite dimension, can be mapped to a single-site quantum impurity embedded in an average medium. As a powerful, numerically exact solver of the quantum impurity problem, the Hirsch-Fye quantum Monte-Carlo (QMC) method (Hirsch and Fye, 1986) is then described. Finally the general motivation of combining the many-body technique-DMFT, and the state-of-the-art band structure method-DFT(LDA) is discussed. This naturally leads to the LDA+DMFT approach. In particular we show how the LDA band-structure is incorporated into the DMFT equations, giving rise to the formalism of the practical LDA+DMFT scheme.

In chapter 3, we apply the LDA+DMFT approach to the prototypical Mott insulator-NiO. First in the introduction the main properties and the previous studies of NiO are reviewed. In addition we point out why it is worthwhile to

perform a LDA+DMFT study of NiO. We then describe the new procedure for implementing the LDA+DMFT scheme, in which a set of WFs are constructed and used as the basis for the DMFT calculation. The LDA+DMFT scheme is applied to calculate the electronic properties of NiO, and the obtained results are presented and compared with experiment. This chapter is closed with comments on the successful aspects and limitations of the present study, and the possible directions of improvement.

The possible extensions of the present LDA+DMFT scheme are discussed in Chapter 4. This consists of two respects: firstly, not only the transition metal d but also ligand p orbitals should be included in the DMFT calculation when there is strong hybridization between them, and secondly the LDA part and DMFT part should be merged self-consistently rather than performed in a subsequent order, as done in the present implementation. Here we follow a fully self-consistent scheme recently proposed by Anisimov *et al.* (2005), and its implementation is a still ongoing work.

Chapter 5 concludes this thesis with a summary and outlook.

1. ELECTRONIC-STRUCTURE CALCULATIONS WITH DENSITY FUNCTIONAL THEORY

Density-functional theory (DFT) is nowadays a popular and successful approach to study the ground-state properties of an interacting many-particle system, including atoms, molecules, and crystalline solids. This approach concentrates on the electron density $n(\mathbf{r})$ instead of the much more complicated many-body wave function $\Psi(\mathbf{r}_1, \mathbf{r}_2, \dots, \mathbf{r}_N)$, the solution of the latter is an impossible task for an interacting system with more than a few electrons. The idea of using electron density $n(\mathbf{r})$ instead of the wave function $\Psi(\mathbf{r}_1, \mathbf{r}_2, \dots, \mathbf{r}_N)$ as the basic variable to study many-body systems dates back to the Thomas-Fermi (TF) model proposed by Thomas (1927) and independently by Fermi (1928) in late 1920s. However, the framework of DFT was put on a firm footing only after the work of Hohenberg and Kohn (1964), known as Hohenberg-Kohn (HK) theorems.

1.1 Density Functional Theory

To get an idea of what the HK theorems are, let us start by considering a system with N interacting electrons moving in an external static potential $v(\mathbf{r})$. For this system the many-electron Hamiltonian reads

$$\hat{H} = \hat{T} + \hat{U} + \sum_i v(\mathbf{r}_i), \quad (1.1)$$

where

$$\hat{T} = \sum_i \frac{\hbar^2 \nabla^2}{2m}, \quad (1.2)$$

$$\hat{U} = \sum_{i < j} \frac{e^2}{|\mathbf{r}_i - \mathbf{r}_j|} \quad (1.3)$$

are the kinetic and electron-electron interaction operator respectively, and m in (1.2) is the electron mass. We note that under the Born-Oppenheimer approximation, a N -electron Coulomb system is specified solely by the form of the

external potential $v(\mathbf{r})$, since both \hat{T} and \hat{U} are universal. HK showed that for a given ground-state density $n(\mathbf{r})$, the external potential $v(\mathbf{r})$ can be uniquely determined up to an unimportant constant (for a proof, see Appendix A). Since $v(\mathbf{r})$ in turn fixes the full N-electron Hamiltonian, it is clear that the ground state wave function Ψ^0 , and in particular the kinetic energy $\langle \hat{T} \rangle_0 = \langle \Psi^0 | \hat{T} | \Psi^0 \rangle$ and the interaction energy $\langle \hat{U} \rangle_0 = \langle \Psi^0 | \hat{U} | \Psi^0 \rangle$, are all functionals of $n(\mathbf{r})$. Therefore one can define a universal functional including only the kinetic and integration energy as

$$F[n] = \langle \Psi^0[n] | \hat{T} + \hat{U} | \Psi^0[n] \rangle = T[n] + U[n] \quad (1.4)$$

which does not refer to any external potential $v(\mathbf{r})$. And $\Psi^0[n]$ here is the ground state wave function associated with some particular density $n(\mathbf{r})$.

Now suppose we have some arbitrary external potential $v(\mathbf{r})$, and associated with it can we define the following energy functional,

$$E_v[n] = \int v(\mathbf{r})n(\mathbf{r})d\mathbf{r} + F[n]. \quad (1.5)$$

Note that in Eq. (1.5) $n(\mathbf{r})$, as the basic variable of the functional, is not necessary to be the ground-state density associated with $v(\mathbf{r})$ here.¹ However, it can be easily shown that $E_v[n]$ assumes its minimum at the ground-state density $n^0(\mathbf{r})$ of the present system, i.e., associated with $v(\mathbf{r})$. Thus we have briefly demonstrated the essential ideas of the HK theorems which state that for an interacting electronic system there exist an energy functional of the electron density, and this functional is minimized by the ground-state density. Combining Eqs. (1.4) and (1.5) $E_v[n]$ can be written as

$$E_v[n] = \int v(\mathbf{r})n(\mathbf{r})d\mathbf{r} + T[n] + U[n]. \quad (1.6)$$

The original proof of the HK theorems is given in the space of V-representable electron densities. Levy (1979) and independently Lieb (1983) generalized the proof to the N-representable² electron-density space through the approach of “constrained search”. Now it has been known that all the non-negative function of electron density is N-representable.

The energy-functional $E_v[n]$ is easy to write down, but its explicit form is not known. Thus one has to make approximations to $T[n]$ and $U[n]$ before doing any practical calculations based on the variational principle. The TF model was actually one particular approximation to $E_v[n]$ in which the electrons are

¹ But it should be the ground-state density corresponding to some other $v'(\mathbf{r})$ in this context. This is the so-called “V-representability”.

² N-representability means that the electron density can be realized for some antisymmetric N-electron wave function, i.e., $n(\mathbf{r}) = N \int \dots \int \Psi^*(\mathbf{r}, \mathbf{r}_2, \dots, \mathbf{r}_N) \Psi(\mathbf{r}, \mathbf{r}_2, \dots, \mathbf{r}_N) d\mathbf{r}_2 \dots d\mathbf{r}_N$.

treated as independent particles and the interaction energy is approximated by the electrostatic energy. This model was frequently used in the past, but there are serious deficiencies within it, e.g., for atoms the electron density decays too slowly far away from the nucleus³, and for molecules and solids the chemical bonds calculated with this model are not stable, and so on. These deficiencies can be largely ascribed to the local approximation to the kinetic energy⁴,

$$T[n] \approx \int d\mathbf{r} t_0[n(\mathbf{r})]. \quad (1.7)$$

Here $t_0[n] = (3\hbar^2/10m)(3\pi^2)^{2/3}n^{5/3}$ is the kinetic energy density of a noninteracting homogeneous electron gas with a constant density n . Actually two kinds of approximations are involved in (1.7), the first is the local approximation which assumes that the kinetic energy density at some particular spatial point only depends on the density precisely at that point, and the second is to use the kinetic energy density of the noninteracting system to replace that of the interacting one since the latter is not known.

The drawbacks arising from the local approximation to $T[n]$ were removed through the Kohn-Sham (KS) approach (Kohn and Sham, 1965), which maps a system with interacting electrons to one with noninteracting electrons moving in an effective potential. This mapping is achieved by introducing auxiliary single-particle orbitals, by means of which the noninteracting part of the kinetic energy can be treated exactly. This represents a substantial improvement over the TF model, and many pathologies are thus cured. Furthermore, a single-particle picture arises with a set of self-consistent equations which are analogous to the Hartree-Fock (HF) equations. The resultant effective potential includes the external static potential, the Hartree or electrostatic potential, and the remaining part known as the exchange-correlation potential. KS equations play a fundamental role in DFT.

Nowadays electronic-structure calculations based on DFT through the KS approach are routinely performed for atoms, molecules and solids, and the application of DFT to organic materials has just appeared. A large number of review articles and books exist, and here we only list a few of them, e.g., Lundqvist and March (1983); Parr and Yang (1989); Jones and Gunnarsson (1989); Dreizler and Gross (1990). An excellent elementary introduction into DFT was given recently by Capelle (2003). In this thesis we are only concerned with the application of DFT to crystalline solids, where the single-particle picture arising from the KS approach leads to a band theory due to the periodicity of the effective potential.

³ The electron density for a single atom calculated with the TF model decays as a power law ($1/r^6$) away from the nucleus, whereas the physically correct behavior should be an exponential decay.

⁴ This is effectively an approximation that the motion of the electrons is treated as independent particles, and should be distinguished from the local density approximation to the exchange-correlation functional.

The band theory of solid crystals, initiated by Bloch, Brillouin and Wilson, has been tremendously advanced since the emergence of DFT.

Practically, it is inevitable to introduce approximations to the exchange-correlation potential. The local density approximation (LDA), which we will discuss below, is the most frequently used one.

1.2 Single-Particle Description and Local Density Approximation

DFT is turned into a tractable framework through Kohn-Sham approach, or Kohn-Sham ansatz (Kohn and Sham, 1965), which assumes that a system of interacting particles can be represented by one of noninteracting particles moving in an effective potential. This potential contains an unknown exchange-correlation term, and approximations have to be employed to deal with this term. In this section we first discuss the Kohn-Sham approach, and then introduce the local density approximation (LDA).

1.2.1 Kohn-Sham Approach

Among the different parts of contributions to the electronic energy, the external potential energy and the classic electron-electron interaction energy can be expressed explicitly in terms of electron density $n(\mathbf{r})$, and all the remaining contributions, denoted as $G[n]$, are not known explicitly as a functional of $n(\mathbf{r})$. Thus we can rewrite the energy functional $E_v[n]$ Eq. (1.6).

$$E_v[n] = \int d\mathbf{r} v(\mathbf{r})n(\mathbf{r}) + \frac{1}{2} \int d\mathbf{r} \int d\mathbf{r}' \frac{n(\mathbf{r})n(\mathbf{r}')}{|\mathbf{r} - \mathbf{r}'|} + G[n]. \quad (1.8)$$

KS further separate $G[n]$ into $T_s[n]$ and $E_{xc}[n]$,

$$G[n] = T_s[n] + E_{xc}[n], \quad (1.9)$$

where the $T_s[n]$ is the kinetic energy for a system of noninteracting electrons with density $n(\mathbf{r})$, and $E_{xc}[n]$ is the remaining parts, defined as the exchange-correlation energy.

Combining Eqs. (1.8) and (1.9), and applying the variational principle, one arrives at the following Euler equation,

$$\frac{\delta T_s[n]}{\delta n(\mathbf{r})} + v(\mathbf{r}) + \phi(\mathbf{r}) + \frac{\delta E_{xc}[n]}{\delta n(\mathbf{r})} = 0, \quad (1.10)$$

where

$$\phi(\mathbf{r}) = \int d\mathbf{r}' \frac{n(\mathbf{r}')}{|\mathbf{r} - \mathbf{r}'|}. \quad (1.11)$$

is the Hartree potential. The original problem given by Eq. (1.10) is mathematically identical to the one of a system of noninteracting electrons moving in an effective potential

$$v_{eff}(\mathbf{r}) = v(\mathbf{r}) + \phi(\mathbf{r}) + \frac{\delta E_{xc}[n]}{\delta(\mathbf{r})}. \quad (1.12)$$

The latter problem can be solved by the single-particle Schrödinger equation,

$$\left(\frac{\hbar^2}{2m} \nabla^2 - v_{eff}(\mathbf{r}) \right) \psi_i(\mathbf{r}) = \epsilon_i \psi_i(\mathbf{r}) \quad (1.13)$$

which is required to yield the same electron density as the interacting electron system⁵,

$$n(\mathbf{r}) = \sum_{i=1}^N |\psi_i(\mathbf{r})|^2. \quad (1.14)$$

Equations (1.11) to (1.14) are the famous KS equations which have to be solved self-consistently.

For crystalline solids, the periodicity can be fully retained in the effective potential $v_{eff}(\mathbf{r})$, and the effective single-particle problem (1.13) naturally leads to the Bloch's energy band theory. In this connection an approximation has been implicitly invoked to interpret the auxiliary single-particle eigenvalues ϵ_i in (1.13) as the physical excitation energies. In practice such an interpretation is found to be a good approximation for weakly correlated systems.

1.2.2 Local Density Approximation

As has been shown, KS theorems guarantee that the ground-state energy of a quantum many-electron system can be obtained by minimizing an energy functional $E_v[n]$ with respect to the electron density, and KS approach maps the problem of minimizing $E_v[n]$ to a set of self-consistent equations for a single electron. Thus KS theorems and KS mapping together provide a single-particle description of interacting many-particle systems. So far these two steps are both exact in principle. However, as mentioned before, for any practical implementation of DFT, one has to introduce approximation to the exchange-correlation energy functional $E_{xc}[n]$ defined in expression (1.9).

⁵ In case that the electron density is not representable by a single Slater determinant, one can replace Eq. (1.14) by $n(\mathbf{r}) = \sum_{i=1}^N f_i |\psi_i(\mathbf{r})|^2$, in which the states above the Fermi level can be occupied and holes can be left below the Fermi level.

The most popular approximation that has been used for decades is the local density approximation (Kohn and Sham, 1965), which is usually expressed as,

$$E_{xc}[n] = \int d\mathbf{r} n(\mathbf{r}) \epsilon_{xc}(n(\mathbf{r})). \quad (1.15)$$

Here $\epsilon_{xc}(n(\mathbf{r}))$ is the exchange-correlation energy per electron for a homogeneous gas of interacting electrons with constant density n . The basic idea behind it is to separate the whole inhomogeneous electron system into infinitely small pieces and treat every piece as if its neighbors do not have influences on it. This kind of approximation has appeared for treating the kinetic energy in TF theory where it is quite problematic. However, the LDA treatment of $E_{xc}[n]$ proved to be very successful and this is due to the reason that the nonlocal correction to $E_{xc}[n]$ is relatively small in cases that the variation of $n(\mathbf{r})$ is not too rapid.

Now let's have a closer look at $\epsilon_{xc}(n)$. $\epsilon_{xc}(n)$ consists of two components: the exchange energy $\epsilon_x(n)$ and correlation energy $\epsilon_c(n)$ per electron. $\epsilon_x(n)$ is known exactly⁶

$$\epsilon_x(n) = -\frac{3e^2}{4} \left(\frac{3n}{\pi}\right)^{1/3}, \quad (1.16)$$

whereas the precise form of $\epsilon_c(n)$ is not known. The study of $\epsilon_c(n)$ by itself is a very difficult problem in many-body theory, and the best description of $\epsilon_c(n)$ so far is given numerically by Quantum Monte Carlo method (Ceperley and Alder, 1980). The practical expression of $\epsilon_c(n)$ in the modern calculations is based on the parameterization of these numerical data.

LDA has been successfully used in the band-structure calculations of quite a large number of solid state systems, but it failed for one particular group of materials, namely those with strongly correlated electrons. Most of the transition metals and their compounds, as well as rare-earth materials, belong to this category. Another example is chemistry where LDA is usually not accurate enough to describe quantitatively the chemical bonding in molecules. These problems call for better approximations beyond LDA, and among many of them we here only mention a particular one which is commonly used in chemistry, known as generalized-gradient approximation (GGA). Instead of considering $\epsilon_{xc}(n(\mathbf{r}))$ is a local function of $n(\mathbf{r})$, GGA takes it as a function of $n(\mathbf{r})$ and its gradient $\nabla n(\mathbf{r})$ (Perdew and Wang, 1986),

$$\epsilon_{xc}(n(\mathbf{r})) = f(n(\mathbf{r}), \nabla n(\mathbf{r})). \quad (1.17)$$

GGA enjoys a great success in chemistry by giving reliable results of the chemical bonding, and often improves over the LDA results for the strong-correlated solid

⁶ See, e.g. Mahan (1990, p. 385), $\epsilon_x(n) = -(3/4\pi)k_F e^2$ where $k_F = (3\pi^2 n)^{1/3}$ is the Fermi wave vector.

materials. Different choices of the form of $f(n, \nabla n)$ represents different kinds of GGA, and one has the freedom to choose a best one appropriate for the particular type of system under investigation.

1.3 The Linear Muffin-Tin Orbital Method

The linear muffin-tin orbital (LMTO) method is one particular technique for solving the one-electron problem in crystalline solids. Among the many methods of solving band-structure problems, the LMTO method is often more favorable because it is relatively easy to implement and computationally cheap, and it has the accuracy required in most cases. In this section we first briefly review the energy band methods in general, and then discuss the LMTO method specifically.

1.3.1 Energy Band Methods

DFT through KS Ansatz offers a self-consistent way of calculating the band structures of crystalline solids. The energy bands of electrons arise from the translational symmetry of crystals and determine many physical properties of the system. To calculate the band structures accurately and efficiently is one of the basic tasks in solid state physics. Lot's of experience had been gained much earlier before DFT was widely accepted as an efficient tool for band-structure calculations.

Indeed, even without considering any self-consistency, solving the Schrödinger equation of a single electron moving in a given, periodic potential is a highly nontrivial problem. To be specific, we consider the following problem

$$\left(\frac{\hbar^2}{2m} \nabla^2 - v(\mathbf{r}) \right) \psi_j^{\mathbf{k}}(\mathbf{r}) = E_j^{\mathbf{k}} \psi_j^{\mathbf{k}}(\mathbf{r}) \quad (1.18)$$

where the potential $v(\mathbf{r})$ is translationally invariant,

$$v(\mathbf{r} + \mathbf{R}) = v(\mathbf{r}), \quad (1.19)$$

with \mathbf{R} being a lattice constant. The eigenfunctions $\psi_j^{\mathbf{k}}(\mathbf{r})$ in Eq. (1.18), known as Bloch functions, have been chosen to be simultaneously the eigenfunctions of both the Hamiltonian operator \hat{H} and the translation operator \hat{T} , and hence are labelled by both the band index j and Bloch vector \mathbf{k} . The justification for doing so is provided by the Bloch theorem,

$$\hat{T}_{\mathbf{R}} \psi_j^{\mathbf{k}}(\mathbf{r}) \equiv \psi_j^{\mathbf{k}}(\mathbf{r} + \mathbf{R}) = e^{i\mathbf{k} \cdot \mathbf{R}} \psi_j^{\mathbf{k}}(\mathbf{r}). \quad (1.20)$$

The Bloch vector \mathbf{k} is a vector in the reciprocal space, and is usually chosen to be restricted inside the first Brillouin zone.

The different energy-band methods differ from one another by the set of functions chosen as the basis to expand the unknown eigenfunctions $\psi_j^{\mathbf{k}}(\mathbf{r})$. Historically, these methods are divided into two classes: one works with fixed, energy-independent basis functions, like plane waves, atomic orbitals, or orthogonalized plane waves (OPW) (Herring, 1940), and the other uses energy-dependent basis, in particular the partial waves. Examples for the latter are the cellular (Wigner and Seitz, 1933), augmented plane wave (APW) (Slater, 1937), and Korringa-Kohn-Rostoker (KKR) (Korringa, 1947; Kohn and Rostoker, 1954) methods. Both of these methods have advantages and drawbacks. The fixed basis method, say LCAO (linear combination of atomic orbitals), has the advantage that the variational procedure for one-electron Hamiltonian leads to an algebraic eigenvalue problem so that all the eigenvalues and eigenvectors at a given \mathbf{k} point can be obtained by a single diagonalization. However, this method requires a large number of atomic orbitals to form a complete basis set, and the Hamiltonian matrix elements involve a lot of two- and three-center integrals which are very difficult to calculate. On the other hand, the methods employing the energy-dependent partial waves as basis functions can have good accuracies with a smaller basis set, but the resultant secular matrix has a nonlinear energy-dependence so that the eigenvalues can only be found one by one, thus requiring much more computation time than the linear problem.

Under this background a linear procedure was proposed by Andersen (1975) in order to combine the positive features of both kinds of energy band methods but avoid their difficulties. The idea is to linearize (Taylor expanded up to first order) the energy-dependence of the partial waves around some arbitrary but fixed energy points. The linear energy-independence vanishes by a proper linear combination of the partial wave functional and their energy derivatives at these energy points (one energy point for each partial wave), leading to energy-independent orbitals. With these energy-independent basis functions, the secular equations of the eigenvalue problem become linear in energy. The linear method was first applied to the muffin-tin orbitals (MTOs) (Andersen and Wooley, 1973) and then to augmented plane waves, leading to linear muffin-tin orbitals (LMTOs) and linear augmented plane waves (LAPWs). The LMTOs and LAPWs, as their conventional counterparts are defined with respect to the muffin-tin potential which is a reasonable approximation to the real crystal potential. In this approximation, a so-called muffin-tin sphere is inscribed inside each atomic polyhedron: inside the sphere the potential is assumed to be spherically symmetric, and out of the spheres it is flat. A schematic behavior of the MT potential is shown in Fig. 1.1. In the next section we will give an illustration of how the LMTOs are constructed.

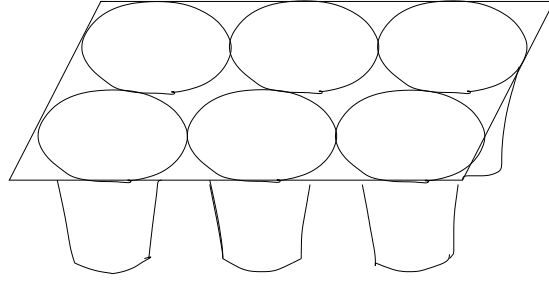


Figure 1.1: A schematic picture of the MT potential. The potential well should go to infinity at the center of the atom.

1.3.2 Linear Muffin-Tin Orbitals

A detailed description of the LMTO method was given by Skriver (1984), which we are following here. To arrive at a final definition of LMTO, several steps are needed to take. First, instead of treating a full MT potential, we only consider a single MT well embedded in a constant potential environment. Namely we are dealing with a single-electron problem with the following potential,

$$v(\mathbf{r}) = \begin{cases} V(r) & r \leq S_{\text{MT}}, \\ V_{\text{MTZ}} & r \geq S_{\text{MT}}, \end{cases} \quad (1.21)$$

where $V(r)$ is the spherically symmetric potential inside the MT sphere, and V_{MTZ} is constant potential outside the sphere, with S_{MT} the radius of the MT sphere. For convenience we define

$$V_{\text{MT}}(r) = v(\mathbf{r}) - V_{\text{MTZ}} = \begin{cases} V(r) - V_{\text{MTZ}} & r \leq S_{\text{MT}}, \\ 0 & r \geq S_{\text{MT}}, \end{cases} \quad (1.22)$$

and

$$\kappa^2 = E - V_{\text{MTZ}}. \quad (1.23)$$

Therefore the Schrödinger equation of a single electron moving in the potential $v(\mathbf{r})$ with behaving like (1.21) reads

$$\left[-\frac{\hbar^2}{2m} + V_{\text{MT}}(r) - \kappa^2 \right] \psi_L(E, \mathbf{r}) = 0. \quad (1.24)$$

Due to the spherical symmetry of the total potential $v(\mathbf{r})$ under consideration, the eigenfunction $\psi_L(E, \mathbf{r})$ can be classified by the combined angular and magnetic quantum number $L = lm$ is, and can be written as a product of a radial part and an angular part, i.e.,

$$\psi_L(E, \mathbf{r}) = i^l Y_l^m(\hat{\mathbf{r}}) \psi_l(E, r). \quad (1.25)$$

The radial part of the Schrödinger equation satisfied by $\psi_l(E, r)$ inside the MT sphere and in the constant potential region respectively look like,

$$\left[\frac{\hbar^2}{2m} \frac{d^2}{dr^2} + \frac{l(l+1)}{r^2} + V_{\text{MT}}(r) - \kappa^2 \right] r\psi_l(E, r) = 0, \text{ for } r \leq S_{\text{MT}}, \quad (1.26a)$$

$$\left[\frac{\hbar^2}{2m} \frac{d^2}{dr^2} + \frac{l(l+1)}{r^2} - \kappa^2 \right] r\psi_l(E, r) = 0, \text{ for } r \geq S_{\text{MT}}. \quad (1.26b)$$

Leaving Eq. (1.26a) aside for a while, let us concentrate on the Helmholtz equation (1.26b) which has two linearly independent solutions. For a positive κ^2 , these are the spherical Bessel function $j_l(\kappa r)$ and Neumann function $n_l(\kappa r)$, and for $\kappa^2 < 0$, i.e., the kinetic energy is negative in the constant potential region, the Neumann function $n_l(\kappa r)$ should be replaced by the first kind Hankel function $-ih_l^{(1)} = n_l - ij_l$. Here we only present the formulations of the positive κ^2 case, and those for $\kappa^2 < 0$ can be obtained by a simple replacement.

Summarizing the above analysis, we can have the partial waves solving the Schrödinger equation of (1.24) ,

$$\psi_L(E, \kappa, \mathbf{r}) = i^l Y_l^m(\hat{\mathbf{r}}) \begin{cases} \psi_l(E, r) & r \leq S_{\text{MT}}, \\ \kappa[n_l(\kappa r) - c_l(E, \kappa)j_l(\kappa r)] & r \geq S_{\text{MT}}. \end{cases} \quad (1.27)$$

Here the coefficient $c_l(E, \kappa)$, usually expressed as $\cot(\eta_l(E, \kappa))$, is determined so that $\psi_L(E, \kappa, \mathbf{r})$ is continuous and differentiable across the boundary of the MT sphere. This requires

$$c_l(E, \kappa) = \cot(\eta_l(E, \kappa)) = \frac{n_l(\kappa S_{\text{MT}})}{j_l(\kappa S_{\text{MT}})} \cdot \frac{D_l(E) - D\{n_l\}}{D_l(E) - D\{j_l\}}, \quad (1.28)$$

where

$$\begin{aligned} D_l(E) &= \frac{S_{\text{MT}}}{\psi_l(E, S_{\text{MT}})} \left. \frac{d\psi_l(E, r)}{dr} \right|_{r=S_{\text{MT}}}, \\ D\{n_l\} &= \frac{S_{\text{MT}}}{n_l(\kappa S_{\text{MT}})} \left. \frac{dn(\kappa r)}{dr} \right|_{r=S_{\text{MT}}}, \\ D\{j_l\} &= \frac{S_{\text{MT}}}{j_l(\kappa S_{\text{MT}})} \left. \frac{dj(\kappa r)}{dr} \right|_{r=S_{\text{MT}}}, \end{aligned} \quad (1.29)$$

are the logarithmic derivative of $\psi_l(E, r)$, $n(\kappa r)$, and $j(\kappa r)$ at the sphere boundary respectively. The $\eta_l(\kappa, E)$ defined in (1.28) can be view as the phase shift of the free spherical wave for $r \rightarrow \infty$ due to the scattering of the MT potential.

The partial waves (1.27) are not suitable for serving basis functions. This is particularly because the presence of the term $-\kappa c_l(E, \kappa)j_l(\kappa r)$ in the constant

potential region make them not normalizable for negative κ^2 . The trick that can be employed here to cure this problem is to subtract this term from $\psi_l(E, \mathbf{r})$ in both regions (inside and outside the MT sphere) while maintaining the continuity and differentiability, ending up with

$$\chi_L(E, \kappa, \mathbf{r}) = i^l Y_l^m(\hat{\mathbf{r}}) \begin{cases} \psi_l(E, r) + \kappa c_l(E, \kappa) j_l(\kappa r) & r \leq S_{\text{MT}}, \\ \kappa n_l(\kappa r) & r \geq S_{\text{MT}}. \end{cases} \quad (1.30)$$

These orbitals $\chi_L(E, \kappa, \mathbf{r})$ are actually the energy dependent MTOs. Although they are not the solutions of the problem (1.24), the Bloch sum of $\chi_L(E, \kappa, \mathbf{r})$ and $\psi_L(E, \kappa, \mathbf{r})$ give the identical results except for the \mathbf{k} points satisfying $|\mathbf{k} + \mathbf{G}|^2 = k^2$ with \mathbf{G} being the reciprocal lattice vector. In addition, they are reasonably localized, and regular over the whole space.

In (1.27) and (1.30), the parameter E and κ are related through Eq. (1.23). However, the continuity and differentiability of $\psi_L(E, \kappa, \mathbf{r})$ and $\chi_L(E, \kappa, \mathbf{r})$ are guaranteed by the chosen value (1.28) of $c_l(E, \kappa)$ irrespective of their possible relation between E and κ . In this connection we can disregard (1.23) and treat κ as an independent parameter. By doing so the tails of $\psi_L(E, \kappa, \mathbf{r})$ and $\chi_L(E, \kappa, \mathbf{r})$ are no longer the exact solution of the Schrödinger equation (1.24) in the region of the constant potential any more, but they have the advantage of being energy independent. Moreover, the head of $\chi_L(E, \kappa, \mathbf{r})$ (i.e., the part inside the MT sphere) can also be made energy independent around a fixed energy E_ν up to the first order by replacing (augmenting) $j_l(\kappa r)$ and $n_l(\kappa r)$ inside the MT sphere by more appropriate functions which are attached to the original functions at the sphere boundary in a continuous and differentiable fashion. For this purpose, we define the augmented Bessel function $J_l(\kappa r)$ as

$$J_l(\kappa r) = \begin{cases} -\dot{\psi}_l(E_\nu, r)/(\kappa \dot{c}_l(E_\nu, \kappa)) & r \leq S_{\text{MT}} \\ j_l(\kappa r) & r \geq S_{\text{MT}} \end{cases} \quad (1.31)$$

where $\dot{\psi}_l$ and \dot{c}_l are the energy derivative of ψ_l and c_l respectively. It is easy to verify that $J_l(\kappa r)$ defined in (1.31) is everywhere continuous and differentiable. A proper definition of the augmented Neumann function $N_l(\kappa r)$ is more delicate. Before giving an explicit form of $N_l(\kappa r)$, it is illustrating to present the following expansion theorem of $n_L(\kappa, \mathbf{r}) = n_l(\kappa r) i^l Y_l^m(\hat{\mathbf{r}})$ and $j_L(\kappa, \mathbf{r}) = j_l(\kappa r) i^l Y_l^m(\hat{\mathbf{r}})$, namely,

$$n_L(k, \mathbf{r}) = 4\pi \sum_{L'} \sum_{L''} C_{LL'L''} j_{L'}(\kappa, \mathbf{r} - \mathbf{R}) n_{L''}^*(\kappa, -\mathbf{R}) \quad (1.32)$$

which is valid inside the sphere $|\mathbf{r}| < R$. Here the Gaunt coefficients $C_{LL'L''}$ are defined as

$$C_{LL'L''} = \int Y_l^m(\hat{\mathbf{r}}) Y_{l'}^{m'}(\hat{\mathbf{r}}) Y_{l''}^{m''}(\hat{\mathbf{r}}) d\hat{\mathbf{r}}. \quad (1.33)$$

The augmented spherical Neumann and Bessel functions are also required to satisfy the above expansion theorem, and this lead to the following definition of $N_l(\kappa r)$, including the angular part,

$$N_L(\kappa, \mathbf{r}) = \begin{cases} 4\pi \sum_{L'} \sum_{L''} C_{LL'L''} \begin{cases} j_{L'}(\kappa, \mathbf{r} - \mathbf{R}) n_{L''}^*(\kappa, -\mathbf{R}) \\ |\mathbf{r} - \mathbf{R}| \leq S_{\text{MT}}, \forall \mathbf{R} \neq \mathbf{0} \end{cases} \\ n_L(\kappa, \mathbf{r}) \quad \text{otherwise.} \end{cases} \quad (1.34)$$

To have a clear understanding of (1.34), one may think of the full MT potential composed of nonoverlapping array of MT wells: inside every MT sphere except the one where the present Neumann function is centered, $N_L(\kappa, \mathbf{r})$ is defined as the linear expansion of the augmented Bessel functions centered at that particular MT sphere. In other regions, both the MT sphere at the origin and the interstitial region, the augmented Neumann function is simply defined as the normal one.

With $J_L(\kappa, \mathbf{r})$ and $N_L(\kappa, \mathbf{r})$ defined, we finally end up with the following definition of the augmented MTO

$$\chi_L(E, \kappa, \mathbf{r}) = i^l Y_l^m(\hat{\mathbf{r}}) \begin{cases} \psi_l(E, r) + \kappa c_l(E, \kappa) J_l(\kappa r) & r \leq S_{\text{MT}}, \\ \kappa N_l(\kappa r) & r \geq S_{\text{MT}}. \end{cases} \quad (1.35)$$

The augmented MTO defined in (1.35) is energy independent up to the first order in $(E - E_\nu)$. It is everywhere continuous and differentiable, and it is orthogonal to the core states. By neglecting the high-order energy dependence of $J_L(\kappa, \mathbf{r})$, i.e., fixing $E = E_\nu$, we are led to the linear (energy independent) MTOs (LMTOs) $\chi_L(\kappa, \mathbf{r})$.

One disadvantage of the MTOs defined above is their infinite range which makes the practical calculations cumbersome. It has nevertheless been shown (Andersen and Jepsen, 1984; Andersen *et al.*, 1986) that these conventional MTOs can be exactly transformed into a set tight-binding (TB) orbitals. These TB-MTOs, basically formed by a linear combination of the conventional ones, are rather localized and particularly suitable for first-principles electronic structure calculations.

1.3.3 The LMTO Band Calculation

Now we can consider solving the band structure problem with single-electron crystal potential modelled by MT approximation, within which the potential is formed by a array of MT wells centered at sites \mathbf{R} of a three-dimensional periodic lattice. In the spirit of the LCAO method, the Bloch function can be represented as

$$\psi^{\mathbf{k}}(E, \mathbf{r}) = \sum_L \alpha_L^{\mathbf{k}}(E) \chi_L^{\mathbf{k}}(\kappa, \mathbf{r}) \quad (1.36)$$

where the coefficients $\alpha_L^{\mathbf{k}}(E)$ are to be determined and $\chi_L^{\mathbf{k}}(\kappa, \mathbf{r})$ is the Bloch sum of the energy independent MTOs

$$\begin{aligned}\chi_L^{\mathbf{k}}(\kappa, \mathbf{r}) &= \frac{1}{\sqrt{\mathcal{L}}} \sum_{\mathbf{R}} e^{i\mathbf{k}\cdot\mathbf{R}} \chi_L(\kappa, \mathbf{r} - \mathbf{R}) \\ &= \frac{1}{\sqrt{\mathcal{L}}} \left(\chi_L(\kappa, \mathbf{r}) + \sum_{\mathbf{R} \neq \mathbf{0}} e^{i\mathbf{k}\cdot\mathbf{R}} \chi_L(\kappa, \mathbf{r} - \mathbf{R}) \right).\end{aligned}\quad (1.37)$$

Here \mathcal{L} is the number of the lattice sites or unitary cells. The last term in (1.37) consists of the contributions from all the MT spheres except the one at the origin. In the region that is inside the sphere centered at the origin and passing through the nearest-neighbor sites but outside the neighboring MT spheres, this term can be written as a one-center expansion,

$$\sum_{\mathbf{R} \neq \mathbf{0}} e^{i\mathbf{k}\cdot\mathbf{R}} \chi_L(\kappa, \mathbf{r} - \mathbf{R}) = \sum_{\mathbf{R} \neq \mathbf{0}} e^{i\mathbf{k}\cdot\mathbf{R}} \kappa N_l(\kappa, \mathbf{r} - \mathbf{R}) \quad (1.38a)$$

$$= \sum_{L'} J_{L'}(\kappa, \mathbf{r}) \mathcal{B}_{L'L}^{\mathbf{k}}(\kappa) \quad (1.38b)$$

where the KKR structure constants $\mathcal{B}_{L'L}^{\mathbf{k}}(\kappa)$, according to the expansion theorem (1.32), should be defined as

$$\mathcal{B}_{L'L}^{\mathbf{k}}(\kappa) = 4\pi \sum_{L''} C_{LL'L''} \sum_{\mathbf{R} \neq \mathbf{0}} e^{i\mathbf{k}\cdot\mathbf{R}} \kappa n_{L''}^*(\kappa, \mathbf{R}). \quad (1.39)$$

The above stated region of convergence is the intersection of the two regions where (1.38a) and (1.38b) are valid respectively. Therefore, inside this region, the Bloch sum of MTOs can be expressed in terms of a one-center expansion,

$$\chi_L^{\mathbf{k}}(\kappa, \mathbf{r}) = \frac{1}{\sqrt{\mathcal{L}}} \left(\chi_L(\kappa, \mathbf{r}) + \sum_{L'} J_{L'}(\kappa, \mathbf{r}) \mathcal{B}_{L'L}^{\mathbf{k}}(\kappa) \right). \quad (1.40)$$

With the set of Bloch summed MTOs $\chi_L^{\mathbf{k}}(\kappa, \mathbf{r})$, by applying standard variational techniques, the band structure problem is reduced to a set of linear equations at each \mathbf{k} point,

$$\sum_{L'} \langle \chi_L^{\mathbf{k}} | H - E | \chi_{L'}^{\mathbf{k}} \rangle \alpha_{L'}^{\mathbf{k}}(E) = 0, \quad (1.41)$$

which has solutions in case that

$$\det \{ \langle \chi_L^{\mathbf{k}} | H - E | \chi_{L'}^{\mathbf{k}} \rangle \} = 0. \quad (1.42)$$

Thus we need to evaluate the secular matrix element $\langle \chi_L^{\mathbf{k}}(\kappa, \mathbf{r}) | H - E | \chi_{L'}^{\mathbf{k}}(\kappa, \mathbf{r}) \rangle$. Due to the translational properties of $\chi_L^{\mathbf{k}}(\kappa, \mathbf{r})$ and H , one can verify that

$$\langle \chi_L^{\mathbf{k}} | H - E | \chi_{L'}^{\mathbf{k}} \rangle = N \langle \chi_L^{\mathbf{k}} | H - E | \chi_{L'}^{\mathbf{k}} \rangle_0 \quad (1.43)$$

where $\langle \rangle_0$ means the integral over the atomic polyhedron at the origin. Within the atomic polyhedron, $\chi_L^{\mathbf{k}}(\kappa, \mathbf{r})$ can be expanded as (1.40), and therefore

$$\begin{aligned} N\langle \chi_L^{\mathbf{k}} | H - E | \chi_{L'}^{\mathbf{k}} \rangle_0 &= \langle \chi_L | H - E | \chi_{L'} \rangle_0 \\ &+ \sum_{L''} [\langle \chi_L | H - E | J_{L''} \rangle_0 \mathcal{B}_{L''L'}^{\mathbf{k}} + \mathcal{B}_{LL''}^{\mathbf{k}} \langle J_{L''} | H - E | \chi_{L'} \rangle_0] \\ &+ \sum_{L''} \sum_{L'''} \mathcal{B}_{LL''}^{\mathbf{k}} \langle J_{L''} | H - E | J_{L'''} \rangle_0 \mathcal{B}_{L''L'}^{\mathbf{k}}. \end{aligned} \quad (1.44)$$

For the spherically symmetric potential, the angular part of the wave functions can be first integrated out, and we are finally left with

$$\begin{aligned} \langle \chi_L^{\mathbf{k}} | H - E | \chi_{L'}^{\mathbf{k}} \rangle &= \langle \chi_l | H - E | \chi_l \rangle_0 \delta_{LL'} \\ &+ [\langle \chi_l | H - E | J_l \rangle_0 + \langle \chi_{l'} | H - E | J_{l'} \rangle_0] \mathcal{B}_{LL'}^{\mathbf{k}} \\ &+ \sum_{L''} \mathcal{B}_{LL''}^{\mathbf{k}} \langle J_{l''} | H - E | J_{l''} \rangle_0 \mathcal{B}_{L''L'}^{\mathbf{k}} \end{aligned} \quad (1.45)$$

The simplification from (1.44) to (1.45) arises from the fact the secular matrix element between two $\chi_L(\kappa, \mathbf{r})$ or $J_L(\kappa, \mathbf{r})$ with two different L indices vanishes. The matrix elements appearing on the righthand side of (1.45), is defined as integrals over radial variable r , e.g.,

$$\langle \chi_l | H - E | \chi_l \rangle_0 \equiv \int_0^\infty dr r \chi_l(\kappa, r) \left[-\frac{d^2}{dr^2} + \frac{l(l+1)}{r^2} + v_{\text{MT}}(r) - \kappa^2 \right] r \chi_l(\kappa, r). \quad (1.46)$$

Within the LMTO method, the integral terms on the righthand side of $\chi_L(\kappa, \mathbf{r})$ can be parameterized and evaluated at different orders of approximations. The detailed way of representing these integrals by a set of parameters can be found in the book of Skriver (Skriver, 1984). Concerning the approximations made to accomplish this, a simple and popularly used one is the so-called atomic sphere approximation (ASA), in which the κ^2 is set to 0 and the atomic polyhedra are replaced by the atomic spheres.

The procedure of constructing LMTOs described above is for the simple case when there is only one atom in a unit cell, but it could be easily extended to the multiatomic case. In that case, the LMTOs should carry one more index r distinguishing the different atoms in the unit cell, namely,

$$\chi_L^{\mathbf{k}} \rightarrow \chi_{rL}^{\mathbf{k}} = \chi_{rlm}^{\mathbf{k}}. \quad (1.47)$$

Thus in general, the LMTOs have three indices r, l, m to label the atom, the angular and magnetic quantum number.

1.4 Wannier Functions

The electronic states in the system with a periodic potential are naturally represented by Bloch functions, labelled by the band index n and reciprocal vector \mathbf{k} . An equivalent representation is provided by Wannier functions (WFs) (Wannier, 1937), defined as a Fourier transformation of Bloch functions. These WFs are hence are labelled by the spatial lattice \mathbf{R} and band index n . The existence of a localized set of WFs, and their general properties have been discussed by various authors over the years, e.g., Koster (1953), Parzen (1953), Kohn (1959; 1973), Des Cloizeaux (1963; 1964; 1964), and Blount (1962). Although the concept of WFs has been employed in the construction of model Hamiltonians and in many theoretical discussions, the quantitative calculations based on WFs did not appear until recently (Marzari and Vanderbilt, 1997; Ku *et al.*, 2002; Pavarini *et al.*, 2004; Anisimov *et al.*, 2005). This state of affairs is partly due to the nonunique nature of WFs so that there is no general and reliable method to calculate them, and partly due to the reason that the Bloch description of the electronic states is usually quite satisfactory. However, in narrow-band systems where the electrons have strongly atomic natures, there is a great need for a suitable set of localized orbitals to describe the system properly. In this case, we consider that the WFs are not just a mathematically unitary transformation of Bloch functions, but rather represent the real electronic structure of the system.

The different ways to calculate WFs can be roughly classified into two categories. The first approach, assumed by Koster (1953), Parzen (1953), and Kohn (1973), attempts to produce the WFs directly through a variational procedure, without knowing the Bloch functions. The other approach, which are is often used and will be used here, is to calculate the WFs from a set of Bloch states that has been already obtained from a energy band calculation. In a single-band case, the WFs are defined as the Fourier transformation of the Bloch functions,

$$W(\mathbf{r} - \mathbf{R}) = \frac{1}{\sqrt{\mathcal{L}}} \sum_{\mathbf{k} \in BZ} e^{i\mathbf{k} \cdot \mathbf{R}} \psi^{\mathbf{k}}(\mathbf{r}) \quad (1.48)$$

where the summation is over the first Brillouin zone (BZ) and N is the number of discrete \mathbf{k} points inside this zone. However, even in the simple transformation above, ambiguity concerning the definition of WFs arises from the indeterminacy of the phase factor $e^{i\phi(\mathbf{k})}$ associated with the Bloch function $\psi^{\mathbf{k}}(\mathbf{r})$. On the other hand, the freedom of choosing $\phi(\mathbf{k})$ can be utilized to obtain a set of well-behaved WFs. For instance, for a one-dimensional lattice with reflection symmetry, one can obtain a set of real, symmetric and exponentially localized WFs by choosing $\psi^{\mathbf{k}}(0)$ to be real (Kohn, 1959).

The practically more interesting case is that a composite group of bands are interconnected among themselves by degeneracies. (See Fig. 1.2). In this case, one

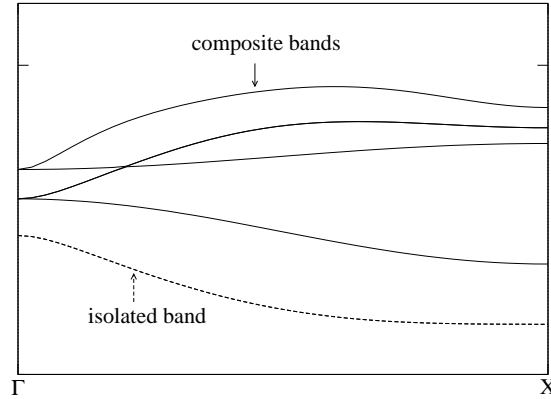


Figure 1.2: A schematic picture of isolated band, and a composite group of bands.

usually does not perform the transformation (1.48) individually for every branch of the bands, but rather construct WFs for the composite bands simultaneously by introducing an additional unitary transformation $U_{mm'}^{\mathbf{k}}$ among the different branches at each \mathbf{k} point, namely,

$$W_m(\mathbf{r} - \mathbf{R}) = \frac{1}{\sqrt{\mathcal{L}}} \sum_{\mathbf{k} \in \text{BZ}} e^{i\mathbf{k} \cdot \mathbf{R}} \sum_{m'} U_{mm'}^{\mathbf{k}} \psi_{m'}^{\mathbf{k}}(\mathbf{r}). \quad (1.49)$$

Two considerations are involved here: firstly it may be possible that no exponentially localized WF can be obtained at all by including only a single branch, and secondly WFs with better localization and higher symmetry can be constructed by treating the composite bands all together. Thus the task of constructing WFs consist in the determination of $U_{mm'}^{\mathbf{k}}$ according to some criterions chosen *a priori*.

Different methods have been developed in the past. In particular, Marzari and Vanderbilt (1997) devised a procedure to obtain the maximally localized WFs by minimizing a functional that representing the total spread $\sum_m \langle r^2 \rangle_m - \langle \mathbf{r} \rangle_m^2$ of these WFs. This minimization procedure starts with some initial guess of the WFs obtained by projecting the trial localized orbitals onto the chosen set of composite Bloch bands and it was found that this initial guess is usually quite good. Ku *et al.* (2002) then discarded the minimization procedure and took only the first step of Marzari and Vanderbilt's method to construct their WFs, by projecting the Gaussian orbitals onto the DFT all-electron eigenstates. Even with this simplified procedure they found remarkably good results concerning the relevant material-specific parameters. Pavarini *et al.* (2004) built up WFs for t_{2g} orbitals in some typical $3d^1$ perovskites by symmetrically orthonormalizing the N -th order muffin-tin orbitals (NMTOs) (Andersen and Saha-Dasgupta, 2000), and employed them in the LDA+DMFT investigation for the Mott transition and the suppression of orbital fluctuations in these systems. Most recently, Anisimov *et al.* (2005) proposed a scheme to calculate WFs by projecting the LMTOs onto the

chosen set of Bloch bands. This scheme is particularly suitable for LDA+DMFT calculations, and will be discussed in detail in chapter **3**.

2. THE LDA+DMFT APPROACH

In the first chapter we discussed the density functional theory and its local density approximation (DFT-LDA) that have been extensively used in the modern band-structure calculation for solid crystalline. We also presented the main idea and formulations of the LMTO method, which is one of the most popular method for performing the DFT-LDA band calculation. However, the DFT-LDA, and in general the single-particle description of solid systems generally fail for the systems with narrow bands and strong electron interactions. For these systems, one has to invoke another approach, namely the model Hamiltonian approach, to explicitly take into account the electron-electron interactions. In this context an appropriate model should on the one hand be able to capture the strongly correlated nature of these systems, but on the other hand be simple enough to allow for an analytical or numerical solution, possibly under some reliable approximation. The one-band Hubbard model is such a “minimal” model aiming at describing in a simplified way the correlated d electrons in transition metals and their compounds. The model Hamiltonians, in spite of their apparent relevance to some basic features of the strongly correlated materials and usefulness in revealing the underlying physical mechanisms, are restricted in their ability to make quantitative predictions. The LDA+DMFT approach is the first attempt to give a quantitative description of the materials with strongly correlated electrons by combining the DFT-LDA band structure calculation and the dynamical mean-field theory (DMFT) for solving the many-body Hamiltonian. This combination is based on the fact that the DFT-LDA calculation is a first-principles method and usually gets the material-specific information quite correctly, and DMFT is most powerful many-body technique for treating the strongly correlated lattice fermionic model. In this chapter we first introduce the Hubbard model, then give a brief review of the dynamical mean-field theory and the quantum Monte-Carlo (QMC) method for solving the DMFT equations, and finally close the chapter with the LDA+DMFT formulations.

2.1 The Hubbard Model

The model referred to as Hubbard model became a standard framework for studying the Mott transition and ferromagnetic metal since it was introduced

(Gutzwiller, 1963; Hubbard, 1963; Hubbard, 1964). The model Hamiltonian consists of two terms

$$H = \sum_{ij,\sigma} t_{ij} (d_{i\sigma}^\dagger d_{j\sigma} + h.c.) + U \sum_i n_{i\uparrow} n_{i\downarrow}, \quad (2.1)$$

with the first term describing the electron hopping from site i to site j , and the second an intraatomic Coulomb repulsion. Here the operator $d_{i\sigma}$ ($d_{i\sigma}^\dagger$) annihilate (creates) an electron at site i with spin σ , $n_{i\sigma} = d_{i\sigma}^\dagger d_{i\sigma}$, and U is the strength of the Coulomb interaction. Usually the hopping of the electrons is restricted to the neighboring site, and is translationally invariant, namely,

$$t_{ij} = \begin{cases} -t, & (t > 0) \\ 0 & \end{cases} \quad \begin{array}{l} i, j \text{ are neighboring sites,} \\ \text{otherwise.} \end{array} \quad (2.2)$$

Apart from the physical parameters t and U , a few other parameters can affect the the feature of the model, and these are the dimension D of the lattice on which the model is defined, the band filling $\delta = N_e/(2\mathcal{L})$ (N being the total electron number, and \mathcal{L} the number of the lattice site), and the temperature.

However, it is extremely difficult to get any exact result of (2.1), except in the case of $D = 1$ where exact solution was worked out by Lieb and Wu (1968) using the Bethe ansatz, and these authors showed that there is no metal-insulator transition for any $U > 0$ and δ . The fact that exact solutions are not possible in $D = 2$ and $D = 3$ cases makes the employment of various approximations unavoidable. To be confident that some particular approximation at hand is a meaningful one, it is important to explore the different limiting situations in which the original model reduces to a simpler one and some reliable results can be obtained. In some particular limiting regime, a good approximation should become exact or at least capture some physical ingredients. The ration U/t is a natural quantity according to which one can have two opposite limiting regimes: the strong coupling regime (defined as $U/t \gg 0$) and weak coupling regime ($U/t \ll 0$). Another important quantity is the dimension D . $D = 1$ is the case where exact solution is available and thus provides an important test for the validity of new approximations one wants to employ. Amazingly, in the opposite limit $D = \infty$ drastic simplification of the Hubbard model (2.1) (and in general fermionic lattice model) occurs under a proper scaling of the hopping term (Metzner and Vollhardt, 1989b), and a nontrivial $D = \infty$ Hubbard model is formed. It is on this particular limit that the dynamical mean-field theory (DMFT) (Georges and Kotliar, 1992; Jarrell, 1992) is based.

While leaving the discusson of $N = \infty$ limit to the next section, let's first have a look at the strong and weak coupling regimes. First of all, in the limit of $U/t \gg 0$ and at half-filling ($\eta = 1/2$), the Hubbard model (2.1) is reduced to an antiferromagnetic Heisenberg model up to the second order in t/U (Anderson,

1959),

$$H = J \sum_{i,j} \mathbf{S}_i \cdot \mathbf{S}_j, \quad (2.3)$$

where the exchange constant $J = t^2/U$, and the the spin \mathbf{S}_i at site i is defined through

$$\begin{aligned} S_i^z &= n_{i\uparrow} - n_{i\downarrow}, \\ S_i^\uparrow &= d_{i\uparrow}^\dagger d_{i\downarrow}, \\ S_i^\downarrow &= d_{i\downarrow}^\dagger d_{i\uparrow}. \end{aligned} \quad (2.4)$$

This implies that the ground state is insulating. However, the magnetic property of the ground state of (2.3) is not exactly known except $D = 1$. While the half-filled Hubbard model is reduced to the antiferromagnetic Heisenberg model for very large U , how about the case that the band filling is slightly less than one half? In that case the additional holes can hop between the lattice sites without costing extra energy, and this requires adding a hopping term to the Heisenberg Hamiltonian (2.3), leading to the so-called t - J model. Nagaoka (1966) rigorously proved that the ground state of the system with a single hole and infinite U (i.e., $U \gg N_e t$) is ferromagnetic. This sheds some lights on the understanding the itinerant ferromagnetism within the Hubbard model, but the condition for Nagaoka's theorem is rather unphysical, and the efforts of extending it to more realistic cases failed.

Apart from the above simplifications, two analytical approaches have proved to be useful for the strong-coupling regime. One is the Gutzwiller variational approach (Gutzwiller, 1963), through which Brinkman and Rice (1970) was able to determine a criterion for the metal-insulator transition for the half-filling case, and in particular the metallic phase was found to be a Fermi liquid. In addition, by using Gutzwiller approximation, the Gutzwiller variational wave function provides a framework for interpolating the strong and weak coupling regimes (for a review, see Vollhardt (1984) and Vollhardt *et al.* (1987)). The other approach is known as slave boson mean-field theory (Barnes, 1976; Barnes, 1977), which in many aspects lead to the same results as the Gutzwiller variational approach, but can be used in a more general context (Kotliar and Ruckenstein, 1986).

The weak coupling regime was also addressed by several authors. However, even in this limit, a proper treatment of the Hubbard model turned out to be highly nontrivial, especially for the bipartite lattice where the antiferromagnetic correlation always sets in at half-filling due to the "perfect nesting" of the Fermi surface. Nevertheless, Metzner and Vollhardt (1989a) showed that the exact second-order contribution to the ground-state energy can be obtained by standard perturbation theory. A general approach to strongly correlated electrons by employing "conserving approximation" (i.e., consistent with microscopic conservation laws)

beyond the mean-field level was developed by Bickers *et al* (1989) and applied to 2D Hubbard model. But in general, these approaches require a large amount of computation efforts and are cumbersome to be performed. Again, a preferable route one may take here is to start from the $D = \infty$ limit where the computation effort is tremendously reduced, and reach the finite dimension by perturbative techniques.

Besides the analytical studies of the Hubbard model within various approximations, numerical investigations have been performed on finite systems. Among these the exact diagonalization (ED) and quantum Monte Carlo (QMC) are the two major tools. ED provides exact results and is only doable for rather small systems due to the exponential growth of the configuration space with the number of sites. QMC, on the other hand, can be used to study relatively larger systems, but suffers from the sign problem for large values of U and numerical instability at low temperatures. QMC technique can be either used directly as an *ab initio* approach or within a variational framework (Yokoyama and Shiba, 1987). ED and QMC can often be employed in a complementary way in which the result of ED offers a check for the efficiency of QMC.

The one-band Hubbard model is the minimal model one can figure out to describe correlated d -electron systems. But one can ask the question: how well does this model represent the physics of the correlated electrons? Obviously the one-band model has neglected the multi-orbital effects and the possible hybridizations between the d orbitals and s , p orbitals. Indeed important effects may be lost through such a simplification. For a material-oriented study, one often needs to generalize the model (2.1) so that the orbital degree of freedom can be taken into account, giving a multi-orbital Hubbard-like model,

$$H = \sum_{i,j,m,m',\sigma} t_{ij}^{mm'} d_{im\sigma}^\dagger d_{jm'\sigma} + \sum'_{i,m,m',\sigma,\sigma'} \frac{U_{mm'}^{\sigma\sigma'}}{2} n_{im\sigma} n_{im'\sigma'} - \sum'_{i,m,m',\sigma} \frac{J_{mm'}}{2} d_{im\sigma}^\dagger d_{im'\bar{\sigma}}^\dagger d_{im'\sigma} d_{im\bar{\sigma}}. \quad (2.5)$$

Here the hopping parameters $t_{ij}^{mm'}$ become a matrix between m orbital on site i and m' orbital on site j . $U_{mm'}^{\sigma\sigma'}$ gives the strength of direct Coulomb interaction between the spin-orbital channels $\{m, \sigma\}$ and $\{m', \sigma'\}$, and the prime on the summation excludes the self-interaction with $m = m'$ and $\sigma = \sigma'$. The $J_{mm'}$ term describes the ‘‘spin-flip’’ effect between two channels and the prime here means $m \neq m'$. In practice, the following relationships among the parameters $U_{mm'}^{\sigma\sigma'}$ and $J_{mm'}$ are assumed,

$$U_{mm'}^{\sigma\sigma'} = U - 2J(1 - \delta_{mm'}) - J\delta_{\sigma\sigma'} \quad \text{and} \quad J_{mm'} = J \quad (2.6)$$

which hold exactly for cubic systems. It should be noted that, in a rigorous derivation of (2.5), there should exist other terms reflecting the physical pre-

cesses like pair hopping and density-dependent hopping, which are nevertheless neglected here for simplicity. The above model (2.5) is frequently used in material investigations in conjunction with the LDA band-structure calculations which provide the model parameters. The one-band Hubbard model is already difficult enough to solve, the task of solving the multi-band model (2.5) is much more challenging. At present the most powerful tool for dealing with this model seems to be DMFT, which we will discuss in the next section.

2.2 Dynamical Mean-Field Theory

The essential idea of DMFT is to replace the fermionic lattice model by a quantum impurity model embedded in an effective medium which needs to be determined self-consistently. By doing so the local dynamics is contained in the impurity problem and the lattice effect is taken care of by the self-consistent condition, in a rather similar philosophy of the Weiss mean-field theory for the classical systems. The DMFT is a dynamical theory, however, in the sense that the local quantum fluctuation is fully accounted for by the impurity model and only the spatial correlations are treated in a mean-field way. Thus it is standing at a higher level than static mean-field theories such as the Hartree-Fock approximation in which both the spatial and local quantum fluctuations are frozen. Similar to the Weiss mean-field theory, DMFT becomes exact in the limit of infinite dimension (or the infinite coordination number). Before presenting the DMFT equations, it is appropriate to have a look at the $D = \infty$ limit for correlated lattice fermions.

2.2.1 The Infinite Dimension Limit

For a number of classical problems (e.g., the Ising model and the spin glasses), many insights into the system can be gained by taking the limit $D \rightarrow \infty$. For the classical spin models, the $D \rightarrow \infty$ leads to the Weiss molecular field theory. In order to keep the total energy finite, the spin coupling constant J (see the Heisenberg model (2.3) for example) has to be rescaled as $J = J^*/Z$ where J^* is a constant and is the coordination number (for a hypercubic lattice, $Z = 2D$). It is interesting to see that this limit is also useful for strongly correlated fermionic lattice model. In their original paper, Metzner and Vollhardt (1989b) pointed out, in the $D \rightarrow \infty$ limit, the diagrammatic treatment of the Hubbard model simplifies substantially while the many-body nature is still preserved. Again, to have a nontrivial model where both the kinetic and interaction energy are finite, the hopping amplitude t (see (2.1) and (2.2)) has to be rescaled, but in a different

way comparing with the spin models, namely,

$$t = \frac{t^*}{\sqrt{2D}}, \quad t^* = \text{const.} \quad (2.7)$$

The reason for such a choice of the scaling can be easily seen from the noninteracting density of states (DOS) of the Hubbard model (2.1) with nearest-neighbor hopping on a supercubic lattice (Metzner and Vollhardt, 1989b),

$$N_D(\varepsilon) = \frac{1}{2t\sqrt{\pi D}} \exp \left[- \left(\frac{\varepsilon}{2t\sqrt{D}} \right)^2 \right], \quad D \rightarrow \infty \quad (2.8)$$

Thus the scaling (2.7) immediately leads to the Gaussian behavior of the noninteracting DOS at infinite dimension,

$$N_\infty(\varepsilon) = \frac{1}{\sqrt{2\pi} t^*} \exp \left[- \frac{1}{2} \left(\frac{\varepsilon}{t^*} \right)^2 \right]. \quad (2.9)$$

Another important example is the Bethe lattice with nearest neighbor hopping. For this lattice the scaling of (2.7) leads to the the semicircular noninteracting DOS for $D = \infty$,

$$N_\infty(\varepsilon) = \frac{1}{2\pi t^{*2}} \sqrt{4t^{*2} - \varepsilon^2}, \quad |\varepsilon| < 2t^*. \quad (2.10)$$

Moreover, due to (2.7), it is easy to see the non-interacting single-particle propagator

$$G_{ij\sigma}^0 \sim \mathcal{O}(1/\sqrt{D}) \quad (2.11)$$

for neighboring i, j , and for general i, j sites one obtains (van Dongen *et al.*, 1989; Metzner, 1989),

$$G_{ij\sigma}^0 \sim \mathcal{O}(1/D^{||\mathbf{R}_i - \mathbf{R}_j||/2}) \quad (2.12)$$

where $||\mathbf{R}_i - \mathbf{R}_j||$ is the distance between i and j under the so-called ‘‘New York metric’’. As a consequence of the property (2.12), it was shown that the off-site contribution of the irreducible self-energy, i.e., Σ_{ij} with $i \neq j$, is infinitely smaller than its on-site counterpart Σ_{ii} for $D \rightarrow \infty$ (Metzner and Vollhardt, 1989b; Müller-Hartmann, 1989b), and thus the full self-energy becomes a purely local quantity,

$$\Sigma_{ij}(\omega) = \Sigma_{ii}(\omega)\delta_{ij}, \quad \text{for } D \rightarrow \infty. \quad (2.13)$$

It follows that its Fourier transformation $\Sigma(\mathbf{k}, \omega)$ becomes momentum-independent,

$$\Sigma(\mathbf{k}, \omega) = \Sigma(\omega). \quad (2.14)$$

Remarkable simplifications of the treatment of the Hubbard-like models arise from (2.14) and this immediately stimulated a number of subsequent works mainly focusing on the Gutzwiller variational wave function, and the weak-coupling expansion of the Hubbard model and related models (for a review, see Müller-Hartmann (1989a), Vollhardt (1991; 1993)).

2.2.2 DMFT Equations — Exact Solution of the $D = \infty$ Hubbard Model

As observed by Müller-Hartmann (1989b), the irreducible self-energy $\Sigma_{ii}(\omega)$, which is purely local, depends only on the site-diagonal full Green's function $G_{ii}(\omega)$ on the the same site. By using this fact, Brandt and Mielsch (1989; 1990; 1991) obtained the exact solution of the infinite dimensional Falikov-Kimball model, which can be thought of as a simplified version of the Hubbard model by permitting only one of the two spin species to hop. Brandt and Mielsch's work provided an illustrating guideline that the lattice problem can be understood by just looking at a single site. Unfortunately, the $D \rightarrow \infty$ Hubbard model does not allow for an analytically exact solution. However, Georges and Kotliar (1992) showed that its dynamics can be described by a single impurity with the effective single-site action (see also Jarrell (1992)),

$$S_{\text{eff}} = U \int_0^\beta d\tau n_\uparrow(\tau) n_\downarrow(\tau) - \int_0^\beta d\tau \int_0^\beta d\tau' \sum_\sigma d_\sigma^\dagger(\tau) \mathcal{G}_0^{-1}(\tau - \tau') d_\sigma(\tau'). \quad (2.15)$$

The $\mathcal{G}_0(\tau - \tau')$ here, serving as the “bare” Green's function for this local site, describes the influences of the environment on the present site. It essentially plays the same role as the Weiss field in the classic models, but now it is not just a constant number but rather (imaginary) time-dependent, so as to account for the quantum fluctuations on this local site. The reason that one is allowed to reduce the original lattice problem to a single-site problem (2.15) is due to the fact that the spatial fluctuations is completely suppressed at $D = \infty$.

The full Green's function and the self-energy (represented in the domain of Matsubara frequency) of the impurity problem can be calculated from (2.15),

$$G_{\text{imp}}(i\omega_n) = \langle d^\dagger(i\omega_n) d(i\omega_n) \rangle_{S_{\text{eff}}}, \quad \text{and} \quad \Sigma_{\text{imp}}(i\omega_n) = \mathcal{G}_0^{-1}(i\omega_n) - G_{\text{imp}}^{-1}(i\omega_n) \quad (2.16)$$

Of course the effective field $\mathcal{G}_0(\tau)$ is not known *a priori*, but it has to be such that the interacting Green's function of impurity problem and the site-diagonal Green's function of the original lattice problem are identical, and so are the self-energies, namely,

$$G_{\text{imp}}(i\omega_n) = G_{ii}(i\omega_n), \quad \Sigma_{\text{imp}}(i\omega_n) = \Sigma(i\omega_n). \quad (2.17)$$

On the other hand, the on-site lattice Green's function is

$$G_{ii}(i\omega_n) = \frac{1}{\mathcal{L}} \sum_{\mathbf{k}} \frac{1}{i\omega_n + \mu - \varepsilon_{\mathbf{k}} - \Sigma(i\omega_n)} = \int_{-\infty}^{\infty} \frac{N_\infty(\varepsilon)}{i\omega_n + \mu - \varepsilon - \Sigma(i\omega_n)} \quad (2.18)$$

where $\varepsilon(\mathbf{k}) = \frac{1}{\sqrt{\mathcal{L}}} \sum_j t_{ij} e^{i\mathbf{k} \cdot (\mathbf{R}_i - \mathbf{R}_j)}$ is the non-interacting single-particle energy. Eq. (2.18) is known as the \mathbf{k} -integrated Dyson equation, and here the lattice

property enters the equation only through the noninteracting density of states $N(\varepsilon)$ ¹. The close set of equations from (2.15) to (2.18) provide a self-consistent way to determine the local Green's function $G(i\omega_n) = G_{ii}(i\omega_n)$ as well as the self-energy $\Sigma(i\omega_n)$. These equations are known as DMFT equations and consist in a mean-field theory of the Hubbard that becomes exact for $D \rightarrow \infty$. The single-site representation of the lattice problem can be derived in a mathematically rigorous manner. The derivation can be carried out in several different ways, among which there are the ‘‘cavity’’ method, the expansion around the atomic limit, and effective medium interpretation (For a comprehensive review, see Georges *et al* (1996)).

Now we can focus on the single-impurity problem (2.15) which is of course still a highly nontrivial problem. Practically, one can consider the action (2.15) as arising from a single impurity coupled to a bath of ‘‘conduction electrons’’, described by the following Hamiltonian,

$$H_{\text{imp}} = \sum_{\mathbf{k},\sigma} \tilde{\varepsilon}_{\mathbf{k}} a_{\mathbf{k},\sigma}^\dagger a_{\mathbf{k},\sigma} + \varepsilon_d \sum_{\sigma} d_{\sigma}^\dagger d_{\sigma} + U n_{\uparrow}^d n_{\downarrow}^d + \sum_{\mathbf{k}} (V_{\mathbf{k}} a_{\mathbf{k},\sigma}^\dagger d_{\sigma} + h.c.) \quad (2.19)$$

where $n_{\sigma}^d = d_{\sigma}^\dagger d_{\sigma}$ and $\tilde{\varepsilon}_{\mathbf{k}}$ is the single-particle energy of the auxiliary bath electrons (represented by operators a^\dagger, a) and should not be confused with the noninteracting single-particle energy $\varepsilon(\mathbf{k})$ of the original lattice problem in (2.18). The Hamiltonian (2.19) is known as single impurity Anderson model (SIAM) (Anderson, 1961), on which substantial experience has been gained during thirty years of studies. After integrating out the degree of freedom of the bath electrons, one ends up with the action (2.15) for the impurity electron with the effective field,

$$\mathcal{G}^{-1}(i\omega_n) = i\omega_n - \varepsilon_d - \int_{-\infty}^{+\infty} d\varepsilon \frac{\Delta(\varepsilon)}{i\omega_n - \varepsilon}, \quad (2.20)$$

in which $\Delta(\varepsilon) = \sum_{\mathbf{k}} |V_{\mathbf{k}}|^2 \delta(\varepsilon - \tilde{\varepsilon}_{\mathbf{k}})$ is the so-called hybridization function and the representation(2.20) is general enough to produce any \mathcal{G}^{-1} . It is worthwhile to point out the interpretation of the single-site action (2.15) in terms of the SIAM is not the unique way, and alternative interpretation in terms of the Wolff model (Wolff, 1961) also exists (Georges *et al.*, 1992; Georges *et al.*, 1996).

Thus, as one can see, the problem of solving the $D = \infty$ Hubbard model is reduced to solving the SIAM iteratively. However, an exact solution of SIAM only exists for a constant hybridization function $\Delta(\varepsilon) = \Delta$ using the Bethe ansatz. Therefore, for a general $\Delta(\varepsilon)$ appearing in a self-consistent procedure, one has to invoke proper approximations or numerical techniques to get a solution of (2.19). The different approaches to treat the single impurity problem correspond to the different methods of solving the DMFT equations. Of these there are

¹ This is not true, however, for the nondegenerate multi-orbital cases, see Section (2.3).

numerical techniques such as QMC, ED, and Wilson numerical renormalization group (NRG), and analytical approaches such as iterative perturbation theory (IPT) and noncrossing approximation (NCA). QMC studies are based on the Hirsch-Fye algorithm (Hirsch and Fye, 1986) and were applied in the DMFT problems independently by Jarrell (1992), Rozenberg, Zhang, and Kotliar (1992) and Georges and Krauth (1992). A detailed discussion of QMC will be given in the next section. ED investigations were carried out by Caffarel and Krauth (1994) and Si *et al* (1994). The application of NRG in the present context were first performed by Sakai and Kuramoto (Sakai and Kuramoto, 1994), and later by Bulla, Hewson and Pruschke (1998) and Bulla (1999). The IPT scheme was first used in the original work of Georges and Kotliar (1992), and then generalized by Kajueter and Kotliar (1996). NCA was first employed by Jarrell and Pruschke (1993a; 1993b), and by Pruschke, Cox, and Jarrell (1993a; 1993b).

It should be pointed out that the above equations (2.15) to (2.18) are valid specially for paramagnetic phase of the Hubbard model. The scheme can be easily extended to phases with long-range magnetic orders and to other strongly correlated fermionic lattice models like the periodic Anderson model and the Kondo lattice model (Georges *et al.*, 1992).

In the next section, we will present the main formalism for the Hirsch-Fye QMC algorithm which is employed in this thesis for solving the impurity problem.

2.2.3 Quantum Monte-Carlo Method

As mentioned above, the Hirsch-Fye algorithm originally devised for the SIAM can be straightforwardly employed as the impurity solver for the DMFT problem. In one-band case this algorithm has empirically proven to be absent of the sign problem and not suffering the numerical instability at low temperatures. More importantly, for the studies of multi-band models and the material-specific calculations, the QMC is practically the only numerical tool so far to deal with the DMFT equations. Therefore QMC plays an indispensable role among the different impurity solvers. Within the QMC method, what one can obtain is the imaginary-time Green's function $G(\tau)$. To get any physically interested quantities, one has to first continue $G(\tau)$ to get the real-time Green's function, which is usually accomplished by the maximum entropy method (MEM) (Jarrell and Gubernatis, 1996).

In the following we will give a discussion of the Hirsch-Fye algorithm, following the review of Georges *et al* (1996). To begin with, we rewrite the SIAM (2.19)

as,

$$H_{\text{imp}} = H_0 + H_1, \quad (2.21a)$$

$$H_0 = \sum_{\mathbf{k}, \sigma} \tilde{\epsilon}_{\mathbf{k}} a_{\mathbf{k}\sigma}^\dagger a_{\mathbf{k}\sigma} + (\epsilon_d + \frac{U}{2}) \sum_{\sigma} d_{\sigma}^\dagger d_{\sigma} + \sum_{\mathbf{k}} (V_{\mathbf{k}} a_{\mathbf{k}\sigma}^\dagger d_{\sigma} + \text{h.c.}), \quad (2.21b)$$

$$H_1 = U n_{\uparrow}^d n_{\downarrow}^d - \frac{U}{2} (n_{\uparrow}^d + n_{\downarrow}^d). \quad (2.21c)$$

Now we consider the the partition function of the SIAM,

$$\mathcal{Z} = \text{Tr} e^{\beta H_{\text{imp}}} = \text{Tr} \prod_{i=1}^{\Lambda} e^{\Delta\tau (H_0 + H_1)} \approx \text{Tr} \prod_{i=1}^{\Lambda} e^{\Delta\tau H_0} e^{\Delta\tau H_1}. \quad (2.22)$$

Here the imaginary time interval $[0, \beta]$ has been equivalently discretized into Λ slices and $\Delta\tau = \beta/\Lambda$. The Trotter breakup is used for the last step and the error involved in this breakup is $\sim \mathcal{O}(\Delta\tau^2)$. The interaction part of the Hamiltonian can be decoupled via a Hubbard-Stratonovich transformation using the auxiliary Ising variables (Hirsch, 1983),

$$e^{\Delta\tau H_1} = \frac{1}{2} \sum_{s=\pm 1} e^{\lambda s (n_{\uparrow}^d - n_{\downarrow}^d)}, \quad (2.23)$$

where $\lambda = \cosh^{-1}(\exp(\Delta\tau U/2))$. From (2.22) and (2.23) we have

$$\mathcal{Z} \approx \frac{1}{2^{\Lambda}} \sum_{\{s\}=\pm 1} Z_{\{s\}}^{\Delta\tau}, \quad (2.24a)$$

$$Z_{\{s\}}^{\Delta\tau} = \prod_{\sigma=\pm 1} \text{Tr} e^{\Delta\tau K} e^{V^{\sigma}(s_1)} \times e^{\Delta\tau K} e^{V^{\sigma}(s_2)} \dots e^{\Delta\tau K} e^{V^{\sigma}(s_{\Lambda})}. \quad (2.24b)$$

Here, $\{s\}$ denotes the set of Ising variables $(s_1, s_2, \dots, s_{\Lambda})$, one variable corresponding to one time slice. In addition,

$$e^{\Delta\tau K} = \begin{pmatrix} \epsilon_d + U/2 & V_{\mathbf{k}_1}^* & V_{\mathbf{k}_2}^* & \dots \\ V_{\mathbf{k}_1} & \tilde{\epsilon}_{\mathbf{k}_1} & 0 & \dots \\ V_{\mathbf{k}_2} & 0 & \tilde{\epsilon}_{\mathbf{k}_2} & \dots \\ \dots & \dots & \dots & \dots \end{pmatrix} \quad (2.24c)$$

stems from the noninteracting part of the Hamiltonian H_0 in (2.21b), and

$$e^{V^{\sigma}(s_i)} = \begin{pmatrix} e^{\sigma s_i \lambda} & 0 & 0 & \dots \\ 0 & 1 & 0 & \dots \\ 0 & 0 & 1 & \dots \\ \dots & \dots & \dots & \dots \end{pmatrix} \quad (2.24d)$$

is associated with the decoupled on-site interaction (2.23). At this point one should distinguish between the physical spin σ and the auxiliary Ising spins which can be 1 or -1 at every time slice.

A crucial observation is that the Ising-spin dependent partition function $Z_{\{s\}}^{\Delta\tau}$ can be expressed as

$$Z_{\{s\}}^{\Delta\tau} = \det O_{\{s\}}^{\uparrow} \cdot \det O_{\{s\}}^{\downarrow}, \quad (2.25)$$

where

$$O_{\{s\}}^{\sigma} = \begin{pmatrix} 1 & 0 & \dots & 0 & e^{\Delta\tau K} e^{V^{\sigma}(s_{\Lambda})} \\ -e^{\Delta\tau K} e^{V^{\sigma}(s_1)} & 1 & \dots & \dots & 0 \\ 0 & -e^{\Delta\tau K} e^{V^{\sigma}(s_2)} & 1 & \dots & \dots \\ \dots & \dots & \dots & 1 & 0 \\ 0 & 0 & \dots & -e^{\Delta\tau K} e^{V^{\sigma}(s_{\Lambda-1})} & 1 \end{pmatrix}. \quad (2.26)$$

(For a proof, see Hirsch (1985) or Blankenbecler, Scalapino and Sugar (1981)). The element of the matrix $O_{\{s\}}^{\sigma}$ is labelled by the combined index $\{l, p\}$ in which l corresponds to the time slice and p to electron orbital respectively. The Ising-spin dependent Green's function $g_{\{s\}}^{\sigma}$, defined as

$$(g_{\{s\}}^{\sigma})_{lp;l'p'} = \frac{1}{\det O_{\{s\}}^{\sigma}} \text{Tr} e^{\Delta\tau K} e^{V^{\sigma}(s_1)} \dots e^{\Delta\tau K} e^{V^{\sigma}(s_{l-1})} a_{p\sigma}(\tau_l) \dots e^{\Delta\tau K} e^{V^{\sigma}(s_{l'-1})} a_{p'\sigma}^{\dagger}(\tau_{l'}) \dots e^{\Delta\tau K} e^{V^{\sigma}(s_{\Lambda})}, \quad (2.27)$$

is related to the matrix $O_{\{s\}}^{\sigma}$ by

$$g_{\{s\}}^{\sigma} = (O_{\{s\}}^{\sigma})^{-1}. \quad (2.28)$$

In (2.27) we have assumed the correspondence that that $a_{1\sigma} = d_{\sigma}$, $a_{2\sigma} = a_{\mathbf{k}_1\sigma}$, $a_{3\sigma} = a_{\mathbf{k}_2\sigma}$, \dots , and so on. The essential ingredient of the Hirsch-Fye algorithm is based on the fact, as first observed by Hirsch and Fye (1986), that Green's functions for two different Ising-spin configurations $\{s\}$ and $\{s'\}$ are connected by a Dyson equation

$$g' = g + (g - 1)(e^{V' - V} - 1)g'. \quad (2.29)$$

In (2.29) we have abbreviated $g \equiv g_{\{s\}}^{\sigma}$, $g' \equiv g_{\{s'\}}^{\sigma}$, and the e^V here should be understood as a diagonal matrix with $(e^V)_{ll'} = e^{V^{\sigma}(s_l)} \delta_{ll'}$ (the form of $e^{V^{\sigma}(s_l)}$ is given in (2.24d)). It is not difficult to see the matrix $(e^{V' - V} - 1)$ in (2.29) has the following behavior,

$$\left[e^{(V' - V)} - 1 \right]_{lp;l'p'} = e^{\lambda\sigma(s_l - s'_l)} \delta_{ll'} \delta_{p1} \delta_{p'1}, \quad (2.30)$$

i.e., it is nonzero only at the impurity site. Therefore, the Dyson equation (2.29) also holds for the Green's function of the impurity site $G_{\{s\}}^{\sigma} \equiv (g_{\{s\}}^{\sigma})_{11}$,

$$G' = G + (G - 1)(e^{V' - V} - 1)G', \quad (2.31)$$

but now $e^{V'-V} - 1$ should be understood as an $\Lambda \times \Lambda$ diagonal matrix with element $e^{\lambda\sigma(s_l - s'_l)} - 1$. Rearranging Eq. (2.31) one can get

$$G' = \left[1 + (1 - G)(e^{V'-V} - 1) \right]^{-1} G \quad (2.32)$$

Eq. (2.32) provides a way to generate the Green's function $G_{\{s'\}}$ for some Ising spin configuration $\{s'\} = (s'_1, s'_2, \dots, s'_\Lambda)$ from the known Green's function $G_{\{s\}}$ for another spin configuration $\{s\} = (s_1, s_2, \dots, s_\Lambda)$. For two general $\{s\}$ and $\{s'\}$, this involves an inversion of a $\Lambda \times \Lambda$ matrix. However, in the special case that only a single spin, say s_l , is flipped, one can verify that (2.32) is reduced to

$$G'_{l_1 l_2} = G_{l_1, l_2} + (G_{l_1, l} - \delta_{l_1 l}) \left(e^{\lambda\sigma(s'_l - s_l)} - 1 \right) \left(1 + (1 - G_{ll})(e^{\lambda\sigma(s'_l - s_l)} - 1) \right)^{-1} G_{ll_2}, \quad (2.33)$$

where l denotes some arbitrary but fixed time slice. Moreover, in this case, it can be shown that the following relation holds,

$$\frac{\det O_{\{s\}}^\sigma}{\det O_{\{s'\}}^\sigma} = \frac{\det g_{\{s'\}}^\sigma}{\det g_{\{s\}}^\sigma} = \frac{\det G_{\{s'\}}^\sigma}{\det G_{\{s\}}^\sigma} = 1 + (1 - [G_{\{s\}}^\sigma]_{ll})(e^{\lambda\sigma(s'_l - s_l)} - 1). \quad (2.34)$$

Now we can consider the physical Green's function for the d site which is given by

$$G_{l_1 l_2}^\sigma = \frac{\sum_{\{s\}} \det O_{\{s\}}^\uparrow \det O_{\{s\}}^\downarrow [G_{\{s\}}^\sigma]_{l_1 l_2}}{\sum_{\{s\}} \det O_{\{s\}}^\uparrow \det O_{\{s\}}^\downarrow}. \quad (2.35)$$

Here the exact calculation of the physical G^σ involves a summation over 2^Λ different spin configurations. This is computationally impossible for a large λ . The QMC method, however, provides an efficient way to evaluate (2.35) by importance sampling according to the probability distribution

$$P(\{s\}) = \frac{\det O_{\{s\}}^\uparrow \det O_{\{s\}}^\downarrow}{\sum_{\{s'\}} \det O_{\{s'\}}^\uparrow \det O_{\{s'\}}^\downarrow}. \quad (2.36)$$

The sampling over the configuration space can be performed according to different rules, and the Metropolis sampling is the most frequently used one. In which $P(\{s\} \rightarrow \{s'\})$, the probability of accepting the trial move for $\{s\}$ to $\{s'\}$, is given by

$$P(\{s\} \rightarrow \{s'\}) = \begin{cases} 1 & \text{if } P(\{s'\}) > P(\{s\}), \\ P(\{s'\})/P(\{s\}) & \text{otherwise.} \end{cases} \quad (2.37)$$

The Hirsch-Fye algorithm can be straightforwardly used to solve the effective impurity model appearing in the DMFT context. For the effective impurity

model, what is known is the Weiss field $\mathcal{G}^\sigma(\tau)$ which is determined in the previous iteration. $\mathcal{G}^\sigma(\tau)$, on the other hand, can be regarded as the spin-dependent Green's function $G_{\{s\}}^\sigma$ with $\{s\} = 0$. The initial Ising-spin dependent Green's function $G_{\{s\}}^\sigma$ for an arbitrary Ising-spin configuration ($s_1 = \pm 1, s_2 = \pm 1 \dots S_\Lambda = \pm 1$) can be obtained from $G_{\{s=0\}}^\sigma = \mathcal{G}^\sigma$ by explicitly using (2.32) (which is valid for arbitrary $\{s'\}$ and $\{s\}$). From then on, the Ising-spin configuration space is visited by once flipping only one spin, and whether the flip is accepted or not is determined by the Metropolis algorithm (2.37). Once the flip is accepted, the Green's function is updated through (2.33). The physical Green's function G^σ is calculated by averaging the Ising-spin dependent Green's functions $G_{\{s\}}^\sigma$. The process is continued until a desired accuracy is reached.

2.2.4 Case Studies with DMFT

To have an idea that what one can get within DMFT, we present two examples of the DMFT solutions of the Hubbard model.

(a) One-band Hubbard model away from half-filling

In the first example, we consider the single-band Hubbard model (2.1) defined on a Bethe lattice with infinite connectivity. For $U = 0$, the DOS has a semicircular behavior (2.10), and the integrated Dyson equation (2.18) reduces to

$$G(i\omega_n) = (\zeta - \text{sgn}[\text{Im}(\zeta)])\sqrt{\zeta^2 - 4t^{*2}}/2t^{*2}, \quad (2.38)$$

with $\zeta = i\omega_n + \mu - \Sigma(i\omega_n)$. In this calculation we fix $U = 10$, and $t^* = 0.5$ giving half-width of the semicircular DOS $W = 1$. The effective impurity problem is solved by the QMC method at a temperature $T = 1160K$ corresponding to $\beta = 10$. The QMC result is treated by MEM to get the spectral functions. In Fig. 2.1 the spectral functions as a function of the electron density are shown. At half-filling $n = 1$, it is quite clear that a Mott insulator is formed with the spectrum equally split into lower Hubbard band (LHB) and upper Hubbard band (UHB), and the Fermi energy is sitting in the middle of the gap. When the electron density is away from the half-filling, a quasiparticle resonance takes place at the Fermi level. There is still a Mott gap formed separating the LHB and UHB, but not at the Fermi level. The UHB is shifted to a higher energy and becoming more dispersive, and its spectrum weight is becoming smaller as n decrease. The studies of the one-band Hubbard model away from half-filling within DMFT were carried out by Pruschke, Cox, and Jarrell (1993b; 1993a) using the QMC method, and Kajueter and Kotliar (1996) using the ITP method respectively.

(b) Two-band Hubbard model with hybridization

In the second example we consider a two-band Hubbard model, with one interacting band and one noninteracting band, and the two bands hybridizing with

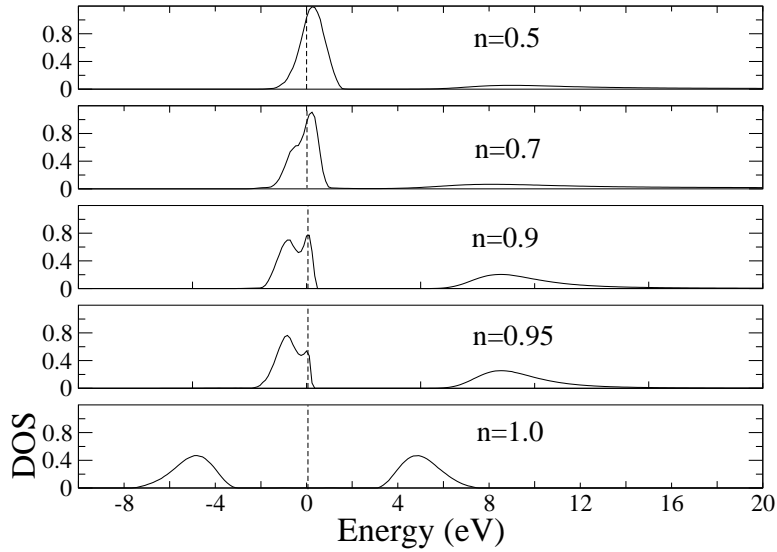


Figure 2.1: The result of the one-band Hubbard model solved by DMFT. The on-site Coulomb interaction $U = 10$ and half of the band width $W = 1$. Fermi energy is set to zero. From top to bottom, electron number per site are 0.5, 0.7, 0.9, 0.95, and 1.0 respectively. The spectrum weights of the UHB are approximately measured as 0.438, 0.658, 0.878, 0.943, and 1.0 respectively

each other. The Hamiltonian reads

$$\begin{aligned}
 H = & - t_p \sum_{\langle i,i'\rangle,\sigma} (p_{i\sigma}^\dagger p_{i'\sigma} + \text{h.c.}) + \epsilon_p \sum_{i,\sigma} n_{i\sigma}^p - t_d \sum_{\langle j,j'\rangle,\sigma} (d_{j\sigma}^\dagger d_{j'\sigma} + \text{h.c.}) + \epsilon_d \sum_{j,\sigma} n_{j\sigma}^d \\
 & + U \sum_i n_{j\uparrow} n_{j\downarrow} + V \sum_{\langle i,j\rangle,\sigma} (p_{i\sigma}^\dagger d_{j\sigma} + \text{h.c.}). \tag{2.39}
 \end{aligned}$$

in which the electrons are classified into a p -type which is free and a d -type which is subject to a on-site Coulomb interaction. These two types of electrons hybridize with each other with a strength V . The model (2.39) is sometimes also addressed as a generalized periodic Anderson model by allowing the originally localized electrons to hop. This model at half-filling case ($n = 2$) has been studied within DMFT by Shimizu, Sakai and Hewson (2000) using NRG method and recently by de' Medici *et al* (2005) using ED and Gutzwiller approximation. For the case of $n = 1$, Ōno, Bulla and Hewson (2001) has obtained a phase diagram within the approximation of linearized DMFT.

In this study we put the p - and d -orbitals on different sublattices of the bipartite Bethe lattice. When the connectivity of the Bethe lattice $q \rightarrow \infty$, the self-consistency equations for the model (2.39) are given by (see e.g., Georges, Kotliar,

and Krauth (1993), or Ōno, Bulla, Hewson (2001)),

$$G_p(i\omega_n)^{-1} = i\omega_n + \mu - \epsilon_p - t_p^2 G_p(i\omega_n) - V^2 G_d(i\omega_n), \quad (2.40a)$$

$$G_d(i\omega_n)^{-1} = i\omega_n + \mu - \epsilon_d - V^2 G_p(i\omega_n) - t_d^2 G_d(i\omega_n). \quad (2.40b)$$

Within DMFT, these equations should be solved together with the effective impurity problem for the d electrons. Again, the impurity problem is solved by the Hirsch-Fye QMC method at $\beta = 10$ and the obtained imaginary Green's function is treated by MEM to get the energy spectrum. At this point we want to point out the model under investigation and the arrangement of the p , d orbitals on the lattice is intended to mimic materials with strong correlations among the transition metal valence d electrons as well as strong hybridizations between the d electrons and the ligand p electrons. The obtained spectra for a fixed set of t_d , t_p , ϵ_d , and ϵ_p parameters and different U , V parameters are shown in Fig. 2.2.

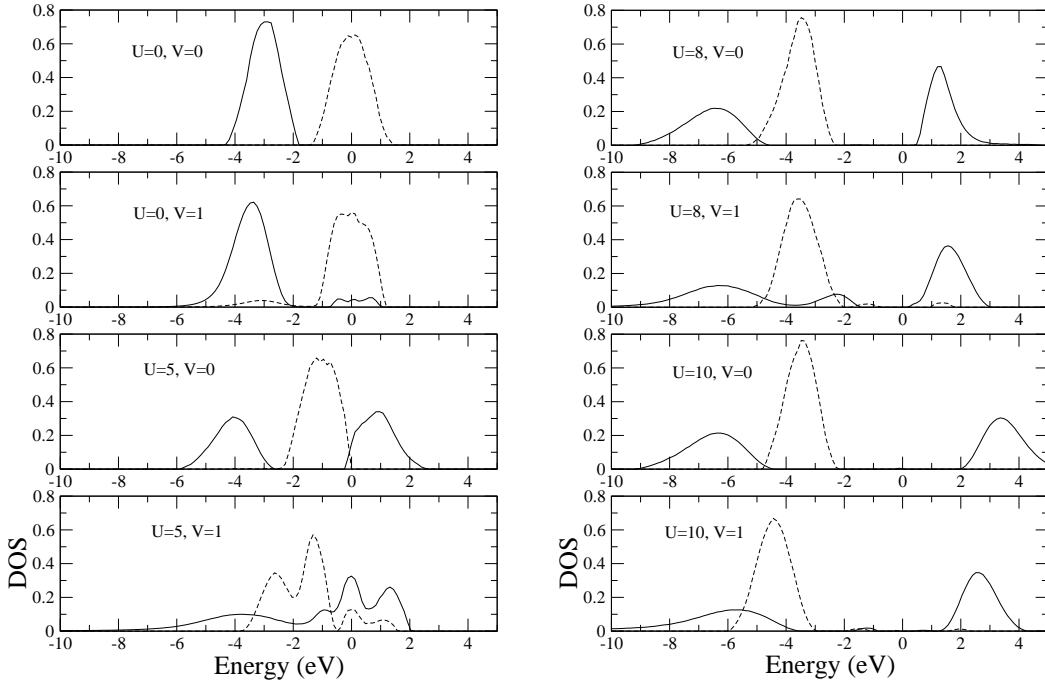


Figure 2.2: The energy spectra of d band (solid line) and p band (dashed line) obtained from the DMFT solution of the two-band Hubbard model. The electron occupation $n = 3$, $\epsilon_p - \epsilon_d = 3$, and the Fermi energy is fixed at 0. The hopping parameters are set as $t_p = t_d = 0.5$ so that the half-width of the noninteracting DOS of both bands is 1. The values of U and V are varied as indicated in the figure.

From Fig. 2.2, one can clearly see the effect of the on-site interaction U of the d electrons and the hybridization between d and p electrons on the electronic

properties of the system. For $V = 0$ and a large U , the d band is split into LHB and UHB by the on-site interaction U , with the fully occupied noninteracting p states sitting in between. This is actually the classic picture for the idea of “charge-transfer” insulator. When V becomes finite, a resonance which has a mixed character of d , p states is formed on the top of the valence bands. These results shed illustrating lights on the understanding of the Mott transition in the materials with strong p - d hybridization.

2.3 The LDA+DMFT Formulation

In the chapter 1 we discussed DFT and its LDA that provide a successful first-principles description of weakly correlated materials. However, usually the LDA fails to describe the strongly correlated materials which are characterized by open d or f shells. These systems exhibit essentially many-body features in their ground-state and excitation properties which can not be captured by the one-electron band theory. The many-body effects such as the Mott metal-insulator transition, Kondo effect and heavy fermion behavior, are usually understood in the framework of simplified model Hamiltonians, among which the Hubbard model and Anderson model are famous examples. DMFT, as a powerful approach to solved these strongly correlated lattice models, has been discussed in the previous section.

Is it possible to develop a first-principles theory for the strongly correlated materials as the DFT-LDA for the weakly correlated one? For this purpose one may first think of a many-body extension of the LDA by supplementing the one-electron LDA Hamiltonian by a Hubbard-like interaction term among the correlated orbitals (Anisimov *et al.*, 1997b; Held *et al.*, 2003). By doing so we are actually separating the electronic states into the weakly correlated ones for which the LDA has already given a sufficient description, and the strongly correlated ones which require a further treatment by solving a many-body problem. Based on these considerations the extended full Hamiltonian reads

$$H = H_{\text{LDA}} + H_{\text{int}} - H^{\text{dc}}, \quad (2.41a)$$

$$H_{\text{LDA}} = \sum_{i\text{r}lm, j\text{r}'l'm', \sigma} \delta_{i\text{r}lm, j\text{r}'l'm'} \varepsilon_{\text{r}lm} n_{i\text{r}lm}^{\sigma} + t_{i\text{r}lm, j\text{r}'l'm'} c_{i\text{r}lm}^{\sigma\dagger} c_{j\text{r}'l'm'}^{\sigma}, \quad (2.41b)$$

$$H_{\text{int}} = \sum_{i, r=r_d, l=l_d} \left[\sum'_{m, m', \sigma, \sigma'} \frac{U_{mm'}^{\sigma\sigma'}}{2} n_{i\text{r}lm}^{\sigma} n_{i\text{r}lm'}^{\sigma'} - \sum'_{m, m', \sigma} \frac{J_{mm'}}{2} c_{i\text{r}lm}^{\dagger\sigma} c_{i\text{r}lm'}^{\dagger\bar{\sigma}} c_{i\text{r}lm'}^{\sigma} c_{i\text{r}lm}^{\bar{\sigma}} \right]. \quad (2.41c)$$

The one-electron LDA Hamiltonian H_{LDA} can be cast into a tight-binding (TB) form as expressed in (2.41b), by choosing the TB-LMTOs (Andersen and Jepsen (1984),

Andersen, Pawłowska, and Jepsen (1986)) as the basis set. $c_{jr'l'm'}^\sigma$ denotes an annihilation operator for an electron in r -th atom of the j -th elementary unit cell with an angular momentum number l and magnetic quantum number m . On top of H_{LDA} , one adds explicitly a many-body interaction term H_{int} for the strongly correlated electrons, as expressed in (2.41c), in exact analogy to the multi-band Hubbard model (2.5) (here we used r_d and l_d to denote the atom and angular momentum channel that these electrons are associated with, usually they are the valence d states of the transition metals). However, the Coulomb interaction among these correlated electrons has been taken into account in an averaged way in the LDA through the one-electron effective potential. Therefore a term H^{dc} , is subtracted to avoid double-counting. Since there is no direct microscopic link between the Hubbard model and LDA, the exact form of H^{dc} in terms of U , J parameters is not known. However, a commonly employed approximation for H^{dc} assumes that the LDA energy E^{dc} for this term is given by (Anisimov *et al.*, 1997b; Held *et al.*, 2003)

$$E^{\text{dc}} = \frac{1}{2}\bar{U}n_d(n_d - 1) - \frac{1}{2}J \sum_{\sigma} n_{d\sigma}(n_{d\bar{\sigma}} - 1). \quad (2.42)$$

with

$$\bar{U} = \frac{U + (M - 1)(U - 2J) + (M - 1)(U - 3J)}{2M - 1}. \quad (2.43)$$

Here M is the number of correlated orbitals, and U , J parameters are related to $U_{mm'}^{\sigma\sigma'}$ and $J_{mm'}$ in (2.41c) through (2.6). Moreover $n_{d\sigma} = \sum_{m=1}^M \langle n_{ir_d l_d m \sigma} \rangle$ is the number of electrons occupying these correlated orbitals with spin σ , and $n_d = \sum_{\sigma} n_{d\sigma}$ the total number of electrons on these orbitals. The correction (2.42) for the LDA energy of the interacting orbitals leads to a correction of one-electron energy ε_{irlm} in (2.41b), namely,

$$\varepsilon_{rlm}^0 = \varepsilon_{rlm} - \frac{\partial E^{\text{dc}}}{\partial n_{rlm}} = \varepsilon_{rlm} - \delta_{rl,r_d l_d} [\bar{U}(n_d - 1/2) + J/2(n_d - 1)], \quad (2.44)$$

with $n_{rlm} = \sum_{\sigma} \langle n_{irlm}^{\sigma} \rangle$. Thus we can rewrite Eqs. (2.41a) and (2.41b) in the following way,

$$H = H_{\text{LDA}}^0 + H_{\text{int}}, \quad (2.45a)$$

$$H_{\text{LDA}}^0 = \sum_{irlm,jr'l'm',\sigma} \delta_{rlm,r'l'm'} \varepsilon_{rlm}^0 n_{irlm}^{\sigma} + t_{irlm,jr'l'm'} c_{irlm}^{\sigma\dagger} c_{jr'l'm'}^{\sigma}. \quad (2.45b)$$

To have a concrete Hamiltonian, the U , J parameters in the interaction term (2.41c) have to be specified. This can be accomplished by a procedure known as “constrained LDA” (Gunnarsson *et al.*, 1989). Eqs. (2.45a), (2.45b) together with (2.41c) represent the *ab-initio* Hamiltonian for a particular material under investigation. For later use, it is more convenient to transform the TB Hamiltonian

(2.45b) to the reciprocal space,

$$(H_{\text{LDA}}^0(\mathbf{k}))_{rlm,r'l'm'} = \frac{1}{\mathcal{L}} \sum_j e^{i\mathbf{k}\cdot(\mathbf{R}_i-\mathbf{R}_j)} (H_{\text{LDA}}^0)_{irlm,jr'l'm'}. \quad (2.46)$$

in which \mathcal{L} is the number of the elementary unit cell in the periodic system (or equivalently, the number of \mathbf{k} points in the first Brillouin zone).

Such a many-body extension of LDA first appeared in the LDA+U approach proposed by Anisimov *et al* (1991) where the interaction term (2.41c) is treated within the Hartree-Fock approximation. Many interesting phenomena, such as orbital and charge ordering in transition metal compounds, can be reproduced by LDA+U. However, for the strongly correlated paramagnetic states, the understanding of which relying on the energy-dependence of the self-energy, LDA+U is too simple to give an adequate description, and more sophisticated methods are needed. The LDA+DMFT approach, first implemented by Anisimov *et al* (1997b) [see also Lichtenstein and Katsnelson (1998)], is such a successful method in which the Hubbard interaction term is treated by DMFT to preserve the many-body nature of the system. The essential ingredient of the LDA+DMFT approach lies in a generalization of the \mathbf{k} -integrated Dyson equation (2.18) to incorporate the material-specific information,

$$G(i\omega_n)_{rlm,r'l'm'} = \frac{1}{\mathcal{L}} \sum_{\mathbf{k}} \left[\frac{1}{i\omega_n + \mu - H_{\text{LDA}}^0(\mathbf{k}) - \Sigma(i\omega_n)} \right]_{rlm,r'l'm'}. \quad (2.47)$$

Here in general an inversion of a matrix with a dimension as large as that of the LDA Hamiltonian matrix is required at each \mathbf{k} point. The self-energy matrix $\Sigma(i\omega_n)$ has non-zero elements only among the interacting orbitals, namely, $\Sigma(i\omega_n)_{rlm,r'l'm'} = \delta_{rl,r_d l_d} \delta_{r'l',r_d l_d} \Sigma_{mm'}(i\omega_n)$. The Weiss Green's function for the interacting orbitals is given by

$$\mathcal{G}_{mm'}^{-1}(i\omega_n) = G(i\omega_n)_{r_d l_d m, r_d l_d m'}^{-1} + \Sigma_{mm'}(i\omega_n). \quad (2.48)$$

Simplification is possible when the energy bands of the interacting orbitals are well separated from other bands, or in another word, the elements in the hybridization block between the interacting orbitals and other ones in the Hamiltonian matrix $H_{\text{LDA}}^0(\mathbf{k})$ are negligibly small. In this case Eq. (2.47) can be reduced to an equation for $M \times M$ matrices,

$$G(i\omega_n)_{mm'} = \frac{1}{\mathcal{L}} \sum_{\mathbf{k}} \left[\frac{1}{i\omega_n + \mu - H_{dd}^0(\mathbf{k}) - \Sigma(i\omega_n)} \right]_{mm'}, \quad (2.49)$$

in which $H_{dd}^0(\mathbf{k})$ denotes the interacting-orbital subblock of the full LDA Hamiltonian $H_{\text{LDA}}^0(\mathbf{k})$. Further simplification occurs in the case that these interacting or-

bitals under consideration are degenerate². In this case $G(i\omega_n)_{mm'} = G(i\omega_n)\delta_{mm'}$, $\Sigma(i\omega_n)_{mm'} = \Sigma(i\omega_n)\delta_{mm'}$, and (2.49) further reduces to a Hilbert transformation of the noninteracting LDA DOS $N^0(\varepsilon)$ of the orbitals under investigation,

$$G(i\omega_n) = \int d\varepsilon \frac{N^0(\varepsilon)}{i\omega_n - \Sigma(i\omega_n) - \varepsilon}. \quad (2.50)$$

In the context of LDA+DMFT, we need to consider a multi-orbital effective impurity problem. The effective action for this problem is given by

$$\begin{aligned} S_{eff} = & - \int_0^\beta d\tau \int_0^\beta d\tau' \sum_{mm'\sigma} d_{m\sigma}^\dagger(\tau) \mathcal{G}_{mm'}^{-1}(\tau - \tau') d_{m'\sigma}(\tau') \\ & + \int_0^\beta d\tau \sum'_{mm'\sigma\sigma'} \frac{U_{mm'}}{2} n_{m\sigma}(\tau) n_{m'\sigma'}(\tau) \\ & - \int_0^\beta d\tau \sum'_{m,m',\sigma} \frac{J_{mm'}}{2} d_{m\sigma}^\dagger(\tau) d_{m'\bar{\sigma}}^\dagger(\tau) d_{m'\sigma}(\tau) d_{m\bar{\sigma}}(\tau). \end{aligned} \quad (2.51)$$

as the multi-orbital generalization of (2.15). Here $d_{m\sigma} = c_{o\ r_{al}d_m}^\sigma$ and $n_{m\sigma} = n_{o\ r_{al}d_m}^\sigma$ with o representing the impurity site, and $\mathcal{G}_{mm'}^{-1}(\tau - \tau')$ is given through the Fourier transform of (2.48). A QMC solution of the impurity problem (2.51) can be obtained by straightforwardly generalizing the Hirsch-Fye algorithm to the multi-orbital case (for details, see, e.g., (Held *et al.*, 2003)). However, in this case it turned out the spin-flip term in (2.51) is very difficult to deal with due to the sign problem arising from the discrete Hubbard-Stratonovich decoupling (2.23). Therefore for simplicity this term is usually ignored in practical LDA+DMFT calculations. Recently it was reported the sign problem associated with the spin-flip term can be cured to some extent by introducing a different decoupling scheme for this term (Sakai *et al.*, 2004). Unfortunately, this improvement has only been implemented for the model studies (Arita and Held, 2005), but not yet for realistic LDA+DMFT calculations.

The LDA+DMFT scheme presented above has been successfully applied to many materials with strongly correlated electrons, e.g., $\text{La}_{1-x}\text{Sr}_x\text{O}_3$ (Anisimov *et al.*, 1997a; Nekrasov *et al.*, 2000), V_2O_3 (Held *et al.*, 2001a; Keller *et al.*, 2004; Keller, 2005), Ce (Held *et al.*, 2001b; McMahan *et al.*, 2003), and $\text{Ca}(\text{Sr})\text{VO}_3$ (Sekiyama *et al.*, 2004). A comprehensive review of the LDA+DMFT approach and its application to various materials is given by Held *et al.* (2003). However, for the case that the hybridization between the interacting orbitals and other ones is

² For materials with cubic symmetry, the crystal-field of the ligand atoms causes the transition metal d orbitals to split into 3-fold degenerate t_{2g} orbitals and 2-fold degenerate e_g orbitals. In cubic perovskites, it is often a good approximation to take only the three t_{2g} orbitals around the Fermi level into account.

strong, the separation of the interacting-orbital subblock $H_{dd}^0(\mathbf{k})$ from the rest part of $H_{LDA}^0(\mathbf{k})$ is not a proper treatment, and thus Eq. (2.49) does not hold to a good approximation. This difficulty arises from the fact that we are actually using LMTOs as the basis for the DMFT calculation, and can be avoided by choosing the Wannier functions instead of the LMTOs as the basis. We will discuss this point in detail when we deal with NiO in the next chapter.

3. LDA+DMFT INVESTIGATION OF NiO

3.1 Introduction

NiO is a prototype Mott insulator (Mott, 1949; Brandow, 1977) which has been under intensive experimental and theoretical investigation for several decades. Historically the theoretical studies of NiO roughly fall into two categories: those performed using first-principles approaches such as the DFT and its various improvements, and those using the localized approach such as the ligand field theory and the configuration-interaction treatment of a cluster model. These studies have led to a good understanding of the underlying physical ingredients in NiO, but a clear, complete picture of NiO is not yet available. This is perhaps due to the fact that both of the abovementioned approaches have some drawbacks and hence can not provide a complete treatment of NiO. While the first-principles studies incorporate the material-specific information without adjustable parameters, they are not able to describe the many-particle features of NiO adequately. On the other hand, the studies within the localized approaches correctly capture the atomic nature of the $3d$ electrons of Ni, but adjustable parameters are involved in these studies to fit the experiment, and more seriously, the band effects are neglected completely which is known to play an important role in NiO. The LDA+DMFT approach, cures the drawbacks of the above methods to some extent, and has proved to be a powerful method for treating strongly correlated materials. In this chapter we will apply this approach to NiO, and before presenting the computation details and results, we first give a short introduction of the physical properties of NiO and a brief review of previous studies.

3.1.1 Crystal Structure

NiO has a rocksalt crystal structure (space group $Fm\bar{3}m$) in its paramagnetic phase (Roth, 1958a; Roth, 1958b). Below its Néel temperature $T_N = 523K$ (Föex, 1948; Tomlinson *et al.*, 1955), NiO is a type-II fcc antiferromagnetic compound (Skull *et al.*, 1951; Roth, 1958a; Roth, 1958b). For this type of ordering, the magnetic moments of Ni ion align ferromagnetically on every (111) plane,

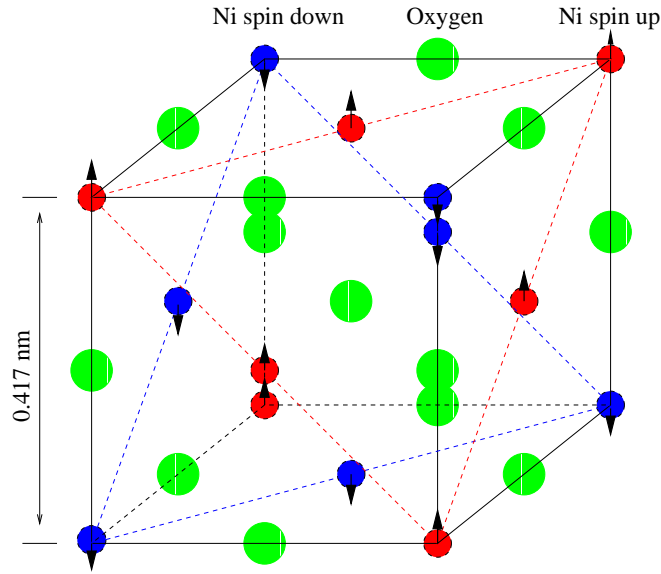


Figure 3.1: Crystal and magnetic structure of NiO in its antiferromagnetic phase; red circle-Ni ion with up spin, blue circle-Ni ion with down spin, blue circle-Oxygen ion. The small rhombohedral distortion is ignored here.

and antiferromagnetically for adjacent planes, as schematically shown in Fig. 3.1. Moreover, the transition from the paramagnetic state to the antiferromagnetic state is accompanied by a tiny rhombohedral distortion (space group $R\bar{3}m$) due to the exchange-striction effect (Bartel and Morosin, 1971). The lattice constant has a small increase from about 4.17 Å to 4.20 Å as the temperature increases from 7 K to 700 K (Bartel and Morosin, 1971). The NaCl crystal structure of NiO in its paramagnetic phase is the simplest possible structure one can expect in transition metal compounds¹, and this simplifies the analysis of its band structure, as can be seen later.

3.1.2 Electronic and Magnetic Properties

The basic experimental facts concerning the electronic and magnetic properties of NiO are as follows: (a) it is a good insulator with an energy gap about 4.0 eV, and this gap remains essentially unchanged above the Néel temperature up to over 1000 K.² (b) The local magnetic moment of Ni ion is about $1.7 - 1.9\mu_B$, and this

¹ On the other hand, this structure is typical for the 3d transition metal monoxides. These compounds, including TiO, VO, MnO, FeO, CoO and NiO, all crystallize in NaCl structure. CuO is the only exception which has a monoclinic structure (Dominguez Rodriguez *et al.*, 1984).

² The melting temperature of NiO is about 2260 K, but the experiment on pure NiO is limited to 1000 K due to the severe stoichiometry problem.

value also persists unchanged above T_N . The magnetic behavior of NiO, e.g., the spin-wave spectrum and the value of the Néel temperature can be well accounted for by a Heisenberg spin Hamiltonian. The susceptibility of the paramagnetic phase roughly follows the Curie-Weiss law with the Weiss constant $\theta \approx -2000$ K. (c) Inside the gap of the optical absorption spectrum, there are structures of Frenkel excitons showing up,³ which can be explained with the ligand field theory (Sugano *et al.*, 1970; Griffith, 1961). These properties reveal the localized nature of the Ni $3d$ electrons, and this further implies the Coulomb repulsion parameter U is quite large.

An efficient technique for investigating the electronic structure is the photoemission spectroscopy (PES), which provide a direct measurement of the electronic energy spectrum of the system if the “matrix element effect” can be neglected for the energy range concerned. Fig. 3.2 shows the X-ray PES (XPS) spectrum of NiO from unpublished data of Kowalczyk *et al.*, first appearing in the review paper of Brandow (1977). Three peaks can be clearly distinguished in this spectrum: a very pronounced main peak on the top of the valence bands, a shoulder near it about 1.6 eV below, and a broad satellite at 7.0 eV below. One issue at the heart of the electronic structure of NiO is how to assign these peaks to the proper final state after the emission of $3d$ electron from the ground state, and this problem is directly related to the nature of the 4 eV insulating gap. In a localized picture, the electronic states are labelled by the shell configuration of the valence electrons, e.g., the ground state of NiO is $3d^8$. Conventionally, the main peak in Fig. 3.2 was ascribed to the d^7 final state, and the satellite is considered to be a $d^8\bar{L}$ state, where \bar{L} denotes a ligand hole, resulting from a charge-transfer from the Oxygen $2p$ state to the Ni $3d$ state accompanying the $3d$ emission. Thus the insulating gap was assumed to be formed due to the excitation process $d^8 + d^8 \rightarrow d^7 + d^9$. However, this picture was revised by Fujimori and Minami (1984) based on a calculation within the configuration-interaction cluster approach. These authors concluded that the main peak is primarily due to $d^8\bar{L}$ final state and the satellite due to d^7 final state. This gives rise to the picture that the gap arises from the process $d^8 + d^8 \rightarrow d^8\bar{L} + d^9$. The latter picture is supported by the subsequent experiments (Sawatzky and Allen, 1984; Hüfner *et al.*, 1984) and has been widely accepted since then. According to a classification scheme by Zaanen, Sawatzky and Allen (1985), an insulating material is called Mott-Hubbard insulator in the former case, and charge transfer insulator in the latter case. In a simple picture of charge transfer insulator, the Oxygen $2p$ bands are located in between the lower and upper Hubbard bands arising from the Ni $3d$ states, and the chemical potential is sitting inside the gap formed between the Oxygen bands and upper Hubbard bands. The hybridization effect will blur this picture to some extent and lead to a resonant state on the top of the valence bands with predominantly

³ Such structures are not observed in the photoemission experiment, however (Sawatzky and Allen, 1984).

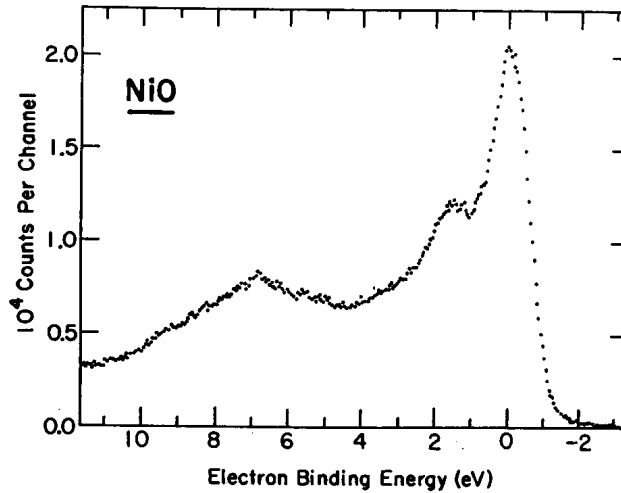


Figure 3.2: X-ray PES data for NiO by S. Kowalczyk, L. Ley, R. Pollack, and Shirley, obtained from a single crystal cleaved in dry nitrogen. The zero energy point is arbitrarily set at the highest point of the main peak. After Brandow (1977).

Oxygen character.

3.1.3 Previous Studies

As the classic example of Mott insulator, NiO is perhaps the best known and thoroughly studied material on which various theoretical approaches have been tried. The paramagnetic band calculations predict NiO to be a metal (Mattheiss, 1972; Shen *et al.*, 1991)⁴, in contrast with the experimental fact. The spin-polarized band calculation based on the local spin density approximation (LSDA) correctly gives an antiferromagnetic ground state (Terakura *et al.*, 1984a; Terakura *et al.*, 1984b), but the obtained insulating gap and the local magnetic moment are considerably smaller than the experimental values. These facts are often taken as the evidence that the LDA (LSDA) are not able to describe the strongly correlated materials. By contrast, the cluster model treated by configuration-interaction method (Fujimori *et al.*, 1984; Fujimori and Minami, 1984) was quite successful in explaining most of the known experimental facts. The success of the cluster model was soon reinforced by the combined x-ray-

⁴ Mattheiss's band calculation is conventional one based on the APW method in combination with the LCAO method, i.e., it is not DFT-based and without selfconsistency. A first DFT-based nonmagnetic band calculation seems to appear in the paper of Shen *et al.* (1991) in the context of comparison between LDA calculations and their experimental results. The two results differ mainly in the distance between the Ni 3*d* bands and O 2*p* bands, with the former being much larger than the latter. But both give a metallic solution.

photoemission (XPS) and bremsstrahlung-isochromat-spectroscopy (BIS) measurements (Sawatzky and Allen, 1984), and finally led to the recognition that NiO is not a Mott insulator in the normal sense, but rather a kind of charge transfer insulator (Zaanen *et al.*, 1985).

For some time it was thought that the purely localized cluster approach is adequate in describing the electronic properties of NiO, but then the angle-resolved photoemission (ARPES) experiments (Shen *et al.*, 1991; Kuhlbeck *et al.*, 1991) revealed that both the localized and band effects play important roles in this system. Especially the dispersion of O $2p$ states can be well accounted for by the LDA band structure. In the meantime, various attempts to calculate the electronic structure of NiO from first-principles beyond L(S)DA persisted, among which the most prominent were the self-interaction-corrected density functional theory (SIC-DFT) (Svane and Gunnarsson, 1991), the LDA+U method (Anisimov *et al.*, 1991), and the GW approximation (Aryasetiawan and Gunnarsson, 1995; Massidda *et al.*, 1997). These methods represent corrections of the single-particle potential or the self-energy in one way or another, and lead to substantial improvements over the L(S)DA results concerning the values of the energy gap and local moment. Since then, many new works have been performed along these lines (Anisimov *et al.*, 1993; Anisimov *et al.*, 1994; Hugel and Kamal, 1997; Shick *et al.*, 1999; Bengone *et al.*, 2000; Faleev *et al.*, 2004; Li *et al.*, 2005), differing in the basis used and/or the detailed ways of doing approximations. Within SIC-DFT and LDA+U method, the occupied and unoccupied states are splitted by the Coulomb interaction U , whereas within LSDA, this splitting is caused by the Stoner parameter I , which is typically one order of magnitude smaller than U . Compared with LSDA, SIC-DFT and LDA+U capture the correct physics for TM oxides, and improve the energy gap and local moment significantly. However, both of SIC-DFT and LDA+U, in which the self-energy is energy-independent, fail to take into account the correlation effects properly and thus can't give a sensible description of the electronic energy spectrum. The GW method goes one step further by calculating the self-energy to the lowest order of the screened interaction W . But its applications to NiO show that the GW approximation is usually not adequate to describe the strongly correlated systems, and different implements can give rise to quite different results (Aryasetiawan and Gunnarsson, 1995; Massidda *et al.*, 1997; Li *et al.*, 2005) concerning the relative positions of the bands and the magnitude of the energy gap. Most recently, an investigation based on the cluster perturbation theory (Eder *et al.*, 2005) which can be viewed as an extension of the local cluster approach was reported.

Although lots of progress has been made in the understandings of NiO, there are still open questions. First of all, although good accordance with experiment has so far been achieved concerning the values of the energy gap and the local moment, the agreement is far from satisfactory with respect to quasiparticle energy spectra. This is not surprising, because the self-energies employed

in previous approaches are either energy-independent, or suffering from uncontrolled approximations. Secondly, almost all the first-principles calculations so far were focused on the antiferromagnetic ground state with only few exceptions (Manghi *et al.*, 1994). However, as is well known, both the band gap and the local magnetic moment persist essentially unchanged above its Néel temperature $T_N \sim 523$ K, and recent experiments showed that the long-range magnetic order has no significant influences on the valence band photoemission spectra (Tjernberg *et al.*, 1996) as well as the electron density distribution (Jauch and Reehuis, 2004). These facts reflect the strongly localized nature of the electronic states in NiO, and can't be understood through Slater's antiferromagnetism approach (Slater, 1951). Therefore, how to produce the paramagnetic insulating state of NiO at high temperatures, without embarking on the long-range magnetic order, is still a very important problem to deal with from the physical point of view. Finally, although the charge transfer nature of the insulating gap of NiO is widely accepted, different voices do persist from both the theoretical side (Hugel and Kamal, 1997; Bengone *et al.*, 2000) and experimental side (Hüfner *et al.*, 1992; Schuler *et al.*, 2005). These authors suggested that NiO be either a Mott-Hubbard insulator, or a mixture of charge-transfer and Mott-Hubbard characters. Indeed, the conclusions concerning the nature of NiO drawn by experimentalists also largely depend on the analysis based on some particular theoretical models. Therefore, it is still highly desirable to have more first-principles investigations of the electronic structure of NiO within different approaches to make the situation more clear.

In this work, we perform a LDA+DMFT calculation of NiO for the paramagnetic insulating phase, based on the procedure proposed by Anisimov *et al* (2005), where the basis of WFs are used in the DMFT calculation. The energy gap, local magnetic moment, and the electronic spectrum are obtained. Since these quantities have no significant dependence on the temperature, we are allowed to compare our results with experimental data at low temperatures and other theoretical results for the ground state. The comparison shows that not only the energy gap and the local moment, but also the electronic spectrum are in good agreement with experiment.

3.2 Method and Results

The LDA+DMFT scheme, in most of its applications so far, is close in spirit to the model approach, namely, the LDA calculation serves to provide the necessary parameters of a many-body model Hamiltonian, and this Hamiltonian is in turn solved by means of DMFT. Since the LDA calculation usually involves a large number of valence s , p , d orbitals originating from all the atoms in the unit cell, it is mandatory to project all the orbitals except for a few relevant ones to be

included in the model Hamiltonian so that DMFT can handle. For transition-metal (TM) compounds, the most relevant orbitals responsible for the physical properties are the TM valence d orbitals. As a matter of fact, in most of the previous studies one just takes the LDA density of states (DOS) of the TM d orbitals as the input for the DMFT calculation, as indicated by the equation (2.50) and this means that one is using the atomic-like LMTO basis for constructing the many-body Hamiltonian (suppose the LDA problem is solved by the LMTO method). However, as already mentioned in the previous chapter, for some materials, e.g., the late TM oxides where there is a strong covalency effect between the TM d orbitals and Oxygen $2p$ orbitals, the atomic-like d orbitals are not the proper basis for the Hubbard-like many-body Hamiltonian. Actually in this case the proper choice of the basis is the d -like Wannier functions (WFs) (Wannier, 1937) which on the one hand have the same symmetry as the atomic-like d orbitals, and on the other hand implicitly take into account of the admixture of Oxygen $2p$ orbitals resulting from the hybridization effect. This is the strategy adopted in a recent work of Anisimov *et al* (2005), where WFs of the d -like bands were constructed from the solution of the LDA band structure, and used as the basis for the DMFT calculation. In the abovementioned work, calculations were carried out for SrVO₃ and V₂O₃ as examples, and in the present work we apply the same procedure to NiO.

To begin with, we perform a standard LDA band calculation for the paramagnetic phase of NiO using the LMTO-ASA (Andersen, 1975) method with the combined correction term included⁵. As has been discussed above, the lattice constant increases from about 4.17 Å to within a temperature range from 7 K to 700 K (Bartel and Morosin, 1971). Such an increase only causes a small deviation of the bands far away from the Fermi energy, but no noticeable change of the Ni $3d$ -derived bands on which we are focusing. In addition, since in future we will compare our result with the low-temperature experimental data anyway, we choose the lattice constant $a = 4.17$ Å throughout this work. The calculated nonmagnetic band structure of NiO along the selected high symmetry lines is shown in Fig. 3.3 (the first Brillouin zone and the denotation of its high symmetry point is shown in Fig. 3.4 for illustrating purpose.) and it is in agreement with those published in literatures (Shen *et al.*, 1991; Eder *et al.*, 2005). Based on the LDA band structure, we can start to construct a set of WFs, which will be used as the basis for the DMFT calculation, following the procedure proposed by Anisimov *et al* (2005). Let's discuss this procedure in some detail below.

⁵ Here we use the Stuttgart TB-LMTO code (Vers. 4.7) for the LDA band calculation. Thanks to Dr. Igor Nekrasov for making the code available.

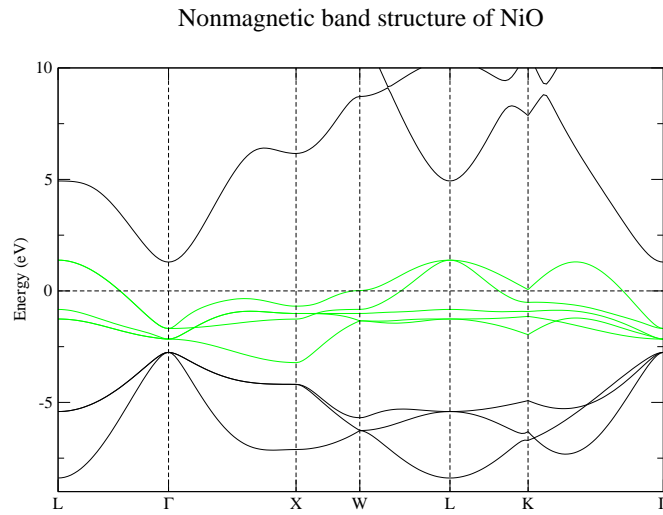


Figure 3.3: Nonmagnetic band structure of NiO obtained by the LMTO method; the Fermi energy is set to zero. The five d -like Bloch bands used for constructing Wannier functions are highlighted by green color

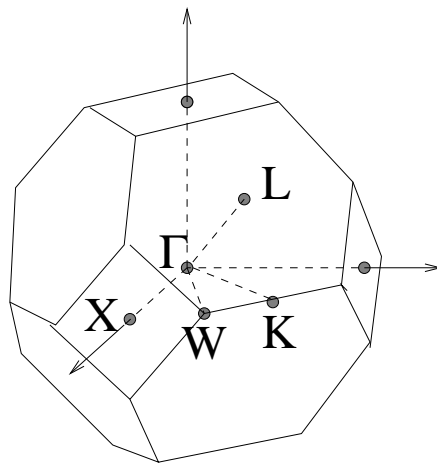


Figure 3.4: The first Brillouin zone of the fcc lattice

3.2.1 Wannier Function Construction

The solution of the LDA band problem is a set of Bloch states $|\psi_i^{\mathbf{k}}\rangle$, given by one-electron Schrödinger equation,

$$\hat{H}_{\text{LDA}}|\psi_i^{\mathbf{k}}\rangle = \varepsilon_i(\mathbf{k})|\psi_i^{\mathbf{k}}\rangle. \quad (3.1)$$

For a given set of Bloch functions, a set of Wannier functions (WFs) can be defined as a Fourier transformation of these Bloch functions. However, as has been discussed in Section 1.4, in this way the WF's can not be uniquely defined. This is because the Bloch functions themselves are determined only up to an arbitrary phase factor, and for the multi-band case, an additional unitary transformation connecting the different Bloch functions at each \mathbf{k} point is involved, as indicated in Eq. (1.49). In another word, it means there exist some degrees of freedom of constructing WF's corresponding to freedom of choice of a unitary transformation matrix $U_{ji}^{(\mathbf{k})}$ for the Bloch functions, namely

$$|W_i^{\mathbf{R}}\rangle = \frac{1}{\sqrt{\mathcal{L}}} \sum_{\mathbf{k}} e^{i\mathbf{k}\cdot\mathbf{R}} |\tilde{\psi}_i^{\mathbf{k}}\rangle. \quad (3.2)$$

with

$$|\tilde{\psi}_i^{\mathbf{k}}\rangle = \sum_j U_{ji}^{(\mathbf{k})} |\psi_j^{\mathbf{k}}\rangle. \quad (3.3)$$

(resulting Bloch function $|\tilde{\psi}_i^{\mathbf{k}}\rangle$ will not be in general case an eigenfunction of the Hamiltonian but has a meaning of Bloch sum of WF's (see below $|\widetilde{W}_n^{\mathbf{k}}\rangle$ in Eq. (3.4))). There is no rigorous way to determine $U_{ji}^{(\mathbf{k})}$, and on the other hand the freedom of choosing $U_{ji}^{(\mathbf{k})}$ can be utilized to obtain WF's with desired properties by exerting additional restrictions. Among others Marzari and Vanderbilt (1997) proposed the condition of maximum localization for WF's, resulting in a variational procedure to calculate $U_{ji}^{(\mathbf{k})}$. To get a good initial guess Marzari and Vanderbilt (1997) proposed choosing a set of localized trial orbitals $|\phi_n\rangle$ and projecting them onto the Bloch functions $|\psi_{i\mathbf{k}}\rangle$. It was found that this starting guess is usually quite good. This fact later led to the simplified calculating scheme proposed by Ku *et al* (2002) where the variational procedure was abandoned and the result of the projection was considered as the final step.

For constructing a set of WF's with some particular symmetry, one can select either a set of Bloch bands (N_1, \dots, N_2), or choose the energy interval (E_1, E_2) in which the bands are located. We first define the nonorthogonalized WF's in reciprocal space $|\widetilde{W}_n^{\mathbf{k}}\rangle$ as the projection of the set of site-centered atomic-like trial orbitals $|\phi_n\rangle$ onto the Bloch functions $|\psi_i^{\mathbf{k}}\rangle$ of the chosen bands,

$$|\widetilde{W}_n^{\mathbf{k}}\rangle \equiv \sum_{i=N_1}^{N_2} |\psi_i^{\mathbf{k}}\rangle \langle \psi_i^{\mathbf{k}} | \phi_n \rangle = \sum_{i(E_1 \leq \varepsilon_i(\mathbf{k}) \leq E_2)} |\psi_i^{\mathbf{k}}\rangle \langle \psi_i^{\mathbf{k}} | \phi_n \rangle. \quad (3.4)$$

Then the real space WFs $|\widetilde{W}_n^{\mathbf{R}}\rangle$ are given by

$$|\widetilde{W}_n^{\mathbf{R}}\rangle = \frac{1}{\sqrt{\mathcal{L}}} \sum_{\mathbf{k}} e^{-i\mathbf{k}\cdot\mathbf{R}} |\widetilde{W}_n^{\mathbf{k}}\rangle. \quad (3.5)$$

In the present work the energy bands which are included in the construction (3.4) are the five d -like bands sitting around the Fermi energy, as highlighted in green in Fig. 3.3. These five Bloch bands are dominated by Ni $3d$ states, but also have considerable contributions from O $2p$ states due to the hybridization effect. Concerning the trial orbitals $|\phi_n\rangle$, the simplest choice would be the Bloch sum of the LMTOs which are also used as the basis for solving the LDA band problem,

$$|\chi_\mu^{\mathbf{k}}(\mathbf{r})\rangle = \frac{1}{\sqrt{\mathcal{L}}} \sum_{\mathbf{R}} e^{i\mathbf{k}\cdot\mathbf{R}} |\chi_\mu(\mathbf{r} - \mathbf{R})\rangle. \quad (3.6)$$

Here the index μ is a combination of rlm where r denote the different atom in the unit cell, and l, m are angular momentum and magnetic quantum numbers respectively (see Eq. (1.47)). In this work n in $|\phi_n\rangle$ (Eq. (3.4)) is chosen to enumerate the five Ni $3d$ LMTOs, namely, those $|\chi_{rlm}^{\mathbf{k}}\rangle$ with r corresponding to Ni ion, $l = d$, and $m = 1, 2, \dots, 5$. Note that a WF in reciprocal space $|\widetilde{W}_n^{\mathbf{k}}\rangle$ defined in (3.4) does not coincide with the Bloch function $|\psi_n^{\mathbf{k}}\rangle$ in the multi-band case due to the summation over band index i in (3.4), but rather with a linear combination of them, i.e., $|\widetilde{\psi}_n^{\mathbf{k}}\rangle$ in Eq. (3.3) after orthonormalization. Actually one can consider them as Bloch sums of WFs analogous to the Bloch sum of the basis functions $\chi_\mu^{\mathbf{k}}(\mathbf{r})$ (Eq. (3.6)). The coefficients $\langle\psi_i^{\mathbf{k}}|\phi_n\rangle$ in (3.4) define (after orthonormalization) the unitary transformation matrix $U_{ji}^{(\mathbf{k})}$ in Eq. (3.3).

By expressing the LDA Hamiltonian in Eq. (3.1) within the basis of TB-LMTOs $|\chi_\mu^{\mathbf{k}}\rangle = |\chi_{rlm}^{\mathbf{k}}\rangle$, the band problem (3.1) reduces to a linear eigenvalue problem. Solving (3.1), one can obtain eigenvalues $\varepsilon_i(\mathbf{k})$ and eigenvectors $c_{\mu i}(\mathbf{k})$, and as well as the Bloch function $|\psi_i^{\mathbf{k}}\rangle$ which are given by

$$|\psi_i^{\mathbf{k}}\rangle = \sum_{\mu} c_{\mu i}(\mathbf{k}) |\chi_\mu^{\mathbf{k}}\rangle. \quad (3.7)$$

For an orthogonal set of LMTO basis $|\chi_\mu^{\mathbf{k}}\rangle$ ⁶, Eq. (3.7) means the coefficients

$$c_{\mu i}(\mathbf{k}) = \langle\chi_\mu^{\mathbf{k}}|\psi_i^{\mathbf{k}}\rangle, \quad c_{\mu i}^*(\mathbf{k}) = \langle\psi_i^{\mathbf{k}}|\chi_\mu^{\mathbf{k}}\rangle. \quad (3.8)$$

By using Eq. (3.4), (3.7) and (3.8), one can arrive at

$$|\widetilde{W}_n^{\mathbf{k}}\rangle = \sum_{i=N_1}^{N_2} |\psi_i^{\mathbf{k}}\rangle c_{ni}^*(\mathbf{k}) = \sum_{i=N_1}^{N_2} \sum_{\mu} c_{\mu i}(\mathbf{k}) c_{ni}^*(\mathbf{k}) |\chi_\mu^{\mathbf{k}}\rangle = \sum_{\mu} \tilde{b}_{\mu n}^{\mathbf{k}} |\chi_\mu^{\mathbf{k}}\rangle, \quad (3.9)$$

⁶ For a set of nonorthogonal set of LMTO basis $|\tilde{\chi}_\mu^{\mathbf{k}}\rangle$, one can first orthogonalize them, $|\tilde{\chi}_\mu^{\mathbf{k}}\rangle \rightarrow |\chi_\mu^{\mathbf{k}}\rangle$, and then take the orthogonalized functions $|\chi_\mu^{\mathbf{k}}\rangle$ as the trial function $|\phi_n\rangle$ in (3.4).

with

$$\tilde{b}_{\mu n}^{\mathbf{k}} \equiv \sum_{i=N_1}^{N_2} c_{\mu i}(\mathbf{k}) c_{ni}^*(\mathbf{k}). \quad (3.10)$$

Eq. (3.9) and (3.10) provide a well-defined way to construct a subset of nonorthogonal WFs from a (large) set of LMTOs.

In order to orthonormalize the WFs (3.9) one needs to calculate the overlapping matrix $O_{nn'}(\mathbf{k})$

$$O_{nn'}(\mathbf{k}) \equiv \langle \widetilde{W}_n^{\mathbf{k}} | \widetilde{W}_{n'}^{\mathbf{k}} \rangle = \sum_{i=N_1}^{N_2} c_{ni}(\mathbf{k}) c_{n'i}^*(\mathbf{k}), \quad (3.11)$$

and its inverse square root $S_{nn'}(\mathbf{k})$ is defined as

$$S_{nn'}(\mathbf{k}) \equiv O_{nn'}^{-1/2}(\mathbf{k}). \quad (3.12)$$

(orthogonality of Bloch states $\langle \psi_n^{\mathbf{k}} | \psi_{n'}^{\mathbf{k}} \rangle = \delta_{nn'}$ was used in the derivation of (3.11).)

From (3.9) and (3.12), the orthonormalized WFs in \mathbf{k} -space $|W_n^{\mathbf{k}}\rangle$ can be obtained as

$$|W_n^{\mathbf{k}}\rangle = \sum_{n'} S_{nn'}(\mathbf{k}) |\widetilde{W}_{n'}^{\mathbf{k}}\rangle = \sum_{i=N_1}^{N_2} |\psi_i^{\mathbf{k}}\rangle \bar{c}_{ni}^*(\mathbf{k}) = \sum_{\mu} b_{\mu n}^{\mathbf{k}} |\chi_{\mu}^{\mathbf{k}}\rangle, \quad (3.13)$$

with

$$\bar{c}_{ni}^*(\mathbf{k}) \equiv \langle \psi_i^{\mathbf{k}} | W_n^{\mathbf{k}} \rangle = \sum_{n'} S_{nn'}(\mathbf{k}) c_{n'i}^*(\mathbf{k}), \quad (3.14)$$

$$b_{\mu n}^{\mathbf{k}} \equiv \langle \chi_{\mu}^{\mathbf{k}} | W_n^{\mathbf{k}} \rangle = \sum_{i=N_1}^{N_2} c_{\mu i}(\mathbf{k}) \bar{c}_{ni}^*(\mathbf{k}). \quad (3.15)$$

The real space site-centered WFs $|W_n^{\mathbf{R}}\rangle$ are given by a simple Fourier transformation of $|W_n^{\mathbf{k}}\rangle$. But here all the calculations can be done in the momentum space, and an explicit calculation of the real space WFs are not needed.

With the set of orthogonal WFs $|W_n^{\mathbf{k}}\rangle$ constructed, one can easily obtain the LDA Hamiltonian matrix $H^{\text{WF}}(\mathbf{k})$ within this basis set. By using Eqn. (3.1) and (3.13), one can get

$$\begin{aligned} H_{nn'}^{\text{WF}}(\mathbf{k}) &= \langle W_n^{\mathbf{k}} | \hat{H}_{\text{LDA}}(\mathbf{k}) | W_{n'}^{\mathbf{k}} \rangle = \sum_{i=N_1}^{N_2} \bar{c}_{ni} \varepsilon_i(\mathbf{k}) \bar{c}_{n'i}^* \\ &= \sum_{\mu, \nu} b_{\mu n}^{\mathbf{k}*} H_{\text{LDA}}(\mathbf{k})_{\mu\nu} b_{\nu n'}^{\mathbf{k}}, \end{aligned} \quad (3.16)$$

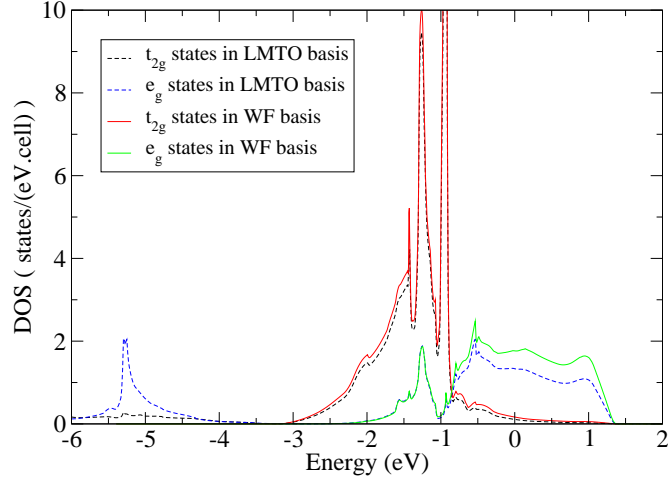


Figure 3.5: LDA partial DOSs in the basis of Ni 3d LMTOs (t_{2g} -black dashed curve, e_g -blue dashed curve) and d -like WFs (t_{2g} -red solid curve, e_g -green solid curve).

where $H_{\text{LDA}}(\mathbf{k})_{\mu\nu} = \langle \chi_{\mu}^{\mathbf{k}} | \hat{H}_{\text{LDA}}(\mathbf{k}) | \chi_{\nu}^{\mathbf{k}} \rangle$.

Thus, we have described a simple and practical procedure to construct a set of WFs which span the same Hilbert space as a specified set of Bloch bands do. The Hamiltonian matrix within this basis set, as indicated in (3.16), can be easily obtained directly from (a subset set of) the eigenvalues and eigenvectors of the LDA band problem. In the case of NiO, at each \mathbf{k} point this leads to a set of five WFs with d symmetry, and $H_{nn'}^{\text{WF}}(\mathbf{k})$ is a 5×5 Hamiltonian matrix.

3.2.2 LDA Results

In the previous section, we have demonstrated the procedure for calculating the WFs for the correlated d -like orbitals, and show that the low-energy Hamiltonian matrix within this basis can be constructed straightforwardly by the solution of the LDA band problem. The more detailed formulation and derivations can be found in the original paper of Anisimov *et al* (2005). In this work the procedure is applied to NiO, and the WFs are constructed so as to span the Hilbert subspace containing the five green Bloch bands across the Fermi level (see Fig. 3.3). Here we first present the density of states (DOS) of these WFs in Fig. 3.5, and as a comparison Ni 3d LMTO DOSs are also shown. Since the WFs constructed in the above procedure have d symmetry, they can also be classified into 3-fold degenerate t_{2g} states and 2-fold degenerate e_g states for the cubic system, like NiO. However, one should keep in mind that these WFs are not pure d states, but rather the anti-bonding-like states resulting from the hybridization between Ni 3d and O 2p states. Actually this is self-evident in Fig. 3.5, where in the Ni

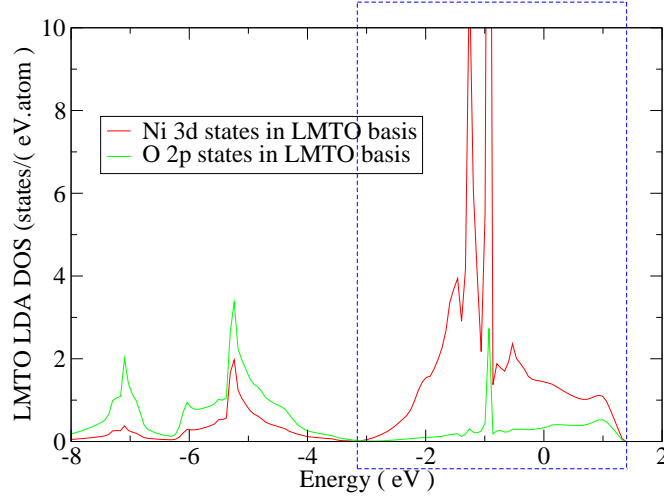


Figure 3.6: LDA partial DOS of Ni 3*d* states (red curve) and O 2*p* states (green curve) in the basis of LMTOs. The blue dashed box indicates the energy window in which the Bloch bands are included in the WF construction.

3*d*-dominant region (from -3 to 1.4 eV), WFs have more spectral weight than LMTOs, with the extra spectral weight mainly coming from the contributions of Oxygen 2*p* states. This point is further illustrated in Fig. 3.6, in which the LMTO DOSs of Ni 3*d* states and O 2*p* states are both shown. By comparing Fig. 3.5 and Fig. 3.6, one can see that the difference between the spectral weights of the WFs and LMTOs in the Ni 3*d*-dominant region (indicated by the dashed box in Fig. 3.6) is well accounted for by the O 2*p* states. On the other hand, these WFs, by its construction, omit the region of higher binding energies which primarily has O character but strongly hybridized with Ni *d* states. Therefore, we do not expect the present calculation would reproduce the well-known satellite structure appearing at higher binding energies, but aim at providing a quantitatively good description of the electronic spectrum around the gap region.

So far we already have the low-energy tight-binding Hamiltonian $H^{\text{WF}}(\mathbf{k})$ expressed in the basis of WFs, and to have a many-body theory of NiO, one needs to supplement $H^{\text{WF}}(\mathbf{k})$ with the multi-orbital Coulomb interaction and Hund-rule's coupling exchange terms. On the other hand, these interaction terms have been taken into account in $H^{\text{WF}}(\mathbf{k})$ in an average way, and therefore in principle a term H^{dc} corresponding to these contributions should be subtracted from $H^{\text{WF}}(\mathbf{k})$ to avoid double-counting. However, in the present case when only the the interacting orbitals are included in the effective Hamiltonian, H^{dc} is just an irrelevant constant and does not really need to be considered.

Based on the above considerations, the full Hamiltonian reads

$$\begin{aligned}
H = & \sum_{\mathbf{k}, n, n', \sigma} H^{\text{WF}}(\mathbf{k})_{nn'} d_{\mathbf{k}n\sigma}^\dagger d_{\mathbf{k}n'\sigma} \\
& + \sum'_{i, n, n', \sigma, \sigma'} \frac{U^{\sigma\sigma'}}{2} d_{i n \sigma}^\dagger d_{i n \sigma} d_{i n' \sigma'}^\dagger d_{i n' \sigma'} - \sum'_{i, n, n', \sigma} \frac{J_{nn'}}{2} d_{i n \sigma}^\dagger d_{i n' \bar{\sigma}}^\dagger d_{i n' \sigma} d_{i n \bar{\sigma}} \quad (3.17)
\end{aligned}$$

in which $d_{i n \sigma}^\dagger$ ($d_{i n \sigma}$) creates (destroys) an electron with spin σ in the n -th Wannier orbital (here n ranging from 1 to 5) centering at lattice site i , and $d_{\mathbf{k}, n, \sigma}^\dagger$ ($d_{\mathbf{k}, n, \sigma}$) is its Fourier transform. Furthermore $U_{nn'}^{\sigma\sigma'}$ denotes the interaction strength between one electron with spin σ in Wannier orbital n and that with spin σ' in orbital n' , and satisfies the relation that $U_{nn'}^{\sigma\sigma'} = U - 2J(1 - \delta_{nn'}) - J\delta_{\sigma\sigma'}$ for the cubic system. In principle the values of the U , J parameters here are accessible from the constrained LDA calculation. However, since now we are using the WFs as the basis, the suitable U values should be smaller than those obtained by the constrained LDA using LMTO basis. This is due to the fact that WFs are more extended than LMTOs. Actually concerning the value of the averaged Coulomb interaction \bar{U} (Eq. (2.43)), we can roughly estimate this value within the WF basis \bar{U}^{WF} from that within LMTO basis U^{LMTO} by $\bar{U}^{\text{WF}} = \bar{U}^{\text{LMTO}}(1 - x)^2$ where x is the admixture of the Oxygen states into the WFs (see Appendix B for details). For the d -band WFs constructed in this work, $x \approx 0.15$, and the constrained LDA calculation within LMTO basis gives $\bar{U}^{\text{LMTO}} = 8$ eV (Anisimov *et al.*, 1991). This leads to an estimated $\bar{U}^{\text{WF}} = 5.78$ eV. Since the results usually don't show significant dependence on the J value, we assume the J value does not change much from LMTO basis to WF basis, and choose $J = 1$ eV which is typical for such systems. From Eq. (2.43), one can obtain U value from \bar{U} and J by $U = \bar{U} + (20/9)J$ in which the number of orbitals $M = 5$ is used. All the above analysis finally give rise to $U^{\text{WF}} \approx 8$ eV.

3.2.3 LDA+DMFT Results and Comparison with Experiment

We solve the above material-specific model (3.17) by means of DMFT (Kotliar and Vollhardt, 2004; Georges *et al.*, 1996; Vollhardt *et al.*, 2005) that represents the original lattice model by a single-impurity model subject to a self-consistent condition. The impurity problem is in turn solved by the quantum Monte-Carlo (QMC) technique (Hirsch and Fye, 1986), and the imaginary Green's function data obtained by QMC are treated by maximum entropy method (MEM) (Jarrell and Gubernatis, 1996) to get the physical spectral function. The QMC simulation can be performed at different temperatures, but the computation effort scales with $1/T^3$ and therefore the calculations are restricted within relatively high

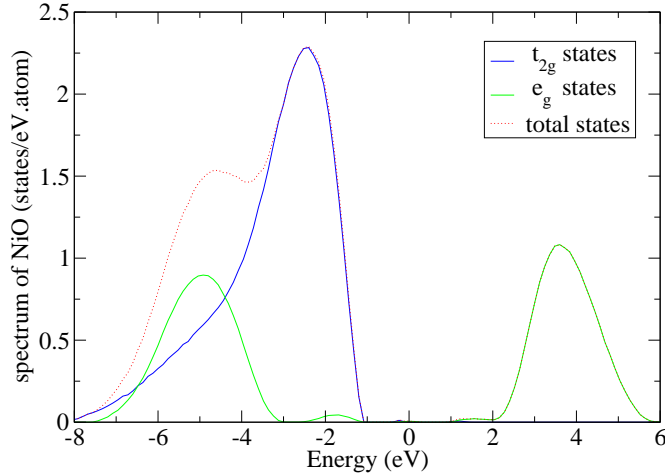


Figure 3.7: Theoretical energy spectrum of NiO obtained by the LDA+DMFT calculation for $T = 1160$ K, and $U = 8$ eV, $J = 1$ eV. t_{2g} states (blue curve) and e_g states (green curve), and total d states (red dotted curve) are shown.

temperatures. The electronic energy spectrum obtained with QMC simulation at $T = 1160$ K (corresponding to $\beta = 10$), and the interaction parameters $U = 8$ eV and $J = 1$ eV are shown in Fig. 3.7. From which one can see that the t_{2g} bands are fully filled and form the main peak below the Fermi level. The e_g bands, on the other hand, are splitted into lower and upper Hubbard bands, and an insulating gap is formed between the occupied t_{2g} bands and unoccupied e_g bands. The occupied e_g bands, together with the lower edge of the t_{2g} bands forms the shoulder below the main peak.

To analyze the effect of the QMC simulation temperature on the spectrum of NiO, we also performed the calculation at $T = 725$ K (corresponding to $\beta = 16$). The result is shown in Fig. 3.8 in comparison with that obtained at $T = 1160$ K. From the comparison one can see the results at two different temperatures do not show any significant difference, and the overall behaviors of the spectra almost fall on top of each other, in agreement with the conclusion from the photoemission experiment (Tjernberg *et al.*, 1996). Since there are always some numerical errors from QMC and some extent of indeterminacy of the MEM spectrum, here we would not associate the small detailed differences between the results at two different temperatures with any physical meanings.

Now it is worthwhile to compare our LDA+DMFT results with experiment. For this purpose we choose the combined XPS+BIS experiment carried out by Sawatzky and Allen (1984) which can be used directly for comparison with theoretical energy spectrum. This experiment was done at room temperature, i.e., in the antiferromagnetic phase. Although the theoretical calculation and the experiment are performed at different magnetic phases, the comparison is justified by

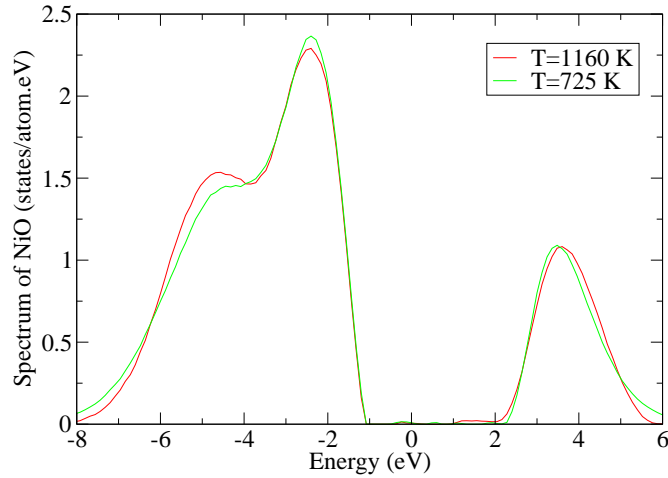


Figure 3.8: Theoretical spectrum of NiO obtained by the LDA+DMFT approach for $U = 8$ eV, $J = 1$ eV at $T = 1160$ K (red curve) and $T = 725$ K (green curve) respectively.

the observation that the electronic structure of NiO is not significantly affected by the magnetic phase transition (Tjernberg *et al.*, 1996; Jauch and Reehuis, 2004), as mentioned earlier in the introduction. Due to the ambiguity involved in the determination of the position of the chemical potential inside the insulating gap⁷, here we shift the position of the chemical potential coming from the theoretical calculation to be in accord with the experimental one. From Fig. 3.9, one can see that concerning the conduction bands, the theoretical spectrum agrees with the experimental BIS data almost perfectly, and moreover the main peak below the Fermi energy is also well reproduced. The second peak appearing in the theoretical spectrum, on the other hand, is relatively far off the experimental shoulder structure. On the other hand, the determination of the exact behavior of the energy spectrum around this region is quite tricky because there is some degree of ambiguity involved in the MEM for energy ranges relatively far away from the Fermi level. Therefore, we leave the proper explanation of the shoulder structure within the LDA+DMFT approach to future studies. A full theory of NiO should allow for the hybridization between Ni $3d$ states and O $2p$ states evolving under the influence of the interactions among d electrons. This requires an explicit inclusion of Oxygen $2p$ states, which is however not performed in this calculation. Therefore we take the present result as the first approximation of the full solution of the NiO problem within the LDA+DMFT approach.

Although the interaction parameter $U = 8$ eV estimated from the constrained LDA calculation gives rise to a theoretical spectrum in excellent agreement with

⁷ In principle, for finite temperatures, the chemical potential position in the gap can be determined exactly, but this requires a rather high accuracy of the calculation and hence is not feasible in the present case.

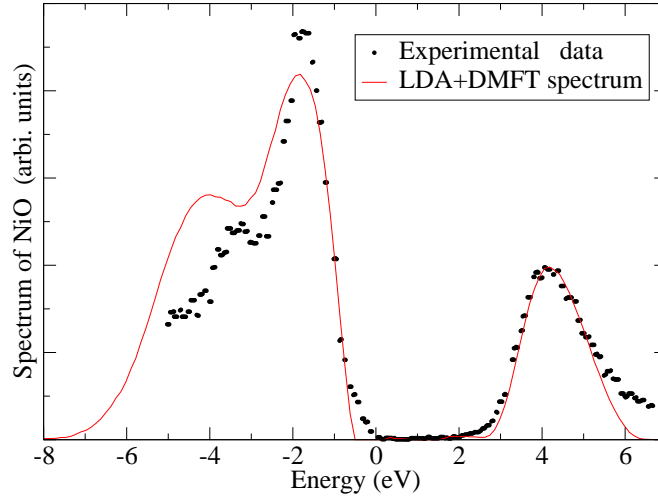


Figure 3.9: Theoretical spectrum obtained by the LDA+DMFT calculation (red curve) for $U = 8$ eV and $J = 1$ eV at $T = 1160$ K, compared with experimental XPS+BIS data (black dots) [after Sawatzky and Allen (1984)]. The zero energy point of the theoretical curve is shifted to fit the energy scale of the experimental data.

experiment, it is interesting to see how the spectrum will change by varying the U value. Therefore we also performed the calculations for $U = 8.5$ eV and 7.5 eV with fixed $J = 1$ eV at $T = 1160$ K respectively. The results are shown in Fig. 3.10, in comparison with that for $U = 8$ eV and the experimental data. To illustrate more clearly the change of the insulating gaps for different U values, the positions of the conduction-band peaks are put together by purpose. From Fig. 3.10, we see that indeed for $U = 8$ eV we get the best agreement with experiment. The Mott insulating gap increases roughly linearly with the U value.

After discussing the electronic energy spectrum, we will then turn to the energy gap and local magnetic moment. In table 3.1 the values of the energy gap and local magnetic moment obtained in this work are presented, in comparison with the experimental results, as well as those obtained within other theoretical approaches. The energy gap 4.4 eV here is measured by the distance between the half-maximum points of the first valence peak and the conduction peak, in the same way as done in the paper of Sawatzky and Allen (1984). Concerning the magnetic moment, it is worth mentioning that the value of $1.70 \mu_B$ is obtained in an indirect way here. This is due to the fact that the basis employed in the DMFT calculation is WFs, and hence the calculated value is not what is measured in experiment, namely, the local moment in the immediate vicinity of Ni ion. Specifically, in this calculation the material-specific model Hamiltonian involves five d -like WFs occupied by eight electrons, and hence gives rise to a magnetic moment $M = 2 \mu_B$ for these WFs (practically we get $M \approx 1.99$ from

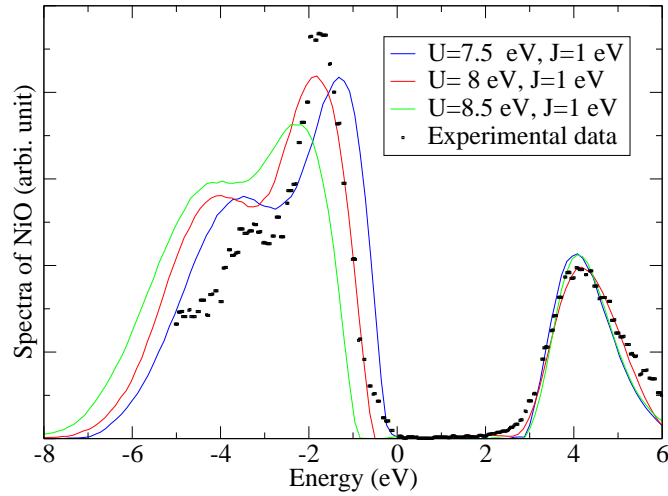


Figure 3.10: Theoretical spectra obtained by the LDA+DMFT calculations for $U = 7.5, 8,$ and 8.5 eV (blue, red, and green curves) respectively with fixed $J = 1$ eV and temperature $T = 1160$ K. Experimental XPS+BIS data [after Sawatzky and Allen (1984)] are also shown for comparison.

our QMC calculation, and the small derivation from $2 \mu_B$ may be due to the numerical error or the minor minus-sign problem present in the present calculation). However, we can roughly estimate the magnetic moment associated with Ni ion by $M(1 - x)$ where M is the moment on Wannier orbitals and x is the contribution of O $2p$ states to WFs⁸. From the LDA band calculations and the construction of WFs we know $x \approx 0.15$, and this gives $M(1 - x) \approx 1.70$ which is comparable to the experimental value and those obtained within other theoretical approaches.

3.3 Conclusions

In this work we applied the LDA+DMFT approach, in its recently developed form, to NiO. Specifically, we constructed a subset of WFs corresponding to the five Bloch bands across the Fermi level from the LDA band structure, and used them as the basis to build up a material-specific multi-band Hubbard-like Hamiltonian. This Hamiltonian is further solved by DMFT. The electronic energy spectrum obtained in this way is in excellent agreement with the experimental XPS+BIS results around the gap region. At the same time, we obtained the energy gap and local magnetic moment which also show good agreement with experimental results and those obtained by other theoretical approaches.

⁸ This relationship is derived under the same argument as that for the interaction parameter U for WFs. See Appendix B

Tab. 3.1: The LSDA, GW, LDA+U, LDA+DMFT (present work) and experimental energy gaps and magnetic moments for NiO

	LSDA	GW ^a	LDA+U ^b	LDA+DMFT	Expt.
Energy gaps (eV)	0.3	3.7	3.7	4.4	4.3 ^c , 4.0 ^d
Moments (μ_B)	1.09	1.83	1.70	1.70	1.64 ^e , 1.77 ^f , 1.90 ^g

^aS. Massidda *et al* (1997)

^bV. I. Anisimov *et al* (1993)

^cG. A. Sawatzky and J. W. Allen (1984)

^dS. Hüfner *et al* (1984)

^eH. A. Alperin (1962)

^fB. E. F. Fender *et al* (1968)

^gA. K. Cheetham and D. A. O. Hope (1983)

However, our present treatment is not a perfect one. In the construction of the material-specific Hamiltonian (3.17), we only include the five “anti-bonding” bands (which have mainly Ni 3*d* characters in the LDA calculation), but the three “bonding” bands (which are the mixture of the Ni 3*d* and O 2*p* states but have more O contributions) below them are completely neglected. Because of this, in the present work, the ratio of the contributions to the WFs from the Ni 3*d* and O 2*p* states depends on the LDA results. This means the valence bands close to the Fermi level have mainly Ni 3*d* characters, and thus the insulating gap is of the Mott-Hubbard type. This seems to be in contradiction with the widely accepted view that NiO is a charge-transfer insulator (Fujimori *et al.*, 1984; Sawatzky and Allen, 1984; Zaanen *et al.*, 1985). However, since different voices concerning this problem have persisted (Hugel and Kamal, 1997; Bengone *et al.*, 2000; Schuler *et al.*, 2005), either saying it is a Mott-Hubbard insulator or a mixture of both types, we can leave this question open for the moment, and hope to clarify this problem in future studies. Another drawback of the present framework is that, by neglecting the “bonding band”, it is not possible for us to reproduce the satellite structure appearing at high binding energies. A proper explanation of this structure from first-principles is another important issue of NiO.

In spite of the limitations of the current scheme, the LDA+DMFT approach is apparently a very promising method to deal with the late transition metal monoxides like NiO, by incorporating the first-principles information and strongly-correlated physics in one theoretical framework. A more complete treatment of NiO within the LDA+DMFT approach would require an explicit inclusion of the Oxygen 2*p* bands in the DMFT calculation, which is an on-going project. As a first approximation, the present results are quite encouraging, and we hope this work will stimulate more theoretical investigations along this direction.

4. TOWARDS A SELF-CONSISTENT LDA+DMFT SCHEME

4.1 General Motivation

In the previous two chapters we have discussed the LDA+DMFT approach, and applied it to NiO. We also pointed out that in most of its practical applications, the LDA+DMFT approach is implemented in a way that is close to the model Hamiltonian approach. Namely, one first performs a LDA band-structure calculation and derives a Hubbard-like many-body Hamiltonian for the correlated “heavy” orbitals, and then solves this Hamiltonian by DMFT. Such a procedure is usually quite successful, but it has apparent limitations for dealing with the materials for which it is not sufficient considering just the correlated orbitals. This is because some other orbitals may also play important roles in the system through their hybridizations with these correlated ones. In the case of NiO, these “other” orbitals are the Oxygen $2p$ ones, and many controversies about NiO arise from their interplay with the Ni $3d$ orbitals. This requires a more sophisticated description of the system beyond the Hubbard-like model, by treating the both kinds of orbitals on the same footing.

Moreover, for such kind of systems, it is expected that the DMFT treatment of the physically relevant orbitals will modify the electron density resulting from the DFT-LDA calculation. Since the LDA band structure uniquely depends on the electron density, the change of the electron density will inversely leads to a change of the LDA band structure, and thus the starting point of the DMFT calculation. Therefore, in principle one needs a global self-consistent loop which allows for a feedback from DMFT to LDA. Such a global loop is similar to the DFT one, but has one more ingredient, namely, a chosen subset of orbitals is treated by DMFT. In another word, the full orbital space is separated into two subspaces, one for the correlated orbitals which are treated by DMFT, and the other for all the rest orbitals which are described by usual DFT-LDA calculation. Implemented in this way, the LDA+DMFT approach is now close in spirit to the usual first-principle electronic structure method.

The above picture of the global self-consistent LDA+DMFT scheme, motivated

by physical considerations, is largely conceptual. A more rigorous formulation of this scheme can be worked out by applying variational principle to a constructed energy functional, similar to the approach used in deriving the Kohn-Sham equations. The new LDA+DMFT energy functional, which can be viewed as an extension of the LDA electronic energy functional, has an additional basic variable, i.e. the local Green's function G_{loc} , besides the electron density $\rho(\mathbf{r})$ (Savrasov and Kotliar, 2001; Lichtenstein *et al.*, 2003). The extremization of this functional can lead to a set of LDA+DMFT equations representing a global self-consistent loop. A recently proposed GW+DMFT scheme (Biermann *et al.*, 2003) is based on the similar idea, but the band structure is now solved by the GW method instead of LDA.

Depending on the basis used to represent the correlated orbitals, the method employed to solve the DMFT equations, and the interface between the band structure calculations and the DMFT calculations, the self-consistent LDA+DMFT scheme can be implemented in different ways. Here we will present a full-orbital calculation scheme proposed recently by Anisimov *et al* (2005) in which the band structure calculation and the DMFT treatment of the strongly correlated orbitals can be coupled in self-consistent way. In this scheme, the LDA band problem is solved within a set of LMTO basis as usual, but the correlated orbitals which will be further treated DMFT are represented by a set of Wannier functions (WFs). These WFs (labelled by index n) span a subspace of the whole Hilbert space defined by the LMTOs (labelled by index μ) used in the LDA calculation. The self-energy obtained within the DMFT calculation, can be transformed from the WF subspace back into the LMTO full-orbital space. With the self-energy in the full-orbital space, one can calculate the full interacting Green's function and of course the total electron density, thus closing the self-consistent loop. In the next section we will give more detailed formulations.

4.2 Flow Diagram and Formulation

The flow diagram of the fully self-consistent LDA+DMFT scheme is shown in Fig. 4.1. Here the basic ingredients are:

1. Solve the LDA band structure within the basis of LMTOs $\chi_{\mu}^{\mathbf{k}}(\mathbf{r})$.
2. From the LDA band structure, the WFs $W_n(\mathbf{r} - \mathbf{R}) = W_n^{\mathbf{R}}(\mathbf{r})$ for a subset of correlated orbitals (specified by a set of Bloch bands from N_1 to N_2 across the Fermi level), and their Bloch sum $W_n^{\mathbf{k}}(\mathbf{r})$ can be calculated, following the procedure described in Sec. 3.2.1. At each \mathbf{k} point, one can derive a low-energy tight-binding Hamiltonian $H_{nn'}^{\text{WF}}(\mathbf{k})$ matrix within the basis $W_n^{\mathbf{k}}(\mathbf{r})$. The transformation from LMTOs to WFs is defined by a set of coefficients

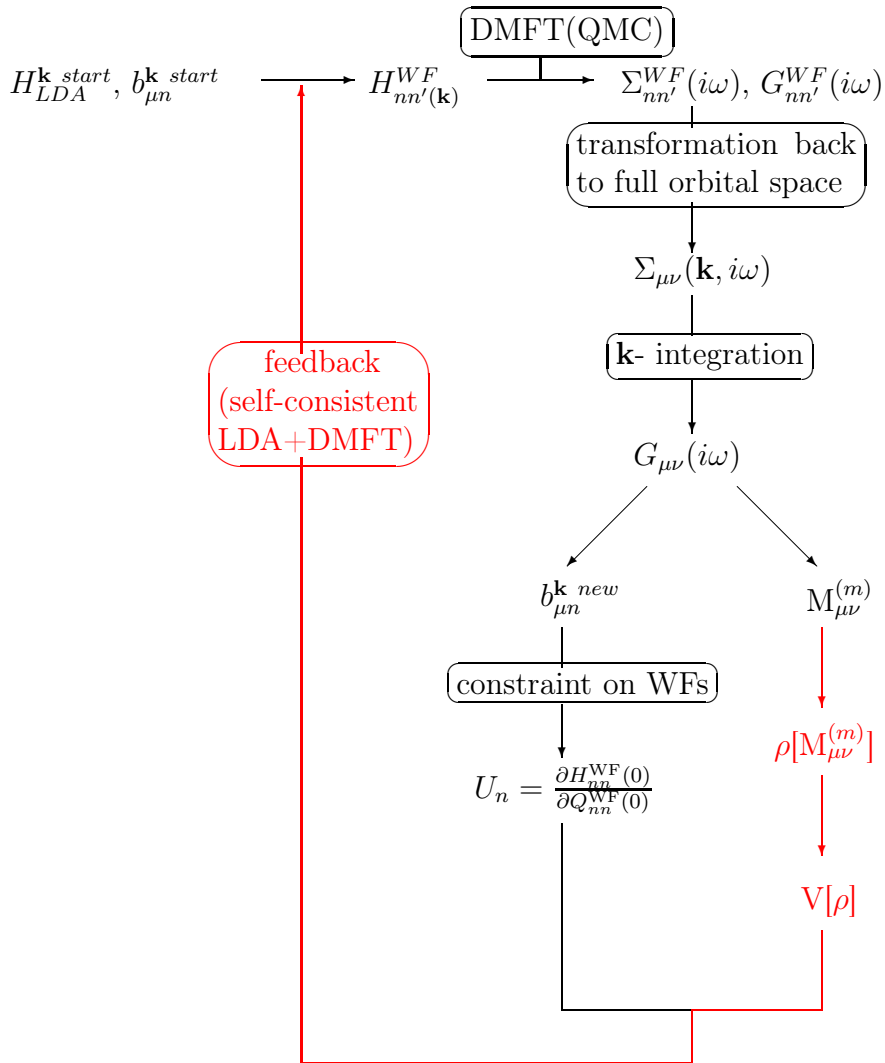


Figure 4.1: Flow diagram of the fully self-consistent LDA+DMFT scheme. The red lines indicate the steps which has not been realized so far (after Anisimov et al. (2005)).

$b_{\mu n}^{\mathbf{k}} = \langle \chi_{\mu}^{\mathbf{k}}(\mathbf{r}) | W_n^{\mathbf{k}}(\mathbf{r}) \rangle$ (see Eq. (3.15) for its definition). The transformation of the full LDA Hamiltonian matrix $H_{\text{LDA}}(\mathbf{k})$ within the LMTO basis to that within subset WF basis $H^{\text{WF}}(\mathbf{k})$ is provided by Eq. (3.16).

3. Calculate the Coulomb interaction parameter U , J within ‘‘constrained’’ LDA, and form a material-specific generalized multi-orbital Hubbard-like Hamiltonian. Here the U , J values are defined for the WFs. The procedure goes similar to the conventional ‘‘constrained’’ LDA for the LMTO basis. For instance, the U value for orbital n is defined as,

$$U_n = \frac{\partial E_{nn}^0}{\partial Q_{nn}^0}, \quad (4.1)$$

where E_{nn}^0 and Q_{nn}^0 are the elements of the energy and occupancy matrix for the set of real-space WFs centering at the origin,

$$\begin{aligned} E_{nn'}^0 &= \langle W_n^0 | \left(\frac{1}{\mathcal{L}} \sum_{i=N_1}^{N_2} \sum_{\mathbf{k}} |\psi_i^{\mathbf{k}}\rangle \varepsilon_i(\mathbf{k}) \theta(E_F - \varepsilon_i(\mathbf{k})) \langle \psi_i^{\mathbf{k}} | \right) | W_{n'}^0 \rangle \\ &= \frac{1}{\mathcal{L}} \sum_{i=N_1}^{N_2} \sum_{\mathbf{k}} \bar{c}_{ni}(\mathbf{k}) \varepsilon_i(\mathbf{k}) \theta(E_F - \varepsilon_i(\mathbf{k})) \bar{c}_{n'i}^*(\mathbf{k}), \end{aligned} \quad (4.2)$$

$$\begin{aligned} Q_{nn'}^0 &= \langle W_n^0 | \left(\frac{1}{\mathcal{L}} \sum_{i=N_1}^{N_2} \sum_{\mathbf{k}} |\psi_i^{\mathbf{k}}\rangle \theta(E_F - \varepsilon_i(\mathbf{k})) \langle \psi_i^{\mathbf{k}} | \right) | W_{n'}^0 \rangle \\ &= \frac{1}{\mathcal{L}} \sum_{i=N_1}^{N_2} \sum_{\mathbf{k}} \bar{c}_{ni}(\mathbf{k}) \theta(E_F - \varepsilon_i(\mathbf{k})) \bar{c}_{n'i}^*(\mathbf{k}). \end{aligned} \quad (4.3)$$

In above equations $\varepsilon_i(\mathbf{k})$ and $|\psi_i^{\mathbf{k}}\rangle$ are the eigenvalues and eigenstates (Bloch states) of the LDA Hamiltonian, and $\bar{c}_{ni}(\mathbf{k})$, $\bar{c}_{n'i}^*(\mathbf{k})$ are defined through Eq. (3.14). In addition E_F is the Fermi energy and $\theta(x)$ is the step function.

4. The many-body Hamiltonian is solved within DMFT, and in particular, the impurity problem is solved by Hirsch-Fye quantum Monte Carlo (QMC) method. From the solution of DMFT, one can obtain the local self-energy $\Sigma_{nn'}^{\text{WF}}(i\omega_n)$ and Green’s functions $G_{nn'}^{\text{WF}}(i\omega_n)$
5. Utilizing the transformation coefficients $b_{\mu n}^{\mathbf{k}}$, the local self-energy $\Sigma_{nn'}^{\text{WF}}(i\omega_n)$ can be converted back (unfolded) into the full Hilbert space

$$\Sigma_{\mu\nu}(\mathbf{k}, i\omega_n) = \sum_{nn'} b_{\mu n}^{\mathbf{k}} (\Sigma_{nn'}^{\text{WF}}(i\omega_n) - E^{\text{dc}}) b_{\nu n'}^{\mathbf{k}*}. \quad (4.4)$$

Here E^{dc} is the double-counting correction for the Coulomb interaction energy which has already been taken into account by LDA. Now the resultant

full self-energy $\Sigma_{\mu\nu}(\mathbf{k}, i\omega_n)$ is free of double-counting. An approximate form for E^{dc} is given by Eq. (2.42) which reduces to

$$E^{dc} = \frac{1}{2}\bar{U}n_d(n_d - 1) \quad (4.5)$$

in the case that the Hund's rule coupling term is neglected. Here n_d should be understood as the total occupancy of the WFs. In the literature other form of E^{dc} exists, e.g.,

$$E^{dc} = \frac{1}{M} \sum_{n=1}^M \text{Re}\Sigma_{nn}(0) \quad (4.6)$$

is used by Lichtenstein *et al* (2003) where M is the number of the correlated orbitals.

6. With $\Sigma_{\mu\nu}(\mathbf{k}, i\omega_n)$, one can calculate the full interacting Green's function

$$G_{\mu\nu}(i\omega_n) = \frac{1}{\mathcal{L}} \sum_{\mathbf{k}} [i\omega_n + \mu - H_{\text{LDA}}(\mathbf{k}) - \Sigma(\mathbf{k}, i\omega_n)]_{\mu\nu}^{-1}. \quad (4.7)$$

Here the matrix inversion is with respect to the LMTO basis.

7. Energy moments can be calculated from the (Matsubara) Green's function

$$M_{\mu\nu}^{(m)} = \frac{1}{\beta} \sum_{i\omega_n=-\infty}^{\infty} (i\omega_n)^m G_{\mu\nu}(i\omega_n). \quad (4.8)$$

Since from QMC calculation, we only have the Green's function value at a finite number (in order of 10) of Matsubara frequencies, the calculation of $M_{\mu\nu}^{(m)}$ with 4.8 is a highly nontrivial problem. The detailed procedure to treat the problem is given in Appendix C.

8. For a given set of LMTOs, the charge density $\rho(\mathbf{r})$ can be obtained as a functional of energy moment, and new effective LDA potential can be constructed $V(\mathbf{r}) = V(\rho(\mathbf{r}))$. This can be schematically illustrated for an orthogonal basis set in the following. In the case only the diagonal energy moments $m_{\mu}^{(n)} = M_{\mu\mu}^{(n)}$ are nonzero and contribute. The spherically averaged charge density can be evaluated as

$$4\pi\rho(r) = \int d\hat{\mathbf{r}} \sum_{j,\mathbf{k}}^{occ} |\psi_j^{\mathbf{k}}(\mathbf{r})|^2 = \sum_{\mu} \int^{E_F} N_{\mu}(\varepsilon) \chi_{\mu}^2(\varepsilon, r) d\varepsilon, \quad (4.9)$$

in which $\chi_{\mu}(\varepsilon, r)$ is the radial part of the energy-dependent partial wave, and $N_{\mu}(\varepsilon)$ is its partial density of states. The linear approximation, which leads to the LMTOs, means that

$$\chi_{\mu}(\varepsilon, r) \approx \chi_{\mu}(\varepsilon_{\nu}, r) + (\varepsilon - \varepsilon_{\mu}) \dot{\chi}_{\mu}(\varepsilon_{\nu}, r). \quad (4.10)$$

The energy moments are defined as

$$m_{\mu}^{(n)} = \int^{E_F} N_{\mu}(\varepsilon)(\varepsilon - \varepsilon_{\nu})^n d\varepsilon, \quad (4.11)$$

and therefore the charge density can be express as a function of energy moments

$$4\pi\rho(r) = \sum_{\mu} \left[m_{\mu}^{(0)}\phi(\varepsilon_{\mu}, r)^2 + 2m_{\mu}^{(1)}\phi(\varepsilon_{\mu}, r)\dot{\phi}(\varepsilon_{\mu}, r) + m_{\mu}^{(2)}\dot{\phi}(\varepsilon_{\mu}, r)^2 \right] \quad (4.12)$$

9. Go back to step 1 and repeat the iteration until self-consistency is reached.

4.3 Difficulties and Challenges

So far the self-consistent scheme discussed above has not been fully realized. The first attempt to implement the scheme described above encounters the following difficulties.

- Approximations have to be made to calculate the energy moments from Matsubara Green's function, since only information at a limited number of Matsubara frequencies is known from QMC. A high accuracy is thus not easy to obtain. We have worked out a procedure to overcome this problem, but it is not fully clear if the accuracy reached so far is enough or not.
- The double counting correction discussed above (Sec. 4.2, point 5.) has to be made in this context, but its exact form is not known. Different approximations used to treat this problem can lead to quite different results. One has to arrive at a better understanding of this problem before one can perform reliable self-consistent calculations.
- To have a good convergence of the full self-consistent scheme, for some transition metal oxides, it seems necessary to include in the DMFT calculation not only the transition metal d orbitals, but also the ligand p orbitals which strongly hybridize with the former. This by itself is a quite challenging problem. We have attempted to do this for NiO, but the present calculations have not produced the right physical scenario, namely, we couldn't find a Mott insulator solution when we treat the Ni $3d$ orbitals and O $2p$ orbitals on the same footing within DMFT. Under the present theoretical framework, the system is modelled as a composition of interacting electrons (Ni $3d$) and noninteracting electrons (O $2p$). Although the total electron number is an integer, the individual (both the interacting and noninteracting) number is not an integer due the the hybridization between them. For the moment it is not fully clear if the failure of getting an insulating solution is due to the present framework, or the way of solving it.

- To get a full energy spectrum, including both Ni $3d$ and O $2p$ states, by maximum entropy method is quite problematic, due to the reason that a large energy range is involved in this case. This makes the problem more difficult, and it is highly desirable to find out a way to improve the MEM performance in future.

Due to the above difficulties and problems, a full implementation of the conceptually appealing scheme is quite challenging, and the studies are still going on.

5. SUMMARY AND OUTLOOK

In this thesis the LDA+DMFT approach, formulated in recent years as an *ab initio* tool to study the strongly correlated materials, was reviewed. The two basic ingredients of this approach, namely the density-functional based band-structure calculation, and the dynamical mean-field theory for solving the many-body Hamiltonian were discussed in chapter 1 and chapter 2 respectively. In chapter 1 we also gave an account of the LMTO method particularly suitable for solving the energy band problem of transition metal compounds. And in chapter 2 a description of the QMC method as the solver of the quantum impurity problem was presented. These two chapters consist in the methodological part of this thesis.

In chapter 3 we applied the LDA+DMFT approach to NiO which is a classic system studied for many years. In this work a new implementation of the LDA+DMFT scheme is employed in which a set of Wannier functions (WFs) are calculated from the band structure and used as the basis of the material-specific many-body Hamiltonian. The results obtained within this approach are in good agreement with experiment concerning the insulating gap, local magnetic moment and energy spectrum. The most successful aspect of the LDA+DMFT approach in this context is that it can reproduce the photoemission (and inverse photoemission) spectrum of NiO at a quantitative level, which is something other theoretical approaches are not able to do. On the other hand, as already pointed out in the conclusion of chapter 3, the present treatment of NiO is not perfect, in the sense that the Oxygen $2p$ -dominated bands are not included in the DMFT calculation, but it is known that the O $2p$ bands play an important role in this system, through its hybridization with Ni $3d$ bands. Therefore, a complete treatment of NiO should allow the hybridization between the Ni $3d$ and O $2p$ electrons and the strong Coulomb interaction among Ni $3d$ electron interplaying with each other. With an extension of its present scheme by including the O $2p$ bands in the DMFT treatment, the LDA+DMFT is a promising method to give a full solution of the NiO problem, considering its present success in producing the experimental photoemission spectrum.

A self-consistent LDA+DMFT scheme was presented in chapter 4. A new feature of this scheme is that the interface between the LDA band-structure calculation and the DMFT calculation is provided by a set of WF's. This set of WF's can be constructed via a transformation from the LMTO basis set. By utilizing the

transformation coefficients relating the LMTOs to the WFs, the feedback from DMFT to LDA can be performed in a well-defined way. So far this proposed scheme has not been fully implemented, and there are some remaining difficulties to overcome before one can really close the self-consistent loop.

Finally we would like to give an outlook for future studies. In the first place, we hope to extend the conventional LDA+DMFT scheme so that the transition metal valence d orbitals and the ligand p orbitals can be treated on the same footing within DMFT. The solution of this problem will also help to close the self-consistent LDA+DMFT loop, the realization of which will be the next aim. In addition, it is also interesting to apply the present scheme to the neighbors of NiO, such as MnO, FeO to see if it is possible to understand the similarities and differences among these isostructured materials within the LDA+DMFT approach.

APPENDIX

A. PROOF THAT THE EXTERNAL POTENTIAL IS A UNIQUE FUNCTIONAL OF THE GROUND-STATE DENSITY

The first Hohenberg-Kohn theorem states that there is a one-to-one mapping between a many-body interacting system and its ground-state density, in another word, the external potential $v(\mathbf{r})$ (which specifies the system) can be uniquely determined (up to an unimportant constant) by the ground-state density $\rho(\mathbf{r})$. The following proof, first given by Hohenberg and Kohn (1964), is valid for systems with nondegenerate ground states. It proceeds by *reductio ad absurdum* (proof by contradiction).

Suppose two different external potential $v(\mathbf{r})$ and $v'(\mathbf{r})$, with ground-state wavefunctions ψ and ψ' respectively, lead to the same ground state density $\rho(\mathbf{r})$. Now, it is clear that unless $v(\mathbf{r}) - v'(\mathbf{r}) = \text{constant}$, $\psi \neq \psi'$ since they satisfy different Schrödinger equations. Let's denote the Hamiltonians and ground-state energies corresponding to ψ and ψ' by H, H' and E, E' respectively. By using the minimal property of the ground-state energy, we have,

$$E = \langle \psi | H | \psi \rangle < \langle \psi' | H | \psi' \rangle = \langle \psi' | H' + V - V' | \psi' \rangle,$$

where $V = \sum_i v(\mathbf{r}_i)$ and $V' = \sum_i v'(\mathbf{r}_i)$. Since $\langle \psi' | H' | \psi' \rangle = E'$, this leads to

$$E < E' + \int \rho(\mathbf{r})(v(\mathbf{r}) - v'(\mathbf{r}))d\mathbf{r}. \quad (\text{A.1})$$

By interchanging the primed and unprimed quantities, we then find in the same way that

$$E' < E + \int \rho(\mathbf{r})(v'(\mathbf{r}) - v(\mathbf{r}))d\mathbf{r}. \quad (\text{A.2})$$

Adding (A.1) and (A.2) gives rise to

$$E' + E < E + E' \quad (\text{A.3})$$

which is of course incorrect. Thus the two different external potentials can not generate the same ground state density, and therefore, up to a constant, the external potential is a unique functional of $\rho(\mathbf{r})$.

76 A. Proof That The External Potential Is A Unique Functional of The Ground-State Density

B. ESTIMATION OF THE LOCAL MAGNETIC MOMENT AND THE COULOMB INTERACTION PARAMETER

As discussed in the context of the LDA+DMFT study of NiO in Sec. 3.2.2, the average Coulomb interaction parameter within the WF basis \bar{U}^{WF} can be estimated from that within the LMTO basis \bar{U}^{LMTO} by $\bar{U}^{\text{WF}} = \bar{U}^{\text{LMTO}}(1-x)^2$, where x is the admixture of the Oxygen $2p$ states into the the WFs. Similarly in Sec. 3.2.3, the local Magnetic moment m_{loc} can be estimated from that associated with a set of WFs m^{WF} (which should be an integer) by $m_{\text{loc}} = m^{\text{WF}}(1-x)$. These two problems are related, and both can be understood in the following way¹.

For simplicity we consider a single Wannier function which is composed of a pure transition metal d atomic-like function (e.g. LMTO) located at the origin and a pure ligand p function centered around some fixed position \mathbf{d} ,

$$\psi^{\text{WF}}(\mathbf{r}) = a\phi_d(\mathbf{r}) + b\phi_p(\mathbf{r} - \mathbf{d}), \quad (\text{B.1})$$

where $|a| \approx 1$ and $|b| \ll 1$. The normalization condition of $\psi^{\text{WF}}(\mathbf{r})$ requires that

$$\int \psi^{\text{WF}*}(\mathbf{r})\psi^{\text{WF}}(\mathbf{r})d\mathbf{r} = |a|^2 + a^*bS + ab^*S^* + |b|^2 = 1, \quad (\text{B.2})$$

where $S = \int \phi_d^*(\mathbf{r})\phi_p(\mathbf{r} - \mathbf{d})d\mathbf{r}$ is the overlap between the d , p orbitals and the normalization of $\phi_d(\mathbf{r})$ and $\phi_p(\mathbf{r})$ are implicitly assumed.

The electron density associated with $\psi^{\text{WF}}(\mathbf{r})$ is

$$\begin{aligned} \rho^{\text{WF}}(\mathbf{r}) &= \psi^{\text{WF}*}(\mathbf{r})\psi^{\text{WF}}(\mathbf{r}) \\ &= |a|^2\rho_d(\mathbf{r}) + a^*b\phi_d^*(\mathbf{r})\phi_p(\mathbf{r} - \mathbf{d}) + ab^*\phi_d(\mathbf{r})\phi_p^*(\mathbf{r} - \mathbf{d}) + |b|^2\rho_p(\mathbf{r} - \mathbf{d}) \end{aligned} \quad (\text{B.3})$$

¹ I would like to thank Professor Anisimov for making this point clear through private communication

In (B.3) the first term $\rho_d(\mathbf{r})$ gives a density confined to the atomic sphere of the transition metal ion, the overlap (second and third) terms are also confined within the immediate vicinity of the transition metal atomic sphere, but the last term $\phi_p(\mathbf{r} - \mathbf{d})$ represents the p electron density confined to the ligand sphere and does not contribute to the local moment m_{loc} associated with the magnetic ion. Based on these considerations, we have

$$\begin{aligned} m_{\text{loc}} &= \int_{\Omega} [|a|^2 \rho_d(\mathbf{r}) + a^* b \phi_d^*(\mathbf{r}) \phi_p(\mathbf{r} - \mathbf{d}) + ab^* \phi_d(\mathbf{r}) \phi_p^*(\mathbf{r} - \mathbf{d})] d\mathbf{r} \\ &\approx |a|^2 + a^* b S + ab^* S^* = 1 - |b|^2, \end{aligned} \quad (\text{B.4})$$

where Ω represents the atomic sphere of the transition metal magnetic ion.

Concerning the Coulomb interaction parameter U , it is defined with respect to some particular basis. For the WF basis,

$$U^{\text{WF}} = \int \frac{\rho^{\text{WF}}(\mathbf{r}) \rho^{\text{WF}}(\mathbf{r}')}{|\mathbf{r} - \mathbf{r}'|} d\mathbf{r} d\mathbf{r}' \quad (\text{B.5})$$

and for the atomic-like basis,

$$U_{dd} = \int \frac{\rho_d(\mathbf{r}) \rho_d(\mathbf{r}')}{|\mathbf{r} - \mathbf{r}'|} d\mathbf{r} d\mathbf{r}' \quad (\text{B.6})$$

Using Eqn. (B.3), (B.5) and (B.6), and assuming only the $d - d$ electron interaction is important, we have,

$$U^{\text{WF}} \approx |a|^4 U_{dd} = (1 - a^* b S - ab^* S^* - |b|^2)^2 U_{dd} \quad (\text{B.7})$$

For the orthogonal (or nearly orthogonal) LMTO basis set, $S \rightarrow 0$, therefore

$$U^{\text{WF}} \approx ((1 - |b|^2)^2) U^{\text{LMTO}} \quad (\text{B.8})$$

Eqn. (B.4) and (B.8) can be generalized to a set of WFs with magnetic moment m^{WF} , and the Oxygen contribution $x = |b|^2$, and we can get

$$m_{\text{loc}} \approx (1 - x) m^{\text{WF}}, \quad (\text{B.9})$$

$$\bar{U}_{\text{WF}} \approx (1 - x)^2 \bar{U}^{\text{LMTO}}. \quad (\text{B.10})$$

These are the relationship used in this work for studying NiO (here We have used the average Coulomb interaction parameter \bar{U} for multiorbital case).

C. ENERGY MOMENT CALCULATION FROM MATSUBARA GREEN FUNCTION

Matsubara Green function $G(i\omega_n + \mu)$ can be expanded in terms of a Laurant series:

$$G_{\alpha,\beta}(i\omega_n + \mu) = \int_{-\infty}^{\infty} \frac{A_{\alpha,\beta}(\epsilon)d\epsilon}{i\omega_n + \mu - \epsilon} \quad (C.1)$$

$$= \frac{M_{\alpha,\beta}^{(0)}}{i\omega_n} + \frac{M_{\alpha,\beta}^{(1)}}{(i\omega_n)^2} + \frac{M_{\alpha,\beta}^{(2)}}{(i\omega_n)^3} + \frac{M_{\alpha,\beta}^{(3)}}{(i\omega_n)^4} \quad (C.2)$$

where

$$M_{\alpha,\beta}^{(n)} = \int_{-\infty}^{\infty} A_{\alpha,\beta}(\epsilon)(\epsilon - \mu)^n d\epsilon \quad (C.3)$$

with $n = 0, 1, 2, 3, \dots$

The energy moments $m^{(n)}$ are calculated by:

$$\begin{aligned} m_{\alpha,\beta}^{(0)} &= \frac{1}{\beta} \sum_{i\omega_n} G_{\alpha,\beta}(i\omega_n) = \frac{1}{\beta} \int_{-\infty}^{\infty} A_{\alpha,\beta}(\epsilon)d\epsilon \sum_{i\omega_n} \frac{1}{i\omega_n + \mu - \epsilon} \\ &= \int_{-\infty}^{\infty} A_{\alpha,\beta}(\epsilon)f(\epsilon - \mu)d\epsilon \end{aligned} \quad (C.4)$$

$$\begin{aligned} m_{\alpha,\beta}^{(1)} &= \frac{1}{\beta} \sum_{i\omega_n} (i\omega_n)G_{\alpha,\beta}(i\omega_n) = \frac{1}{\beta} \int_{-\infty}^{\infty} A_{\alpha,\beta}(\epsilon)d\epsilon \sum_{i\omega_n} \frac{i\omega_n}{i\omega_n + \mu - \epsilon} \\ &= \int_{-\infty}^{\infty} A_{\alpha,\beta}(\epsilon)(\epsilon - \mu)f(\epsilon - \mu)d\epsilon \end{aligned} \quad (C.5)$$

$$\begin{aligned} m_{\alpha,\beta}^{(2)} &= \frac{1}{\beta} \sum_{i\omega_n} (i\omega_n)^2 G_{\alpha,\beta}(i\omega_n) = \frac{1}{\beta} \int_{-\infty}^{\infty} A_{\alpha,\beta}(\epsilon)d\epsilon \sum_{i\omega_n} \frac{(i\omega_n)^2}{i\omega_n + \mu - \epsilon} \\ &= \int_{-\infty}^{\infty} A_{\alpha,\beta}(\epsilon)(\epsilon - \mu)^2 f(\epsilon - \mu)d\epsilon \end{aligned} \quad (C.6)$$

Here $f(\epsilon - \mu)$ is just the Fermi function:

$$f(\epsilon - \mu) = \frac{1}{\beta} \sum_{i\omega_n} \frac{1}{i\omega_n + \mu - \epsilon} = \frac{1}{e^{\beta(\epsilon - \mu)} + 1} \quad (\text{C.7})$$

In practice, we only have a finite number of Matsubara frequencies, it means that on summing over $i\omega_n$ in (4), (5) and (6), one has to do some truncation at a particular point $n = n_{max}$. For instance, the zeroth moment $m^{(0)}$ is calculated in the following way:

$$m_{\alpha,\beta}^{(0)} = \frac{1}{\beta} \sum_{|\omega_n| \leq \omega_{n_{max}}} \left(G_{\alpha,\beta}(i\omega_n) - \frac{M_{\alpha,\beta}^{(0)}}{i\omega_n} \right) + \frac{M_{\alpha,\beta}^{(0)}}{2} + \Delta m_{\alpha,\beta}^{(0)} \quad (\text{C.8})$$

with

$$\begin{aligned} \Delta m_{\alpha,\beta}^{(0)} &= \sum_{|\omega_n| > \omega_{n_{max}}} \frac{M_{\alpha,\beta}^{(1)}}{(i\omega_n)^2} + \frac{M_{\alpha,\beta}^{(2)}}{(i\omega_n)^3} + \frac{M_{\alpha,\beta}^{(3)}}{(i\omega_n)^4} + \dots, \\ &= -2M_{\alpha,\beta}^{(1)} \sum_{\omega_n > \omega_{n_{max}}} \frac{1}{(\omega_n)^2} + 2M_{\alpha,\beta}^{(3)} \sum_{\omega_n > \omega_{n_{max}}} \frac{1}{(\omega_n)^4} + \dots \end{aligned} \quad (\text{C.9})$$

The minimal n_{max} should be chosen so that the series in (9) converges sufficiently fast, and hence the evaluation of $\Delta m_{\alpha,\beta}^{(0)}$ in terms of the coefficients $M_{\alpha,\beta}^{(n)}$ rather than $G_{\alpha,\beta}(i\omega_n)$ themselves is doable. The estimation of $M_{\alpha,\beta}^{(n)}$ is relatively easy because for that purpose one only needs a few $G_{\alpha,\beta}(i\omega_n)$ at high frequencies. Similarly:

$$m_{\alpha,\beta}^{(1)} = \frac{1}{\beta} \sum_{|\omega_n| \leq \omega_{n_{max}}} \left[(i\omega_n) G_{\alpha,\beta}(i\omega_n) - M_{\alpha,\beta}^{(0)} - \frac{M_{\alpha,\beta}^{(1)}}{i\omega_n} \right] + \frac{M_{\alpha,\beta}^{(1)}}{2} + \Delta m_{\alpha,\beta}^{(1)} \quad (\text{C.10})$$

with

$$\begin{aligned} \Delta m_{\alpha,\beta}^{(1)} &= \sum_{|\omega_n| > \omega_{n_{max}}} \frac{M_{\alpha,\beta}^{(2)}}{(i\omega_n)^2} + \frac{M_{\alpha,\beta}^{(3)}}{(i\omega_n)^3} + \frac{M_{\alpha,\beta}^{(4)}}{(i\omega_n)^4} + \dots, \\ &= -2M_{\alpha,\beta}^{(2)} \sum_{\omega_n > \omega_{n_{max}}} \frac{1}{(\omega_n)^2} + 2M_{\alpha,\beta}^{(4)} \sum_{\omega_n > \omega_{n_{max}}} \frac{1}{(\omega_n)^4} + \dots \end{aligned} \quad (\text{C.11})$$

$$m_{\alpha,\beta}^{(2)} = \frac{1}{\beta} \sum_{|\omega_n| \leq \omega_{n_{max}}} \left[(i\omega_n)^2 G_{\alpha,\beta}(i\omega_n) - (i\omega_n) M_{\alpha,\beta}^{(0)} - M_{\alpha,\beta}^{(1)} - \frac{M_{\alpha,\beta}^{(2)}}{i\omega_n} \right] + \frac{M_{\alpha,\beta}^{(2)}}{2} + \Delta m_{\alpha,\beta}^{(2)} \quad (\text{C.12})$$

with

$$\begin{aligned}
\Delta m_{\alpha,\beta}^{(2)} &= \sum_{|\omega_n| > \omega_{n_{max}}} \frac{M_{\alpha,\beta}^{(3)}}{(i\omega_n)^2} + \frac{M_{\alpha,\beta}^{(4)}}{(i\omega_n)^3} + \frac{M_{\alpha,\beta}^{(5)}}{(i\omega_n)^4} + \dots, \\
&= -2M_{\alpha,\beta}^{(3)} \sum_{\omega_n > \omega_{n_{max}}} \frac{1}{(\omega_n)^2} + 2M_{\alpha,\beta}^{(5)} \sum_{\omega_n > \omega_{n_{max}}} \frac{1}{(\omega_n)^4} + \dots \quad (\text{C.13})
\end{aligned}$$

By this procedure, the energy moments can be calculated with the minimal set of Matsubara Green functions, but with arbitrarily good accuracy, only if the $M^{(n)}$'s are evaluated exactly.

For SrVO₃, $n_{max} \approx 1000$, and for NiO, $n_{max} \approx 500$

It is possible to extrapolate the number of Matsubara frequencies to this order from QMC data, but the accuracy is still to be checked.

BIBLIOGRAPHY

- Alperin, H. A.: 1962, *J. Phys. Soc. Jpn. Suppl. B* **17**, 12
- Andersen, O. K.: 1975, *Phys. Rev. B* **12**, 3060
- Andersen, O. K. and Jepsen, O.: 1984, *Phys. Rev. Lett.* **53**, 2571
- Andersen, O. K., Pawłowska, Z., and Jepsen, O.: 1986, *Phys. Rev. B* **34**, 5253
- Andersen, O. K. and Saha-Dasgupta, T.: 2000, *Phys. Rev. B* **62**, R16 219
- Andersen, O. K. and Wooley, R. G.: 1973, *Mol. Phys.* **26**, 905
- Anderson, P. W.: 1959, *Phys. Rev.* **115**, 2
- Anderson, P. W.: 1961, *Phys. Rev.* **124**, 41
- Anisimov, V. I., Aryasetiawan, F., and Lichtenstein, A. I.: 1997a, *J. Phys. Cond. Matter* **9**, 767
- Anisimov, V. I., Kondakov, D. E., Kozhevnikov, A. V., Nekrasov, I. A., Pchelkina, Z. V., Allen, J. W., Mo, S.-K., Kim, H.-D., Metcalf, P., Suga, S., Sekiyama, A., Keller, G., Leonov, I., Ren, X., and Vollhardt, D.: 2005, *Phys. Rev. B* **71**, 125119
- Anisimov, V. I., Kuiper, P., and Nordgren, J.: 1994, *Phys. Rev. B* **50**, 8257
- Anisimov, V. I., Poteryaev, A. I., Korotin, M. A., Anokhin, A. O., and Kotliar, G.: 1997b, *J. Phys. Cond. Matter* **9**, 7359
- Anisimov, V. I., Solovyev, I. V., Korotin, M. A., Czyżyk, M. T., and Sawatzky, G. A.: 1993, *Phys. Rev. B* **48**, 16929
- Anisimov, V. I., Zaanen, J., and Andersen, O. K.: 1991, *Phys. Rev. B* **44**, 943
- Arita, R. and Held, K.: 2005, *Orbital-selective Mott-Hubbard transition in the two-band Hubbard model*, cond-mat/0504040
- Aryasetiawan, F. and Gunnarsson, O.: 1995, *Phys. Rev. Lett.* **65**, 3221
- Barnes, S. E.: 1976, *J. Phys. F* **6**, 1375
- Barnes, S. E.: 1977, *J. Phys. F* **7**, 2637
- Ōno, Bulla, R., and Hewson: 2001, *Eur. Phys. J. B* **19**, 375
- Bartel, L. C. and Morosin, B.: 1971, *Phys. Rev. B* **3**, 1039
- Bengone, O., Alouani, M., Blöchl, P., and Hugel, J.: 2000, *Phys. Rev. B* **62**, 16 392
- Bickers, N. E., Scalapino, D. J., and White, S. R.: 1989, *Phys. Rev. Lett.* **62**, 961
- Biermann, S., Aryasetiawan, F., and Georges, A.: 2003, *Phys. Rev. Lett.* **90**, 086402
- Blankenbecler, R., Scalapino, D. J., and Sugar, R. L.: 1981, *Phys. Rev. D* **24**, 2278

- Blount, R. I.: 1962, *Solid State Physics*, Vol. 13, Academic, New York
- Blümer, N.: 2002, *Ph.D. thesis*, Universität Augsburg
- Born, M. and Oppenheimer, J. R.: 1927, *Ann. Physik* **84**, 457
- Brandow, B.: 1977, *Adv. Phys.* **26**, 651
- Brandt, U. and Mielsch, C.: 1989, *Z. Phys.* **75**, 265
- Brandt, U. and Mielsch, C.: 1990, *Z. Phys.* **79**, 295
- Brandt, U. and Mielsch, C.: 1991, *Z. Phys.* **82**, 37
- Brinkman, W. F. and Rice, T. M.: 1970, *Phys. Rev. B* **2**, 4302
- Bulla, R.: 1999, *Phys. Rev. Lett.* **83**, 136
- Bulla, R., Hewson, A. C., and Pruschke, T.: 1998, *J. Phys. Cond. Matter* **10**, 8365
- Caffarel, M. and Krauth, W.: 1994, *Phys. Rev. Lett.* **72**, 1545
- Capelle, K.: 2003, A bird's-eye view of density-functional theory, VIII'th Brazilian Summer School on Electronic Structure, p. 1, cond-mat/0211443
- Ceperley, D. M. and Alder, B. J.: 1980, *Phys. Rev. Lett.* **45**, 566
- Cheetham, A. K. and Hope, D. A. O.: 1983, *Phys. Rev. B* **27**, 6964
- Cloizeaux, J. D.: 1964, *Phys. Rev.* **135**, A698
- de' Medici, L., Georges, A., Kotliar, G., and Biermann, S.: 2005, *Phys. Rev. Lett.* **95**, 066402
- Des Cloizeaux, J.: 1963, *Phys. Rev.* **129**, 554
- Des Cloizeaux, J.: 1964, *Phys. Rev.* **135**, A685
- Dominguez Rodriguez, A., Castaing, J., and Marquez, R.: 1984, *Basic Properties of Binary Oxides*, Univ. of Seville Press
- Dreizler, R. M. and Gross, E. K. U.: 1990, *Density Functional Theory*, Springer, Berlin
- Eder, R., Dormeich, A., and Winter, H.: 2005, *Phys. Rev. B* **71**, 045105
- Faleev, S. V., van Schilfgaarde, M., and Kotani, T.: 2004, *Phys. Rev. Lett.* **93**, 126406
- Fender, B. E. F., Jacobson, A. J., and Wegwood, F. A.: 1968, *J. Chem. Phys.* **48**, 990
- Fermi, E.: 1928, *Z. Phys.* **48**, 73
- Fock, V.: 1930, *Z. Phys.* **61**, 126
- Föex, M.: 1948, *Compt. Rend. Acad. Sci.* **227**, 193
- Fujimori, A. and Minami, F.: 1984, *Phys. Rev. B* **30**, 957
- Fujimori, A., Minami, F., and Sugano, S.: 1984, *Phys. Rev. B* **29**, 5225
- Georges, A. and Kotliar, G.: 1992, *Phys. Rev. B* **45**, 6479
- Georges, A., Kotliar, G., and Krauth, W.: 1993, *Z. Phys. B* **92**, 313
- Georges, A., Kotliar, G., Krauth, W., and Rozenberg, M. J.: 1996, *Rev. Mod. Phys.* **68**, 13
- Georges, A., Kotliar, G., and Si, Q.: 1992, *Int. J. Mod. Phys. B* **6**, 705
- Georges, A. and Krauth, W.: 1992, *Phys. Rev. Lett.* **69**, 1240
- Griffith, J. S.: 1961, *The Theory of Transition-Metal Ions*, Cambridge University, Cambridge

- Gunnarsson, O., Andersen, O. K., Jepsen, O., and Zaanen, J.: 1989, *Phys. Rev. B* **39**, 1708
- Gutzwiller, M. C.: 1963, *Phys. Rev. Lett.* **10**, 159
- Hartree, D. R.: 1928, *Proc. Cambridge Philos. Soc.* **24**, 89
- Held, K., Keller, G., Eyert, V., Anisimov, V. I., and Vollhardt, D.: 2001a, *Phys. Rev. Lett.* **86**, 5345
- Held, K., McMahan, A. K., and Scalettar, R. T.: 2001b, *Phys. Rev. Lett.* **87**, 276404
- Held, K., Nekrasov, I. A., Keller, G., Eyert, V., Blümer, N., McMahan, A. K., Scalettar, R. T., Pruschke, T., Anisimov, V. I., and Vollhardt, D.: 2003, Realistic investigations of correlated electron systems with LDA+DMFT, in *Psi-k Newsletter*, Vol. #56, p. 65, http://psi-k.dl.ac.uk/newsletters/News_56/Highlight_56.pdf
- Herring, C.: 1940, *Phys. Rev.* **57**, 1169
- Hirsch, J. E.: 1983, *Phys. Rev. B* **28**, 4059
- Hirsch, J. E.: 1985, *Phys. Rev. B* **31**, 4403
- Hirsch, J. E. and Fye, R. M.: 1986, *Phys. Rev. Lett.* **56**, 2521
- Hohenberg, P. and Kohn, W.: 1964, *Phys. Rev.* **136**, B864
- Hubbard, J.: 1963, *Proc. Roy. Soc. London A* **276**, 238
- Hubbard, J.: 1964, *Proc. Roy. Soc. London A* **281**, 401
- Hüfner, S., Osterwalder, J., Riesterer, T., and Hulliger, F.: 1984, *Solid State Commun.* **52**, 793
- Hüfner, S., Reinert, P. S. I. S. F., and Schmitt, H.: 1992, *Z. Phys. B* **86**, 207
- Hugel, J. and Kamal, M.: 1997, *J. Phys. Cond. Matter* **9**, 647
- Jarrell, M.: 1992, *Phys. Rev. Lett.* **69**, 168
- Jarrell, M.: 1993a, *Z. Phys. B* **90**, 187
- Jarrell, M.: 1993b, *Phys. Rev. B* **90**, 187
- Jarrell, M. and Gubernatis, J. E.: 1996, *Physics Reports* **269**, 133
- Jauch, W. and Reehuis, M.: 2004, *Phys. Rev. B* **70**, 195121
- Jones, R. O. and Gunnarsson, O.: 1989, *Rev. Mod. Phys.* **61**, 689
- Kajueter, H. and Kotliar, G.: 1996, *Phys. Rev. Lett.* **77**, 131
- Keller, G.: 2005, *Ph.D. thesis*, Universität Augsburg
- Keller, G., Held, K., Eyert, V., Anisimov, V. I., and Vollhardt, D.: 2004, *Phys. Rev. B* **70**, 205116
- Kohn, W.: 1959, *Phys. Rev.* **115**, 809
- Kohn, W.: 1973, *Phys. Rev. B* **7**, 4388
- Kohn, W. and Rostoker, N.: 1954, *Phys. Rev.* **94**, 1111
- Kohn, W. and Sham, L. J.: 1965, *Phys. Rev.* **140**, A1133
- Korringa, J.: 1947, *Physica* **13**, 392
- Koster, G. F.: 1953, *Phys. Rev.* **89**, 67
- Kotliar, G. and Ruckenstein, A. E.: 1986, *Phys. Rev. Lett.* **57**, 1362
- Kotliar, G. and Vollhardt, D.: 2004, *Phys. Today* **57(3)**, 53
- Ku, W., Rosner, H., Pickett, W. E., and Scalettar, R. T.: 2002, *Phys. Rev. Lett.*

- 89**, 167204
- Kuhlenbeck, H., Odörfer, G., Jaeger, R., Illing, G., M. Menges, T. M., Freund, H.-J., Pöhlchen, M., Staemmler, V., Witzel, S., Scharfschwerdt, C., Wennemann, K., Liedtke, T., and Neumann, M.: 1991, *Phys. Rev. B* **43**, 1969
- Levy, M.: 1979, *Proc. Natl. Acad. Sci. (USA)* **76**, 6062
- Li, J.-L., Rignanes, G.-M., and Louie, S. G.: 2005, *Phys. Rev. B* **71**, 193102
- Lichtenstein, A. I. and Katsnelson, M. I.: 1998, *Phys. Rev. B* **57**, 6884
- Lichtenstein, A. I., Katsnelson, M. I., and Kotliar, G.: 2001, *Phys. Rev. Lett.* **87**, 067205
- Lichtenstein, A. I., Katsnelson, M. I., and Kotliar, G.: 2003, Spectral density functional approach to electronic correlations and magnetism in crystals, in A. Gonis, N. Kioussis, and M. Ciftan (eds.), *Electron Correlations and Materials Properties 2*, Chapt. Phenomological Studies of Correlation Effects, Kluwer, New York, cond-mat/0211076
- Lieb, E. H.: 1983, *Int. J. Quantum. Chem.* **24**, 243
- Lieb, E. H. and Wu, F. Y.: 1968, *Phys. Rev. Lett.* **20**, 1445
- Lundqvist, S. and March, N. H.: 1983, *Theory of the Inhomogeneous Electron Gas*, Plenum, New York
- Mahan, G. D.: 1990, *Many-Particle Physics*, Plenum Press, New York and London
- Manghi, F., Calandra, C., and Ossichi, S.: 1994, *Phys. Rev. Lett.* **73**, 3129
- Marzari, N. and Vanderbilt, D.: 1997, *Phys. Rev. B* **56**, 12 847
- Massidda, S., Continenza, A., Posternak, M., and Baldereschi, A.: 1997, *Phys. Rev. B* **55**, 13494
- Mattheiss, L. F.: 1972, *Phys. Rev. B* **5**, 290
- McMahan, A. K., Held, K., and Scalettar, R. T.: 2003, *Phys. Rev. B* **67**, 75108
- Metzner, W.: 1989, *Z. Phys.* **B77**, 253
- Metzner, W. and Vollhardt, D.: 1989a, *Phys. Rev. B* **39**, 4462
- Metzner, W. and Vollhardt, D.: 1989b, *Phys. Rev. Lett.* **62**, 324
- Mott, N. F.: 1949, *Phys. Soc. London Sect. A* **62**, 416
- Müller-Hartmann, E.: 1989a, *Int. J. Mod. Phys. B* **3**, 2169
- Müller-Hartmann, E.: 1989b, *Z. Phys. B* **74**, 507
- Nagaoka, Y.: 1966, *Phys. Rev.* **147**, 392
- Nekrasov, I. A., Held, K., Blümer, N., Poteryaev, A. I., Anisimov, V. I., and Vollhardt, D.: 2000, *Eur. Phys. J. B* **18**, 55
- Nekrasov, I. A., Keller, G., Kondakov, D. E., Kozhevnikov, A. V., Pruschke, T., Held, K., Vollhardt, D., and Anisimov, V. I.: 2005, *Comparative study of correlation effects in CaVO_3 and SrVO_3* , cond-mat/0501240, accepted for *Phys. Rev. B*
- Nekrasov, I. A., Pchelkina, Z. V., Keller, G., Pruschke, T., Held, K., Krimmel, A., Vollhardt, D., and Anisimov, V. I.: 2003, *Phys. Rev. B* **67**, 085111
- Parr, R. G. and Yang, W.: 1989, *Density-Functional Theory of Atoms and Molecules*, Oxford University Press, Oxford

- Parzen, G.: 1953, *Phys. Rev.* **89**, 237
- Pavarini, E., Biermann, S., Poteryaev, A., Lichtenstein, A. I., Georges, A., and Andersen, O. K.: 2004, *Phys. Rev. Lett.* **92**, 176403
- Perdew, J. P. . and Wang, Y.: 1986, *Phys. Rev. B* **33**, 8800
- Pruschke, T., Cox, D. L., and Jarrell, M.: 1993a, *Europhys. Lett* **21**, 593
- Pruschke, T., Cox, D. L., and Jarrell, M.: 1993b, *Phys. Rev. B* **47**, 3553
- Roth, W. L.: 1958a, *Phys. Rev.* **110**, 1333
- Roth, W. L.: 1958b, *Phys. Rev.* **111**, 772
- Rozenberg, M. J., Chitra, R., and Kotliar, G.: 1999, *Phys. Rev. Lett.* **83**, 3498
- Rozenberg, M. J., Zhang, X. Y., and Kotliar, G.: 1992, *Phys. Rev. Lett.* **69**, 1236
- Sakai, O. and Kuramoto, Y.: 1994, *Solid State Commun.* **89**, 307
- Sakai, S., Arita, R., and Aoki, H.: 2004, *Phys. Rev. B* **70**, 172504
- Savrasov, S. Y. and Kotliar, G.: 2001, *Spectral Density Functionals for Electronic Structure Calculations*, cond-mat/0106308
- Savrasov, S. Y., Kotliar, G., and Abrahams, E.: 2001, *Nature* **410**, 793
- Sawatzky, G. A. and Allen, J. W.: 1984, *Phys. Rev. Lett.* **53**, 2339
- Schuler, T. M., Ederer, D. L., Itza-Ortiz, S., Woods, G. T., Callcott, T. A., and Woicik, J. C.: 2005, *Phys. Rev. B* **71**, 115113
- Sekiyama, A., Fujiwara, H., Imada, S., Suga, S., Eisaki, H., Uchida, S. I., Takegahara, K., Harima, H., Saitoh, Y., Nekrasov, I. A., Keller, G., Kondakov, D. E., Kozhevnikov, A. V., Pruschke, T., Held, K., Vollhardt, D., and Anisimov, V. I.: 2004, *Phys. Rev. Lett.* **93**, 156402
- Shen, Z.-X., List, R. S., Dessau, D. S., Wells, B. O., Jepsen, O., Arko, A. J., Bartlett, R., Shih, C. K., Parmigiani, F., Huang, J. C., and Lindberg, P. A. P.: 1991, *Phys. Rev. B* **44**, 3604
- Shick, A. B., Lichtenstein, A. I., and Pickett, W. E.: 1999, *Phys. Rev. B* **60**, 10763
- Shimizu, Y., Sakai, O., and Hewson, A. C.: 2000, *J. Phys. Soc. Jap.* **69**, 1777
- Si, Q., Rozenberg, M. J., Kotliar, G., and Ruckenstein, A. E.: 1994, *Phys. Rev. Lett.* **72**, 2761
- Skriver, H. L.: 1984, *The LMTO Method*, Springer-Verlag, Berlin Heidelberg New York Tokyo
- Skull, C. G., Strauser, W. A., and Wollan, E. O.: 1951, *Phys. Rev.* **83**, 333
- Slater, J. C.: 1937, *Phys. Rev.* **51**, 846
- Slater, J. C.: 1951, *Phys. Rev.* **82**, 538
- Sugano, S., Tanabe, Y., and Kamimura, H.: 1970, *Multiplets of Transition-Metal Ions in Crystals*, Academic, New York
- Svane, A. and Gunnarsson, O.: 1991, *Phys. Rev. Lett.* **65**, 1148
- Terakura, K., Oguchi, T., Williams, A. R., and Kübler, J.: 1984a, *Phys. Rev. B* **30**, 4734
- Terakura, K., Williams, A. R., Oguchi, T., and Kübler, J.: 1984b, *Phys. Rev. Lett.* **52**, 1830
- Thomas, L. H.: 1927, *Proc. Cambridge Philos. Soc.* **23**, 542

- Tjernberg, O., Söderholm, S., Chiaia, G., Girard, R., Karlsson, U. O., Nylén, H., and Lindau, I.: 1996, *Phys. Rev. B* **45**, 10 245
- Tomlinson, J. R., Domash, L., Hay, R. G., and Montgomery, C. W.: 1955, *J. Am. Chem. Soc.* **77**, 909
- van Dongen, P. G. J., Gebhard, F., and Vollhardt, D.: 1989, *Z. Phys.* **76**, 199
- Vollhardt, D.: 1984, *Rev. Mod. Phys.* **56**, 99
- Vollhardt, D.: 1991, *Physica B* **169**, 277
- Vollhardt, D.: 1993, in V. J. Emery (ed.), *Correlated Electrons Systems*, World Scientific, Singapore
- Vollhardt, D., Held, K., Keller, G., Bulla, R., Pruschke, T., Nekrasov, I. A., and Anisimov, V. I.: 2005, *J. Phys. Soc. Jap.* **74**, 136
- Vollhardt, D., Wölfle, P. ., and Anderson, P. W.: 1987, *Phys. Rev. B* **36**, 006703
- Wannier, G.: 1937, *Phys. Rev.* **52**, 191
- Wigner, E. P. and Seitz, F.: 1933, *Phys. Rev.* **43**, 804
- Wolff, P. A.: 1961, *Phys. Rev. B* **124**, 1030
- Yokoyama, H. and Shiba, H.: 1987, *J. Phys. Soc. Jap.* **56**, 1490
- Zaanen, J., Sawatzky, G. A., and Allen, J. W.: 1985, *Phys. Rev. Lett.* **55**, 418

CURRICULUM VITAE

Personal Data

Name	Xinguo Ren
Date of Birth	September 25, 1976
Place of Birth	Henan, China
Nationality	Chinese

Education and Studies

Ph.D in Physics	Expected in Dec. 2005, University of Augsburg, Germany. Advisor: Professor Dieter Vollhardt Dissertation Topic: "LDA+DMFT Investigation of NiO"
M.S. in Physics	2001, Chinese Academy of Sciences, China Advisor: Professor Yue Yu Thesis: "The Methods of Hartree-Fock Approximation and Exact Diagonalization in Two-Dimensional Electron System"
B.S. in Physics	1998, Nankai Univerisity, Tianjin, China Advisor: Professor Xue-Qian Li Thesis: "The Possible Source of Heavy Neutral Particles in Cosmic Rays"

Research Interests

- *ab initio* electronic-structure calculations with density functional theory.
- Realistic modelling of strongly correlated systems with the LDA+DMFT approach.
- Mott-Hubbard metal-insulator transition in electronic systems.
- Two-dimensional electronic systems.

ACKNOWLEDGEMENTS

In the first place I want to express my sincere gratitude to Prof. Dr. Dieter Vollhardt for offering me an opportunity to work on challenging topics under his supervision. It is his guidance that led me into a new research area of condensed matter physics, namely, investigating the strongly correlated materials from first principles. From numerous discussions with him, what I have learned is not only the scientific knowledge, but also the way of thinking about physics, which is invaluable for my future academic career.

My special thanks go to Dr. Georg Keller and Dr. Igor Nekrasov for their generous helps when I started to learn the LDA+DMFT method. I also appreciate that they have been always available for discussions and answering questions during all these years.

I also want to thank Prof. Dr. Vladimir Anisimov, Prof. Dr. Thomas Pruschke, Ivan Leonov, Dr. Karsten Held, Priv.-Doz. Dr Volker Eyert, and Priv.-Doz Ralf Bulla for helpful discussions. They have helped to broaden my knowledge of the LDA+DMFT approach and strongly correlated materials in one way or another.

Additionally, I would like to thank all the members of the groups of Prof. Dr. Dieter Vollhardt, and Prof. Dr. Arno Kampf for the friendly and pleasant environment they have created. Among them are Priv.-Doz. Stefan Kehrein, Dr. Marcus Kollar, Dr. Sabine Tornow, Dr. Sanjeev Kumar, Markus Schmid, Michael Sekania, Hyun Jung Lee, Dmitry Lobaskin, Martin Eckstein, and Andreas Hackl.

Finally I am deeply indebted to my parents to whom I owe everything.